NORDA Technical Note 143

Naval Ocean Research and
Development Activity
NSTL Station, Mississippi 39529

NORDA Parabolic Equation Workshop, 31 March - 3 April 1981

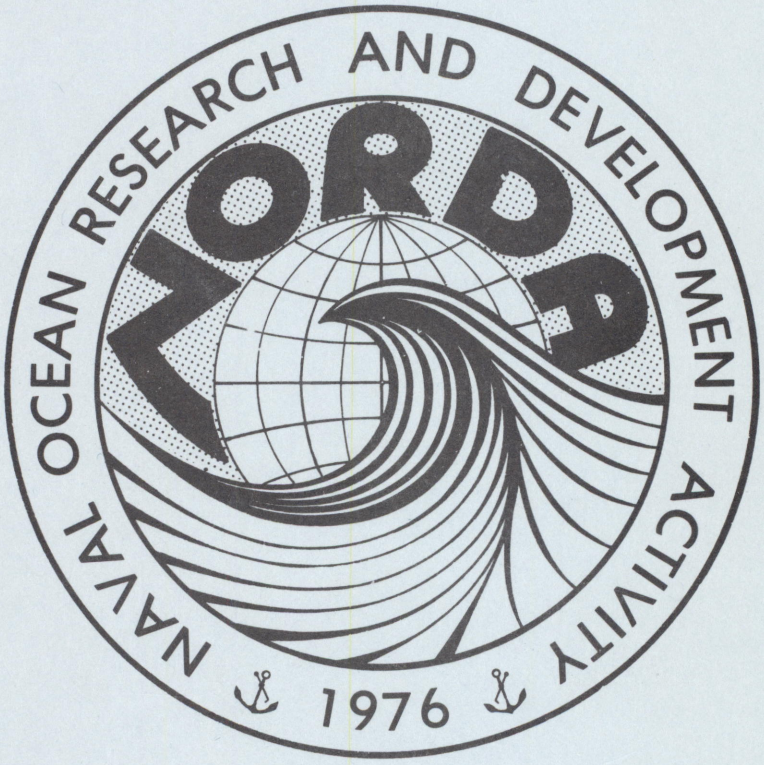

James A. Davis
DeWayne White
Numerical Modeling Division
Ocean Science and Technology Laboratory

Raymond C. Cavanagh
Planning Systems, Inc.
McLean, Va.

Prepared for : The Surveillance
Environmental Acoustic Support
(SEAS) Project, NORDA Code 520

September 1982

ABSTRACT

A Parabolic Equation (PE) workshop sponsored by the Surveillance Environmental Acoustic Support (SEAS) Project and hosted by NORDA's Numerical Modeling Division was held at NSTL from 31 March to 3 April 1981. The purpose of the workshop was to provide a forum for those active in theoretical and applied PE development and to compare computer results for a set of ocean acoustic problems. Fifteen formal presentations were given, and thirteen different PE models were exercised against four test cases. The test cases ranged from one that any PE should be able to handle to one that is a challenge for every PE. This report describes the results of that workshop and includes the theoretical bases for the models, the model descriptions, results of the test cases, and abstracts of the formal presentations.

CONTENTS

NORDA PARABOLIC EQUATION WORKSHOP

I. INTRODUCTION

The advantages of the parabolic approximation (PA) to the elliptic wave equation for use in obtaining solutions to ocean acoustic problems were first made known to the underwater acoustic scientific community through an AESD workshop[1] (sponsored by LRAPP) on non-ray tracing techniques of acoustic propagation modeling held in May 1973. That workshop concerned itself primarily with mode theory solutions to a set of test cases for range-independent environments, but also included the Parabolic Equation (PE) results of Hardin and Tappert[2] for those same problems. As is now well known, the primary advantage of PE is its applicability to ocean acoustic problems with range-dependent environments. See, for example, Tappert[3] for the origin and history of the development and application of PE to various fields, especially the pioneering applications of Leontovich and Fock[4].

Since that AESD workshop in 1973 there has been a literal explosion of the development and application of PE to solutions of underwater sound problems. No attempt is made in this report to try to include what is now an extensive PE bibliography. Because of advances over the last several years in PE models for the range-dependent environment problems in ocean acoustics, the Surveillance Environmental Acoustic Support Project (SEAS, NORDA Code 520) sponsored a "PE Workshop" hosted by NORDA's Numerical Modeling Division (OSTL Code 320). The workshop was held at NSTL from 31 March to 3 April 1981. Objectives of the workshop were to (a) provide a forum for those presently active in theoretical and applied PE development to exchange ideas, describe the PE programs, identify problems or deficiencies in the PE approach, and to stimulate new ideas and approaches; (b) compare computer results for a set of identical ocean acoustic problems; and (c) collectively identify range dependent environment problems that could provide a set of benchmark test cases. An anticipated result of the workshop is the identification of one (or perhaps several) PE transmission loss model that could meet the needs of the SEAS program. This supported version would be a "state-of-the-art" model derived from a combination of the most promising features of existing PE models. The workshop was a success in terms of achieving objectives (a) and (b) above; however, objective (c) was not achieved--there was little discussion of possible benchmark test cases. This report describes the results of the workshop, but does not include recommendations made to SEAS as a consequence of it.

The workshop was divided into two parts: half devoted to the test cases and half devoted to presentations of new PE developments. In the test problem portion a brief description of each PE program exercised against the test cases was given and the predicted transmission loss presented. Thirteen different PE models were exercised against the test problems, with reference normal-mode calculations supplied by the SACLANT ASW Research Centre. In the second half of the workshop, fifteen half-hour presentations on recent PE research and implementations were given. Attendance at the workshop was limited to invitees. The attendees and their organizational affiliations are given in Table 1.

This report addresses itself almost entirely to the test case portion of the workshop (Sections II-IX). Although the new development portion occupied half of the workshop period, it was decided that a semi-detailed exposition of those presentations was a major task and beyond the scope of this report. Abstracts are, however, reproduced in Appendix A.

Table 1. Attendees and organizational affiliation

NAME	ORGANIZATION
Dr. R. Baer	Naval Research Laboratory
Mr. H. Brock	Naval Research Laboratory
Dr. H. Bucker	Naval Ocean Systems Center
Dr. R. Cavanagh	Planning Systems Incorporated
Dr. S. Chin-Bing	Naval Ocean Research and Development Activity
Dr. J. Davis	Naval Ocean Research and Development Activity
Dr. L. Dozier	Science Applications Incorporated
CDR. K. Evans	Naval Ocean Research and Development Activity
Dr. R. Evans	Ocean Data Systems Incorporated
Dr. K. Gilbert	Naval Ocean Research and Development Activity
Mr. D. Gordon	Naval Ocean Systems Center
Dr. R. Greene	Science Applications Incorporated
Dr. J. Hanna	Science Applications Incorporated
Miss E. Holmes	Science Applications Incorporated
Dr. F. Jensen	SACLANT ASW Research Centre
Dr. D. Lee	Naval Underwater Systems Center
Dr. L. Nghiem-Phu	Daubin Systems Corporation
Dr. D. Palmer	Ocean Acoustics Laboratory (NOAA/AOML)
Prof. J. Papadakis	University of Rhode Island
Mr. R. Patton	Bell Telephone Laboratories
Mr. N. Paz	U. S. Naval Oceanographic Office
Mr. M. Pedersen	Naval Ocean Systems Center
Mr. J. Perkins	Naval Research Laboratory
Mr. D. Seals	Bell Telephone Laboratories
Mr. C. Spofford	Science Applications Incorporated
Prof. F. Tappert	University of Miami
Dr. D. Thomson	Defence Research Establishment Pacific (Canada)
Mr. D. White	Naval Ocean Research and Development Activity
Dr. D. Wood	Naval Undersea Systems Center
Dr. R. Uenkataraman	Bell Telephone Laboratories

To assist in the interpretation of results from the various PE's that were exercised against the test cases, theoretical bases are presented in Section II for a generalized PE, standard PE, small modifications to PE, a C_o-independent PE, and higher-order corrections to PE. That section ends with a summary of the accuracy of the various forms. Section III discusses numerical algorithms for solving PE, such as split-step, finite difference, and finite element techniques. Included as well are summaries of treatments of interface and boundary conditions and techniques for obtaining the initial field. Abstracts describing the PE's exercised against the test cases are given in Appendix B.

Given the groundwork that facilitates an understanding of the component parts of each PE and allows proper perspective of their interrelationships, the test cases and results are presented in Sections IV-IX. Section IV discusses the rationale for the test problems and some "ground rules" for participants. The test cases themselves are addressed in Sections V-VIII, and each section includes (1) description of the case and what it was designed to test and (2) model results, analysis, and summary. These sections, taken in turn, are as follows:

Section V.	Test Case 1 - Range Dependent Surface Duct
Section VI.	Test Case 2 - Bilinear Profile
Section VII.	Test Case 3 - Range Independent Shallow Water Environment
Section VIII.	Test Case 4 - Basin/Slope/Shelf Configuration for a Geoacoustical Bottom.

A summary of the workshop is given in Section IX.

II. FORMS OF THE PARABOLIC EQUATIONS

A. INTRODUCTION

Since there are a number of approximations to the Helmholtz Equation that lead to what are commonly referred to as "Parabolic Equations" (PE's), it is important at the start to define and distinguish the various forms presented at the workshop. Following Tappert's exposition presented at the start of the workshop and also Reference 3, we introduce a generalized PE (attributed to Claerbout[5,6] and called "GPE" here) from which the various PE's can be systematically derived and which gives a framework for identifying differences among them. See also McDaniel[7] for a discussion of splitting matrices and derivations of parabolic approximations.

The treatment here will be brief, but should help the reader understand the relationships among the various forms of PE. Such an overview thus facilitates interpretation of results from the PE models that were exercised against the test problems.

In this section then we will derive a generalized PE and, in turn, derive standard PE, discuss small modifications to PE (CMOD and CPA), outline the derivation of a C_o-independent PE, derive higher order corrections to PE or "high angle" PE's, and finally estimate the accuracy of the various forms.

B. GENERAL PE (GPE)

We begin by deriving a generalized PE following Tappert[3]. The acoustic pressure $p(r,z)$ in a cylindrically symmetric medium of constant density ρ having a harmonic point source at $(0,z_s)$ satisfies the following equation:

$$p_{rr} + (p_r/r) + p_{zz} + k_o^2 n^2 p = -(4\pi/r)\ p_s\ \delta(r)\delta(z - z_s) \quad , \tag{1}$$

where r is the radial variable, z the depth, $k_o = \omega/C_o$, ω is the angular frequency, C_o is some arbitrary reference sound speed, $n(r,z) = C_o/C(r,z)$ is the index of refraction, and p_s the source strength. Eq. 1 is solved subject to interface conditions of continuity of p and p'/ρ where p' is the normal derivative. A pressure-release surface ($p(r,0) = 0$) and radiation boundary conditions as z and r go to infinity are assumed.

Away from the source we introduce the function u(r,z) defined by

$$p = u/r^{\frac{1}{2}} \quad , \tag{2}$$

and make the far-field approximation $k_o r \gg 1$ to obtain the Helmholtz far-field equation

$$u_{rr} + u_{zz} + k_o^2 n^2 u = 0 \quad . \tag{3}$$

Defining the operators

$$P = \frac{\partial}{\partial r} \tag{4}$$

and

$$Q = \left(\frac{1}{k_o^2} \cdot \frac{\partial^2}{\partial z^2} + n^2\right)^{\frac{1}{2}} \tag{5}$$

we can then write

$$(P^2 + k_o^2 Q^2)u = 0 \quad . \tag{6}$$

At this point we wish to "factor" the operators in Eq. 6. There are various factorizations (see Ref. 7 for example), but we will use that of Claerbout[5] and write Eq. 6 as

$$(P + ik_oQ)(P - ik_oQ)u + ik_o[P,Q]u = 0 \quad ,$$

where

$$[P,Q]u = PQu - QPu$$

is the commutator of the operators P and Q. If the medium is range independent, or weakly range dependent, the commutator can be ignored and with the assumption of only "outgoing" waves we arrive at GPE:

$$Pu = ik_oQu \quad . \tag{7}$$

GPE, according to Tappert, is the most complete PE which is evolutionary in range and neglects backscattering. For range-independent environments and only outgoing waves it is exact within the limits of the far-field approximation. It provides the basis for obtaining the various forms of "marching out" PE's, i.e., partial differential equations in first order with respect to r (hence the name "Parabolic", as opposed to the Helmholtz Elliptic partial differential equation). These forms will follow as a result of approximations to the pseudo-differential operator Q, whose properties preclude the solution of GPE itself.[3] For later convenience we also write Eq. 7 as

$$Pu = ik_o(1 + q)^{\frac{1}{2}}u \quad , \tag{8}$$

with

$$Q = (1 + q)^{\frac{1}{2}} \quad ,$$

$$q = \varepsilon + \mu \quad ,$$

$$\varepsilon = n^2 - 1 \quad ,$$

and

$$\mu = \frac{1}{k_o^2} \cdot \frac{\partial^2}{\partial z^2} \quad .$$

It is important, finally, to note that in a range-dependent environment GPE (and approximations to it) has an intrinsic error, [P,Q]u. Conditions under which the commutator is small have not been rigorously defined, although Claerbout[6], Tappert[3], and De Santo[12] provide frameworks within which to address the problem. Until more is learned, users of PE's must be wary of cases in which refraction index or boundary conditions are more than weakly range dependent.

C. STANDARD PE (SPE)

Standard PE, which we will refer to as SPE, is that PE reported by Hardin and Tappert at the AESD workshop[2]. Although it is a first-order, small q approximation, SPE has the advantage of being particularly amenable to efficient numerical solution (viz., the Split-step algorithm discuss below). It is easily derived from Eq. 8 by making a Taylor series expansion of Q

$$Q = (1 + q^2)^{\frac{1}{2}} = 1 + (q/2) - (q^2/8) + (q^3/16) + \cdots \tag{9}$$

and retaining only the first two terms to obtain

$$Pu = ik_o(1 + (q/2))u \quad .$$

The introduction of the envelope function

$$\psi(r,z) = u(r,z)\exp(-ik_o r) \tag{10}$$

leads to

$$P\psi = i(k_o q/2)\psi \quad , \tag{11}$$

or to SPE in a more familiar form

$$2ik_o\psi_r + \psi_{zz} + k_o^2(n^2 - 1)\psi = 0 \quad . \tag{12}$$

SPE is thus derived from the Helmholtz far-field equation by assuming $[P,Q]u = 0$, neglecting backscatter, and neglecting q^2 and higher order-terms in the expansion of $Q = \sqrt{1 + q}$.

In the usual derivation of SPE the envelope function is introduced in Eq. 3 to yield

$$P^2\psi + 2ik_oP\psi + k_o^2q\psi = 0 \quad . \tag{13}$$

The $P^2\psi$ term is then neglected by making the "parabolic" approximation, i.e., assuming

$$|P^2\psi| << |2ik_oP\psi| \quad .$$

This approximation, which in a special sense assumes that ψ is a slowly varying function of r, is implied by the approximations listed above in obtaining SPE from GPE. For SPE to be a good approximation to GPE (in the sense of some norm $||\cdot||$) the neglected terms in the expansion of $(1 + q)^{\frac{1}{2}}$ must be small, i.e.,

$$||q||^2 = ||\varepsilon + \mu||^2$$

must be small compared to one.

Modal analysis by McDaniel[8] for a range-independent environment shows that given the correct field at some range r_o, the mode depth functions for SPE are identical to those for the far-field Helmholtz equation. However, the phase at range r for the n-th mode depends on k_o and is given by

$$((k_o^2 + k_n^2)/2k_o)(r - r_o) \quad ,$$

as opposed to $k_n(r - r_o)$ for the far-field Helmholtz equation. The SPE phase can also be written in terms of an equivalent angle θ_n with respect to the horizontal as

$$(k_o/2)(1 + \cos^2\theta_n)(r - r_o) \quad ,$$

where

$$k_n = k_o \cos\theta_n \quad .$$

The ratio of the SPE mode function to the correct mode function for the n-th mode is therefore given by

$$R_{spe} = \exp(i2k_o s^2 (r - r_o)) \quad , \tag{14}$$

where

$$s = (\sin(\theta_n/2))^2 \quad . \tag{15}$$

Notice that the phase error in Eq. 14 depends on the choice of k_o. One can select k_o such that the phase error is zero for a single mode, i.e., $k_o = k_n$, but not for all modes. If the modes are contained in a sufficiently small band (i.e., the spectrum of the operator $[k_o Q]$ is concentrated near k_o), k_o can be selected to be in the center of the band and the resulting phase errors and their consequences on the field may be small. This so-called "narrow band" case is usually interpreted as a "small angle" restriction; the horizontal components of the true wave numbers $k_n = k_o \cos\theta_n$ are confined to a small band about k_o, and the equivalent geometric rays are nearly horizontal ($\theta_n \approx 0$). As noted here and by Fitzgerald[9] and Brock, Buchal and Spofford[10] the angles need not be small, but rather limited to a small aperture so that $k_o \cos\theta_n$ is nearly constant. For a wide band the phase errors can be large with significant consequences on the field.

The next two PE forms discussed (CMOD and CPA) are intended to reduce phase errors while retaining those features of SPE which allow for efficient computer solution.

D. CMOD

A modification to SPE that is designed to reduce the associated phase errors or improve the narrow band limitations has been developed by Brock, Buchal and Spofford[10]. This modification, referred to as CMOD, is not, insofar as we know, easily derivable from GPE. SPE phase errors have been viewed as the result of errors in each mode's horizontal wave number (k_n), which can be thought of as errors in each mode's phase velocity (ω/k_n). CMOD is based on the idea of constructing a "pseudo problem whose (SPE) phase velocities are equal to the elliptic phase velocities of the corresponding modes in the original problem"[10]. This is accomplished by utilizing the WKB approximation to identify a mapping of the modal turning point depths in the original problem into the turning point depths of the same mode in the pseudo problem. Carried out exactly this produces a zero phase error, but the depth functions are then in error away from the mode turning points. If the main contribution to the field of any mode is at a depth in the vicinity of its turning point, then this will be a small error and will be independent of range in a range-independent environment. Use of the WKB approximation, however, does not reduce the phase error to exactly zero; therefore, there are small phase errors as well as depth function errors.

CMOD employs a frequency independent mapping, given by

$$(n,z) \rightarrow (m,y) \cong ((2n - 1)^{\frac{1}{2}},\ zn^{\frac{1}{2}}) \quad . \tag{16}$$

With this mapping the form of the PE equation is unchanged, i.e., u(r,y) satisfies

$$Pu = ik_o[\frac{m^2 + 1}{2} + \frac{1}{2k_o{}^2}\frac{\partial^2}{\partial y^2}]u \quad , \tag{17}$$

or in terms of the envelope function

$$2ik_o\psi_r + \psi_{yy} + k_o{}^2(m^2 - 1)\psi = 0 \quad , \tag{18}$$

which is the same form as SPE given by Eq. 12.

Analysis of phase and amplitude errors of SPE using CMOD is complicated even for the range-independent environment case. See Reference 10 for details and cautions regarding its use in problems having isovelocity regions.

E. CPA

Palmer[11] showed that, in a range-independent environment, an integral operator applied to parameterized solutions of SPE yielded a solution to the Helmholtz equation. The SPE solution was, in fact, found to be the result of a stationary phase approximation to the integral. An expansion about the stationary phase point yields a relation of form

$$\begin{aligned}\Phi(r,z) = \{&1 - (q/4) + (q^2/8) + \cdots \\ &+ ik_o r\,(-(q^2/8) + \cdots) \\ &+ (1/12)(ik_o r)^2(q/2)^4 + \cdots\}\psi(r,z) \quad ,\end{aligned} \tag{19}$$

where ψ is the SPE envelope and Φ is the Helmholtz equation envelope. Note that the first and fourth terms listed give

$$\begin{aligned}\Phi(r,z) &\approx (1 - i(k_o r q^2/8))\psi(r,z) \\ &\simeq \psi + (ir/2k_o)\psi_{rr} \quad .\end{aligned} \tag{20}$$

DeSanto[12] used a similar, but different, integral operator to relate Φ and ψ for a general, range-dependent environment. Again, expansion about the stationary phase point leads to a result much like Eq. 19, but includes the effects of range-dependent n(r,z). DeSanto, Perkins, and Baer suggested using Eq. 20 to improve SPE, and showed examples of the improvement[13]. This modified solution is termed the Corrected Parabolic Approximation, or CPA, and takes the form, at each range step,

$$\psi_c(r) = \psi(r) + (i\Delta/2k_o)\tilde{\psi}_{rr}(r) \quad , \tag{21}$$

where $\psi(r)$ is the SPE solution, Δ is the range step, and $\tilde{\psi}_{rr}(r)$ is a finite-difference approximation to ψ_{rr} which utilizes $\psi(r-\Delta)$, $\psi(r)$, $\psi(r+\Delta)$. See Ref. 13 for details of the implementation.

CPA can be derived directly from GPE via the second-order expansion of Q:

$$P\psi \simeq ik_o((q/2) - (q^2/8))\psi \quad , \tag{22}$$

and the approximations:

$$\tilde{\psi}_{rr} \simeq -(k_o^2 q^2/4)\psi, \tag{23}$$

for $q_r \simeq 0$,

$$\psi_c(r + \Delta) \simeq e^{ik_o((q/2) - (q^2/8))\Delta} \cdot \psi(r) \quad , \tag{24}$$

for q, q^2, and q_r small. Tappert emphasized at the workshop that this modification is valid only for small q, in which case the correction is small anyway. A phase error analysis below confirms and quantifies this. He suggested that a more useful (more accurate) solution to second order in q is obtained via Claerbout's rational-linear method (see Subsection G).

Modal analysis of CPA for a range-independent environment leads to

$$R_{cpa} = (1 + \gamma^2)^{\frac{1}{2}} \exp i(2k_o s^2(r - r_o) - \tan^{-1}\gamma) \quad , \tag{25}$$

where R is the ratio of the CPA mode function to the Helmholtz mode function,

$$\gamma = 2k_o(r - r_o)(s - s^2)^2 \quad , \tag{26}$$

and as before $s = \sin^2(\theta_n/2)$. Thus, for the general case CPA contains an amplitude and a phase error. Notice that the first term in the exponential is the SPE phase error, Eq. 14, and the second term is a modification to that phase error.

For small s (small θ_n, and only the lowest-order terms in amplitude and phase), R_{cpa} reduces to

$$R_{\substack{cpa \\ s\to o}} \sim (1 + 2k_o^2 s^4(r - r_o)^2)\exp(i4k_o s^3(r - r_o)) \quad . \tag{27}$$

In this event CPA provides a more accurate phase than SPE at the expense of a small amplitude error. Note, however, that when s is not small (i.e., the "wide band" case) the error is not small. This is the case for any small q approximation.

F. C_o-INDEPENDENT PE

As has been noted in Section C, SPE's accuracy depends on $||\varepsilon + \mu||$ being small. Tappert[3] has shown however that it is possible to improve on SPE by either (1) requiring $||\varepsilon||$ to be small but relaxing the condition on μ and thereby allowing wide beamwidths, or (2) requiring $||\mu||$ to be small but relaxing the condition on ε and thereby allowing large variations in the index of refraction. Tappert uses formal operator expansions for Q that are linear in one of μ or ε and valid to all orders in the other. His result for small $||\mu||$ is

$$Pu = ik_o[n + \frac{1}{4k_o^2}(\frac{nz^2}{n^3} - \frac{nzz}{n^2}) + \frac{1}{2k_o^2}\frac{\partial}{\partial z}\frac{1}{n}\frac{\partial}{oz}]u \quad . \tag{28}$$

This is Tappert's C_o- or k_o-independent PE equation. That it is k_o-independent is easily seen since k_o and n always appear in the combination $k_o n$.

Modal solution of Eq. 28 for a range-independent environment, to compare with the modal solution of the far-field Helmholtz equation, is complicated by the fact that the depth functions are different, and we shall not attempt that analysis here. If, however, the z derivative of n can be ignored, then Eq. 28 reduces to SPE and the corresponding SPE phase errors persist.

Tappert also derives a small $||\varepsilon||$ PE, but since it was not exercised against the workshop test problems we refer the reader to Reference 3.

G. RATIONAL LINEAR PE APPROXIMATION

In contrast to Tappert's small $||\mu||$ or small $||\varepsilon||$ improvement over the linear q representation of the operator Q that results in SPE, there are higher order approximations of Q that are correct to order q^2. These are generally referred to as "Rational Linear" approximations, and take the following form

$$Q = (1 + q)^{\frac{1}{2}} \simeq \frac{a + bq}{c + dq} \quad . \tag{29}$$

To obtain SPE from this form, let a=1, b=1/2, c=1, and d=0. Claerbout[5,6], who apparently was the first to use a rational linear approximation for PE, has suggested the values: a=1, b=3/4, c=1, and d=1/4, so that Q is approximated as

$$Q = \frac{1 + (3q/4)}{1 + (q/4)} \quad . \tag{30}$$

Expansion of the denominator of Eq. 30 leads to

$$Q = 1 + (q/2) - (q^2/8) + (q^3/32) + \cdots \quad , \tag{31}$$

and comparison of Eq. 31 with the Taylor series expansion of Q given by Eq. 9 shows that it is correct to order q^2 and is therefore a higher-order (also higher-

angle) approximation to Q than employed to obtain SPE. Use of Q given by Eq. 30 in Eq. 7 leads to the governing equation for u:

$$(1 + (q/4))Pu = ik_o(1 + (3q/4))u \quad . \tag{32}$$

Notice that this is linear in q, i.e., a partial differential equation that is of second order in the z derivative, whereas retention of the q^2 term in the Taylor series expansion of Q given by Eq. 9 would result in an equation of fourth order in the z derivative. If we introduce the envelope function ψ, Claerbout's rational linear approximation becomes

$$(q/4)\psi_r + \psi_r = (ik_o q/2)\psi \quad . \tag{33}$$

If the first term in Eq. 33 is set equal to zero, the result is SPE, Eq. 12.

Claerbout's PE, Eq. 33, can be arrived at more directly from Eq. 13 by: (1) initially neglecting the $P^2\psi$ term, (2) applying P and solving for $P^2\psi$, and (3) back substituting the $P^2\psi$ term in Eq. 13. This rationale is employed by Thomson (this report) and is given in Ref. 6.

Greene (this report) has suggested another rational linear approximation to Q given by

$$Q = \frac{0.99986 + 0.79624q}{1.0 + 0.3099q} \quad , \tag{34}$$

where the numerical coefficients (a,b,c, and d) have been determined by minimizing the maximum error of the phase of the propagating modes over a range of angles from 0 to 40°, i.e., k_n/k_o between 1.0 and 0.77. Notice that Greene's coefficients in Eq. 34 are nearly the same as Claerbout's in Eq. 30. Application of Greene's mini-max technique for a range of angles other than 0-40° will of course alter the numerical values of a, b, c, and d.

Any rational linear approximation (i.e., of form given by Eq. 29) leads to the following envelope function:

$$\alpha\psi_r + \gamma\psi_{zzr} = \beta\psi + \omega\psi_{zz} \quad , \tag{35}$$

where

$$\alpha = c + d(n^2 - 1) \quad ,$$

$$\beta = ik_o((a - c) + (b - d)(n^2 - 1)) \quad ,$$

$$\gamma = d/k_o^2 \quad ,$$

and

$$\omega = i(b - d)/k_o \quad .$$

Eq. 35 avoids the numerical specifics and introduces a convenient notation for a later section of this report.

Note that the rational linear approximation, regardless of the choice of a,b,c, and d, has the same mode depth functions as the far-field Helmholtz equation in a range-independent environment (as would any order Taylor series expansion of Q), and yet is second order in the z derivative in range-dependent environments (unlike a higher-order Taylor series expansion of Q).

Modal analysis for a range-independent environment for Claerbout's PE, Eq. 33, results in the error ratio:

$$R_{cb} = \exp(i2k_o(r - r_o)s^3/(1 - s + s^2)) \quad , \tag{36}$$

where again $s = \sin^2(\theta/2)$ and $k_n = k_o\cos\theta_n$. Notice that the amplitude is correct and that the phase error is of order s^3 as $s \to 0$, while the SPE error is of order s^2 (Eq. 14). The error in Greene's approximation is of order 1 as $s \to 0$, but is consistently "small" over the range of angles $0 \leq \theta_n \leq 40°$.

H. SUMMARY OF PE FORMS AND ACCURACY

This section (II) has endeavored to logically relate various PE forms to a general PE, which in turn is closely related to the Helmholtz equation. GPE (in the far-field approximation) is exact when the environment is range-independent and only "one-way" propagation is present. If $n_r \neq 0$ then errors are made. Tappert[3] gives a qualitative ranking of those errors, and DeSanto[12] implicitly estimates them in relating SPE solutions to solutions of the Helmholtz equation, but rigorous quantitative estimates remain to be derived. The error could be large whenever a PE is used and must be kept in mind.

The next type of error is that incurred in making approximations to GPE. GPE is not amenable to numerical solution; the operator $(1 + q)^{1/2}$ is "non-local" and cannot be represented by a finite sum of linear differential operators. The most popular approximation to GPE to date has been "SPE", a small q expansion and, as we discuss in Section III, its widespread use is a result of an efficient numerical algorithm (Tappert and Hardin's split-step) for its solution.

Error estimates of SPE and other PE's have, to date, concentrated on modal analysis for range-independent environments. Although such an approach ignores the effect of environmental range dependencies, it is useful in estimating local errors and their cumulative effect. As outlined in Section C, SPE has phase errors. Because of this, a number of PE's have been developed to improve on SPE.

(1) CMOD - A physically intuitive correction to SPE whose quantitative improvement over SPE is not easy to calculate, but which has been demonstrated in some deep water ocean acoustic problems[10].

(2) CPA - Error estimates here indicate an improvement over SPE for small angle propagation. It has a demonstrated advantage for some realistic problems[13].

(3) Tappert's C_o-Independent PE - An improvement over SPE, but not amenable to error analysis. Tests have not been documented (other than presented here in the test problem sections), and the method may have limited applicability since large variation in the index of refraction (large ε) is usually important for wide angle propagation (large μ).

(4) Rational Linear Approximation - Both the Claerbout and Greene approximations offer the potential for a significant improvement over SPE--for "wide angle" propagation. In modal terms, the correct depth functions are retained, while the phase errors are significantly reduced for angles up to 40° or more.

III. METHOD OF SOLUTION

A. INTRODUCTION

The primary numerical advantage of the parabolic approximation is that it yields a first-order differential equation in the range variable (r), and can therefore be solved by marching out in range from a given "initial" field. This section is then devoted to a discussion of numerical methods--techniques for solving a given PE form on a computer. In practice the solution is obtained by laying down a numerical grid in depth z, solving for the field at the grid points, and advancing in range to the next range increment. The two basic types of approaches are the split-step algorithm and classical finite difference/finite element techniques. An integral part of each approach is its treatment of interfaces/boundaries, approximations to the radiation conditions, and, of course, the initial field.

In this section we address Split-Step SPE (Part B), finite difference methods for SPE (Part C), and a comparison of the two methods (Part D). Part E describes approaches for high angle (rational linear) PE and finally Part F presents various ways to obtain the initial field.

B. SPLIT STEP SPE

The split-step algorithm was historically the first technique employed in solving SPE for underwater acoustic problems; it is therefore appropriate to start with this approach. To facilitate comparisons among numerical solutions to SPE, we first introduce the operators:

$$x = (ik_o q/2) = A + B \tag{37}$$

with

$$A = \frac{i}{2k_o}\frac{\partial^2}{\partial z^2} \tag{38}$$

and

$$B = (ik_o/2)(n^2 - 1) \quad . \tag{39}$$

Write SPE, Eq. 11, as

$$\psi' = x\psi = (A + B)\psi \quad , \tag{40}$$

where the prime is understood to be the r derivative.

Now, given the value of ψ at some range r_n, i.e., $\psi_n = \psi(r_n,z)$, the value of ψ at a new range $r+\Delta$, i.e., $\psi_{n+1} = \psi(r_n+\Delta, z)$, can be approximated from Eq. 40 as

$$\psi_{n+1} = e^{\tilde{x}\Delta} \cdot \psi_n + E \quad , \tag{41}$$

where $\tilde{x}$ approximates the behavior of x over the interval Δ, and where E is an error term (equal to zero if $\tilde{x}$=x and x is r independent). The actual error depends, as we shall see later, on how the exponential operator is split and on how x is approximated by $\tilde{x}$ in a range-dependent environment.

The split-step algorithm usually takes one of two forms. The first approach, originally proposed by Tappert[2], is to split the exponential operator as follows:

$$e^{(A + B)\Delta} \simeq e^{B\Delta} \cdot e^{A\Delta} \tag{42}$$

and exploit the Fourier transform to calculate the two z derivatives inherent in exp $(A\Delta)$. ψ_{n+1} is thus found by means of the algorithm

$$\psi_{n+1} = e^{B\Delta} F^{-1}(e^{-\frac{is^2\Delta}{2k_o}} F(\psi_n)) \quad , \tag{43}$$

where F is the Fourier transform from z to s and F^{-1} is the inverse transform from s to z. The second approach, later suggested by Tappert[15], is to split the exponential operator as

$$e^{(A + B)\Delta} = e^{\frac{A\Delta}{2}} \cdot e^{B\Delta} \cdot e^{\frac{A\Delta}{2}} \tag{44}$$

and solve for ψ_{n+1} by the algorithm

$$\psi_{n+1} = F^{-1}[e^{-i\frac{s'^2\Delta}{4k_o}} F\{e^{B\Delta}F^{-1}(e^{-i\frac{s^2\Delta}{4k_o}}F(\psi_n))\}] \quad . \tag{45}$$

In either case appropriate boundary conditions are required in order to numerically implement this approach. The physical conditions are that p=0, or ψ=0, at z=0 and $\psi \to 0$ as $z \to \infty$. Since one cannot numerically deal with an infinite transform, the latter (radiation) boundary condition must be approximated. The usual approach[14] is to add an attenuating layer of thickness D to the physical depth H and set ψ=0

at $z=z_{max}=H+D$. The attenuating layer is modeled with a complex index of refraction of the form

$$n^2(z) = n^2(H) + i\alpha(z);\ H \leq z \leq z_{max} \quad , \tag{46}$$

where $\alpha(z)$ is the assumed attenuation profile in the layer. The choice of D and α is arbitrary only to the extent that no significant energy should return into the problem from this "false" bottom. Usually D is taken to be $H/3$[14], i.e., $z_{max} = 4H/3$, and α is exponentially increasing with depth. With this approximation to the radiation condition, the Fourier transforms in Eqs. 43 and 45 can be replaced by a discrete FFT (in fact, by a fast sine transform since $p=0$ at $z=0$ and $z=z_{max}$). The advantages of the split-step FFT are that it is energy conserving, unconditionally stable, and computationally efficient[2]. The disadvantages are that it requires a uniform z-grid, periodic boundary conditions and, as we shall see, small step-size for large propagation angles (subject, of course, to the limits of SPE itself). In order to handle realistic ocean acoustic problems rapid variations ("discontinuities") in sound speed, attenuation and density must be taken into account. Sound speed and attenuation are both included in the index of refraction, and the remedy is simple but costly: model discontinuities by a continuous change over a relatively small depth interval and force a larger transform size for proper sampling in depth.

Density variations or discontinuities are a special problem. Tappert[3] has shown that if one introduces a new variable into Eq. 1

$$\tilde{p} = p\rho^{-\frac{1}{2}}$$

and proceeds as in Section C with $\tilde{u}=\tilde{p}\ r^{1/2}$, $\tilde{\psi}=\tilde{u}\ \exp(-ik_o r)$, the resulting equation for $\tilde{\psi}$ is exactly of the form of SPE for ψ (Eq. 11), except that n^2 (which can also contain absorption) is replaced by $\tilde{n}^2$ where

$$\tilde{n}^2 = n^2 + \frac{1}{2k_o^2} \cdot \rho^{\frac{1}{2}} \cdot \nabla \cdot (\rho^{-3/2}\nabla\rho) \quad .$$

Large gradients or discontinuities in ρ can make $\tilde{n}$ deviate considerably from unity (thus violating conditions for validity of SPE). Tappert concludes that a "smearing out" of such rapid or discontinuous changes is necessary and suggests an analytic form for such a smearing[3]. Quite apart from the particular analytic form, the end result is a larger transform size and smaller range step.

C. FINITE DIFFERENCE FOR SPE

An alternative numerical technique for solution of SPE is provided by finite difference techniques. A primary advantage of this approach is that it does not require a uniform z mesh and discontinuities in sound speed and density can be more accurately approximated without exorbitant increases in mesh points.

A standard finite difference approach, Crank-Nicholson, applied to SPE (Eq. 11) for constant z and r mesh has the following form:

$$\frac{1}{\Delta}\left(\psi_{\ell}^{n+1} - \psi_{\ell}^{n}\right) + \frac{1}{2\delta^2}\left[\left(\psi_{\ell+1}^{n+1} - 2\psi_{\ell}^{n+1} + \psi_{\ell-1}^{n+1}\right) + \left(\psi_{\ell+1}^{n} - 2\psi_{\ell}^{n} + \psi_{\ell-1}^{n}\right)\right]$$

$$+ \frac{k_o^2}{2}\left[\left(n^2 - 1\right)_{\ell}^{n+1} \psi_{\ell}^{n+1} + \left(n^2 - 1\right)_{\ell}^{n} \psi_{\ell}^{n}\right] = 0 \quad , \tag{47}$$

where ℓ is the z mesh index with interval δ, and n is the r-mesh index with interval Δ. By rearranging Eq. 47 and introducing $\bar{\psi}$ as the column vector whose components are the ψ_{ℓ}'s, we obtain the matrix form

$$C_L \bar{\psi}^{n+1} = C_R \bar{\psi}^{n} \quad . \tag{48}$$

Since C_L and C_R are tridiagonal matrices (even for variable z and r mesh), Eq. 48 is easily solved implicitly.

Crank-Nicholson is just one of many finite-difference schemes applicable to SPE. Others offer different orders of accuracy, ease of implementation, and speed. In any of these, attenuation can be incorporated by use of a complex index of refraction. Rapid variations in sound speed and density are easily accommodated by the variable mesh (δ) and the flexibility to satisfy the interface conditions, i.e. continuity of pressure p and p'/ρ (p' is the normal derivative).

Radiation conditions as $z \to \infty$ are typically handled as for split-step, i.e., with a false bottom. An exception to this is the use of impedance boundary conditions by Papadakis (this report), given in terms of an integral along the bottom interface

$$p(r,z_B) = -\frac{i^{\frac{1}{2}}\rho_B}{(2k_o\pi\rho)^{\frac{1}{2}}} \cdot \int_o^r e^{i\frac{k_o}{2}(n_B^2 - 1)(r-s)} \cdot (r-s)^{\frac{1}{2}}\, p_z(s,z_B)\,ds \quad , \tag{49}$$

where z_B is the interface depth below which there is a half space with density ρ_B and index of refraction n_B. This technique avoids the introduction of a non-physical subbottom layer and offers a possible savings through elimination of about 25% of the mesh points and evaluating Eq. 49 instead.

D. SPLIT-STEP VS. FINITE DIFFERENCE FOR SPE

In this section we will compare the range-step dependent and frequency dependent errors incurred in using the split-step algorithm and finite differencing to solve SPE. Included in the results are estimates made by Brock[14], Buchal and Tappert[16], McDaniel[7], DiNapoli and Deavenport[17], and Jensen and Krol[18].

Assume that the value of $\psi_n = \psi(r_n,z)$ is available at range r_n. A power series solution to SPE in the form of Eq. 40 is given to third order in Δ by

$$\psi_{n+1} = \left[1 + x\Delta + (x' + x^2)\frac{\Delta^2}{2} + (x'' + 2x'x + xx' + x^3)\frac{\Delta^3}{6}\right]_n \psi_n \quad , \tag{50}$$

where the prime indicates an r derivative and x, x' and x" are evaluated at r_n.

Consider first the errors inherent in the exponential solution of SPE defined by Eq. 41, i.e., even if $\tilde{x}=x$, the solution is in error whenever $x' \neq 0$. If $\tilde{x}$ is x evaluated at r_n, then an expansion of the exponential for small Δ leads to the local error (difference between the solution of Eq. 44 and Eq. 45):

$$E(x(r_n)) = \frac{\Delta^2}{2} x_n' \psi_n + O(\Delta^3)\psi_n \quad , \tag{51}$$

whereas if $\tilde{x}$ is x evaluated at $r_n+\frac{\Delta}{2}$, the error is (to third order in Δ):

$$E(x(r_n + \tfrac{\Delta}{2})) = \frac{\Delta^3}{24} (x'' - 2xx' + 2x'x)_n \psi_n \quad . \tag{52}$$

Thus, errors of order Δ^2 can be incurred even before the exponential operator exp (A+B) is split. These errors persist in what follows.

Now consider the split-step algorithm given by Eq. 42. If $\tilde{x}$ is x evaluated at r_n the error is

$$E_{ss}^{A,B}(x(r_n)) = \frac{\Delta^2}{2} (x' + [A,B])_n \psi_n \quad . \tag{53}$$

This is of order Δ^2 and depends on the range dependence of x (through n) and on the commutator of A and B. Comparing Eqs. 51 and 53 we see that the splitting introduces an additional error, involving [A,B]. Excluding boundary considerations

$$[A,B]\psi_n = -\frac{1}{4}(n^2)_{zz}\psi_n + 2(n^2)_z(\psi_n)_{zz} \quad . \tag{54}$$

The magnitude of [A,B] is therefore seen to depend on the z gradient of the index of refraction and is independent of frequency. On the other hand

$$x' = \frac{i}{2} k_o \frac{\partial n^2}{\partial r} = B' \quad ,$$

and is linear in frequency. The $x'\Delta^2$ error term can be removed by taking $\tilde{x}$ equal to x evaluated at $r_n + \frac{\Delta}{2}$ with the result

$$E_{ss}^{A,B}(x(r_n + \tfrac{\Delta}{2})) = \frac{\Delta^2}{2} [A,B]_n \psi_n \quad . \tag{55}$$

This is to be compared with Eq. 52 where the operator was not split.

Consider now the splitting given by Eq. 44 with $\tilde{x}$ equal to x evaluated at r_n. The resulting error is

$$E_{ss}^{\frac{A}{2},B,\frac{A}{2}}(x(r_n)) = \frac{\Delta^2}{2} x_n' \psi_n \quad , \tag{56}$$

identical to Eq. 51 and an improvement over the previous splitting but still of order Δ^2. If on the other hand $\tilde{x}$ is x evaluated at $r_n + \frac{\Delta}{2}$ the error becomes

$$E_{ss}^{\frac{A}{2},B,\frac{A}{2}}(x(r_n + \tfrac{\Delta}{2})) = \frac{\Delta^3}{24}\,(B'' + 2(B'A - AB') + [A,[A,B]] + 2[B,[A,B]])_n\psi_n \quad (57)$$

and is now of order Δ^3. Notice that the term containing the commutators is explicitly linear in frequency as are other terms. Also notice that since A is not a function of r, Eq. 57 differs from Eq. 52 only in the commutator terms. These additional error terms are a consequence of splitting the operator exp ($x\Delta$).

Before proceeding further it is important to understand that the error in the above formulations and those we will see later depend on the r dependence of n. If n' is small the error will be small, and if n' is large the error will be large--thereby requiring a small range step. Regardless of the size of n' one can always choose Δ to make the local error as small as one likes. However, SPE (as well as GPE) is based on the assumption that n' is small, i.e., $[P,Q] \approx 0$. Thus, in a problem where n' drives the range step-size error, SPE may be a poor approximation.

We next consider the finite difference approaches. One scheme for solving Eq. 40 is given by

$$\frac{\psi_{n+1} - \psi_n}{\Delta} = x_n \frac{\psi_{n+1} + \psi_n}{2} \quad , \quad (58)$$

and results in an error

$$E_{FD} = \frac{x'\Delta^2}{2}\psi_n \quad , \quad (59)$$

i.e., of order Δ^2, linear in frequency, and identical to Eqs. 51 and 56. However, use of the Crank-Nicholson algorithm

$$\frac{\psi_{n+1} - \psi_n}{\Delta} = \frac{x_{n+1}\,\psi_{n+1} + x_n\psi_n}{2} \quad (60)$$

results in an error given by

$$E_{CN} = -\frac{\Delta^3}{12}\,(x'' + 2x'x + xx' + x^3)\psi_n \quad (61)$$

and is of order Δ^3 and cubic (through x^3) in frequency.

We have seen that the accuracy of split-step or finite difference algorithms depends on how the range dependence of x is approximated. For x simply evaluated at range steps, the best that one can do is order Δ^2, whereas a linear approximation for x between range points allows order Δ^3. Therefore, in summary, in a range-dependent environment with x linearly approximated between range points: (1) the splitting originally proposed by Tappert (Eq. 42), has a local error (Eq. 55) of order Δ^2 independent of frequency; (2) the later splitting (Eq. 44) has a local

error (Eq. 57) of order Δ^3 and linear in frequency; and (3) standard Crank-Nicholson (Eq. 60) has a local error (Eq. 61) of order Δ^3 and cubic in frequency. See References 7, 14, 16, 17, and 18 for more in-depth analyses.

Range-step-size predictors are obviously important for practical implementation of any technique, and we refer the reader to References 14 and 19 for discussion of some of the techniques that are utilized.

The advantage of split-step over Crank-Nicholson is that it is more efficient at higher frequencies (linear vs. cubic) permitting a larger range step size. Its disadvantage is that a uniform z-grid is required, and in situations involving rapid variations in depth of, for example, sound speed, a large transform size is required (small z-mesh interval). The finite difference technique, on the other hand, does not require a uniform grid, allowing for the flexibility of a judicious choice of mesh points and consequent reduction in mesh points.

E. HIGH ANGLE PE

1. General

The rational linear approximation of Section G is not appropriate for solution by the split-step approach because of the variable coefficients. The techniques employed in the programs presented at the workshop all used standard integration in r, but employed special representations in z as follows: Greene used cubic splines to represent the z-dependence for his rational linear approximation, whereas Thomson used central differences and Gilbert used finite elements for the discrete z-representation of Claerbout's rational linear approximation. Error analysis in range is, in general, the same as for SPE except that the x operator must be appropriately redefined. While we do present the various discrete techniques for representing the z-dependent part of the rational linear approximation we do not include a corresponding error analysis. Such an analysis is beyond the scope of this report.

2. Cubic Splines

Integration over r of Greene's Rational Linear Approximation, Eq. 35, using the trapezoidal rule on the right hand side and neglecting the r dependence of the index of refraction leads to

$$(\alpha - \tfrac{\Delta\beta}{2})^n \psi^{n+1} + (\gamma - \tfrac{\Delta\omega}{2})^n \psi_{zz}^{n+1} = (\alpha + \tfrac{\Delta\beta}{2})^n \psi^n + (\gamma + \tfrac{\Delta\omega}{2})^n \psi_{zz}^n \quad , \tag{62}$$

where superscripts n and n+1 refer to $r=r_n$ and r_{n+1}, respectively.

In order to treat the z dependence, the following spline interpolation function can be introduced for ψ:

$$\psi = \psi_\ell \tilde{v} + \psi_{\ell+1} v + \frac{1}{6} \delta_\ell^2 \{ g_\ell (\tilde{v}^3 - \tilde{v}) + g_{\ell+1} (v^3 - v) \} \quad , \quad z_\ell \leq z \leq z_{\ell+1} \quad , \tag{63}$$

where

$$\delta_\ell = z_{\ell+1} - z_\ell \quad ,$$

$$v = (z - z_\ell)/\delta_\ell \quad , \tag{64}$$

$$\tilde{v} = 1 - v \quad ,$$

and where ψ_ℓ is the evaluation of ψ at $z=z_\ell$. The g_ℓ are parameters to be determined. In this formulation ψ and ψ_{zz} are continuous, and the conditions on ψ at the boundaries $z=z_1$ and $z=z_n$ require $g_1=g_n=0$. With continuity conditions for ψ and $\rho^{-1}\psi_z$, Eq. 63 yields a set of linear equations in ψ_ℓ and g_ℓ which can be written in matrix notation as

$$M\bar{g} = N\,\bar{\psi} \quad . \tag{65}$$

Here M and N are tridiagonal and $\bar{g}$ and $\bar{\psi}$ are column vectors consisting of the g_ℓ and ψ_ℓ.

Now, use of the interpolation function of Eq. 63 in Eq. 62 leads to an equation of the form

$$A_L^n \bar{\psi}^{n+1} + b_L \bar{g}^{n+1} = A_R^n \bar{\psi}^n + b_R \bar{g}^n \quad , \tag{66}$$

where A_L^n and A_R^n are diagonal matrices and b_L and b_R are constants. Finally, multiplying Eq. 66 by M and using Eq. 65 to eliminate $M\bar{g}$ we arrive at the implicit form

$$C_L^n \bar{\psi}^{n+1} = C_R^n \bar{\psi}^n \quad . \tag{67}$$

This equation can be solved numerically in an efficient manner since C_L^n and C_R^n are tridiagonal. Note that this formulation assumes $\rho = \rho(z)$, and results in ψ_{zz} being continuous when in fact it should be discontinuous for discontinuous ρ or index of refraction. However, this condition can be remedied with a slight modification to the above procedure and still retain the tridiagonality.

3. Heterogeneous Approximation

Thomson solves Claerbout's rational linear approximation in the form appropriate for depth-dependent density. This form can be derived from the Helmholtz equation directly or by first deriving GPE for variable density and then introducing the appropriate expansion similar to that used in Section II-G. Without reproducing the derivation here, we simply state the result that GPE for $\rho = \rho(z)$ is identical to that given by Eq. 8 except that q is redefined as $\tilde{q}$ where

$$\tilde{q} = n^2 - 1 + \frac{\rho}{k_o^2}\frac{\partial}{\partial z}\cdot\frac{1}{\rho}\cdot\frac{\partial}{\partial z} \quad . \tag{68}$$

Likewise, the Claerbout approximation to GPE for this same case is identical to Eq. 32 except that again q is replaced by $\tilde{q}$. Introduction of the envelope function ψ then leads to Claerbout's rational linear approximation for variable density:

$$(1 + \frac{\tilde{q}}{4})\psi_r = \frac{ik_o}{2}\,\tilde{q}\,\psi \quad . \tag{69}$$

Integration of Eq. 69 over an interval $r_{n+1}-r_n$, assuming constant coefficients over the interval, leads to

$$(1 + \frac{\tilde{q}}{4})^n(\frac{\psi^{n+1} - \psi^n}{\Delta}) = ik_o\tilde{q}^n(\frac{\psi^{n+1} + \psi^n}{2}) \quad . \tag{70}$$

Standard central differencing in z is next employed to evaluate all but the ρ dependent part of $\tilde{q}$. To evaluate this Thomson uses the "heterogeneous approximation"20

$$\rho\,\frac{\partial}{\partial z}\cdot\frac{1}{\rho}\frac{\partial}{\partial z}\psi = (\tfrac{1}{2})(1 + \rho_\ell/\rho_{\ell+1})\,\frac{(\psi_{\ell+1} - \psi_\ell)}{\delta^2}$$

$$+ (\tfrac{1}{2})(1 + \rho_\ell/\rho_{\ell-1})\,\frac{(\psi_\ell - \psi_{\ell-1})}{\delta^2} \quad . \tag{71}$$

As in the spline formulation, the result is a tridiagonal system of equations that is easily solved numerically. This formulation, however, does model density discontinuities although the discontinuities in n are not explicitly treated.

4. Finite Elements

Gilbert solves Claerbout's rational linear approximation for variable density $\rho(z)$ using the method of finite elements. The discretized equations in r and z were actually derived by using a variational technique to minimize the appropriate Lagrangian density. However, for simplicity, we will present a different but equivalent derivation here.

We start with Claerbout's rational linear approximation for variable density $\rho(z)$ (Eq. 70). The z-dependence is now treated by the following interpolation function:

$$\psi(z) = \Sigma\, C_j\phi_j(z) \quad , \tag{72}$$

where

$$[C_1,\ C_2,\ \cdots,\ C_{2L-1},\ C_{2L}] = (\psi_1,\ v_1,\ \psi_2,\ v_2,\ \cdots\cdots,\ \psi_L,\ v_L) \quad . \tag{73}$$

In this expression the ϕ_j are cubic polynomials within and zero outside a z-grid interval, and the ψ_ℓ and v_ℓ are ψ and $\rho^{-1}\psi_z$ at the z-grid points.

Insertion of the representation for ψ given by Eq. 72 into Eq. 70, multiplication by $\rho^{-1}\phi_k$, and integration over z leads to a linear system of equations that can be expressed in matrix form as

$$[M^n - ik_o\Delta N^n]\bar{C}^{n+1} = [M^n + ik_o\Delta N^n]\bar{C}^n \quad , \tag{74}$$

where M and N are block tridiagonal with 2x2 blocks, and $\bar{C}$ is the column vector of C_j's. This system of equations can be solved numerically in an efficient manner, but at a slower rate (for the same z-mesh) than the tridiagonal systems of Greene and Thomson. However, discontinuities in both ρ and n are treated explicitly and can be input as arbitrary functions of z. This method need not use cubic polynomials for ϕ_j, and can be easily generalized. In fact, for linear ϕ_j the result is essentially equivalent to using second order differences for ψ and leads to a tridiagonal system.

F. INITIAL CONDITIONS AND WAVENUMBER FILTERS

As stated before, the principal advantage of PE over elliptic equation approaches is that PE allows numerical solutions which march out in range from an initial field. However, because of the sensitivity of the solutions to these initial data and the inherent far-field nature of the PE approximations, careful specification of the depth dependence of the field at starting range r_o is required.

Both initially and down range it is advantageous (and sometimes necessary) to limit the size of the vertical wavenumbers or angles of propagating energy. The choice of limit depends on: the particular version of PE (regions of validity of small angle SPE, high angle PE, etc.), the boundary conditions (especially attenuation of high angle energy by the bottom), computational constraints (depth-mesh spacing and range step decrease as angular aperture increases), and application (e.g., study of narrow beam vertical arrays).

For a range-independent environment the exact initial field can be obtained by a normal mode solution. In a range-dependent environment, especially for sources near bottom slopes, it is not practical to obtain the exact initial field, and only a number of approximate approaches are available. One is to obtain the field from a ray theory calculation, but this technique has its disadvantages and was not used by any of the PE's exercised at the workshop. The techniques that were used fell into two categories: (1) normal modes and (2) point-source simulations, each of which can be "filtered" to limit vertical wavenumbers. These approaches, as exercised by models for the workshop test cases, are discussed in order below.

The normal mode startup is straightforward. Under the assumption that the ocean is stratified near the source, the normal mode solution, $v(r_o,z)$, to the elliptic wave equation for the initial environment is calculated, and related to the initial PE field $\psi(r_o,z)$ by:

$$\psi(r_o,z) = r_o^{\frac{1}{2}}\, v(r_o,z)e^{-ik_o r_o} \quad . \tag{75}$$

The value of r_o is arbitrary but is usually on the order of several wavelengths. Such a starter can of course be used at any range, and has the advantage of being exact, in a range-independent context. One can also predetermine the maximum angle (vertical wavenumber) of propagating energy at the source by truncating the normal mode sum at the appropriate eigenvalue. However, it may not always be necessary to use the initial environment to obtain the normal mode solution as is demonstrated by Gilbert in Sec. VII for Test Case 3, where he greatly simplified the initial environment and truncated the normal mode sum.

Instead of depending on a normal-mode calculation to initialize PE, certain implementations use an analytical initial field at r_o designed to closely match

the spherical-wave solution of the elliptic equation for a point source at depth z_s in a homogeneous environment

$$p(r,z) = \frac{e^{ik_o R}}{R}, \quad R = (r^2 + (z - z_s)^2)^{\frac{1}{2}} \quad . \tag{76}$$

This approach is based on assumptions that neither boundary nor refraction effects are important to range r_o and that the far-field approximation obtains, $k_o r_o >> 1$.

Following this logic and at the same time seeking to reduce the energy of large-angle propagation, Tappert[3] has proposed an initial PE field with envelope of form

$$\psi(r_o,z) = S \exp(-(z - z_s)^2/W^2) \quad , \tag{77}$$

where S and W are to be determined. When normalized, this function of z has the form of a Gaussian density function with mean z_s and variance $W^2/2$, and is thus termed a "Gaussian source." If not truncated, its wavenumber (k_z) power spectrum (Fourier-transform modulus squared) is also Gaussian, with mean 0 and variance $W^2/4$. When limited to $|z| \leq z_{max}$, the transform has sidelobes caused by the convolution of the Gaussian with a shape of form (siny)/y where y is $(z_{max} \cdot k_z)$.

Following Brock[14], the solution of the PE equation in a homogeneous medium with the starting field given by Eq. 77 yields

$$\psi(r,z) = s(1 + i\frac{2r}{k_o W^2})^{-\frac{1}{2}} \exp(-\frac{(z - z_s)^2}{W^2(1 + \frac{i2r}{k_o W^2})}) \quad . \tag{78}$$

By matching the elliptic (Eq. 76) and parabolic (Eq. 78) solutions for small angle ($r >> |z-z_s|$), one obtains

$$S = \frac{1}{W}(\frac{2}{k_o})^{\frac{1}{2}}$$

and

$$W = 2^{\frac{1}{2}}/k_o \quad .$$

According to Tappert[3] some of the advantages of the Gaussian form are: (1) It is a "natural" for a small angle approximation ($|z-z_s| << r$); (2) In the limit of $|z| >> W$, it is smooth and has minimal sidelobes in both z and k space; (3) The phase is correct for a point source in a homogeneous medium, and the depth dependence is correct to "second order in angle" (i.e. to second order in $|z-z_s|/r$).

The principal disadvantages of the Gaussian field were pointed out by D. Wood and J. Hanna in talks at the workshop: (1) It is symmetric about the source-depth and hence not appropriate near boundaries; (2) In wavenumber (angle) space it "rolls off" slowly--thereby allowing energy corresponding to high angles to propagate and

at the same time reducing the energy for small angles (i.e., it does not match the field of a wavenumber-limited point source).

There are, of course, alternatives to the Gaussian initial field which also simulate a wavenumber-limited point source. Thomson's model (this workshop), employs a weighted (sinx)/x form with $x = \beta(z-z_s)$, whose transform (in the limit of $z >> \beta$) is a rectangular "boxcar" function with value zero for $|k| > \beta$ and constant for $|k| < \beta$. Garon, Hanna, and Rost[21] and Hanna (this workshop) described the source function for the SAI PE in the context of a digital (wavenumber) filter. The shape of the inital angular (wavenumber) spectrum is specified in a digitized form. The transform gives the initial depth-dependent field. This allows for special source shapes, and can easily accommodate changes in the z-mesh size. Both the Thomson and Hanna approaches give a sharper cut off of angles than the Gaussian field--thereby allowing large z-mesh size and range step.

For reasons mentioned above, it is usually desirable to limit propagating angles (wave numbers) not only at the source, but also down range. Some versions of PE (e.g., SAI) accomplish this by applying a wavenumber filter to the Fourier-transformed solution at each range step. This is especially efficient for the split-step algorithm since the transform is available at each step. Without such a filter, it is possible for PE solutions to accumulate contributions from what are equivalent to modes with angles outside PE's realm of applicability.

IV. TEST CASES - GENERAL

A. INTRODUCTION

To provide a basis for comparing and analyzing PE programs, four test problems were devised, each designed to test some aspect of the program's capabilities. The tests are obviously not exhaustive but do focus on some of the capabilities required to meet the needs of the SEAS program. The choice of test cases was subject to the following constraints: (1) the number of cases should be small; (2) input parameters that define the problems should be relatively simple (thereby ruling out many range dependent environment cases); and (3) computer costs for execution should be kept as low as possible (thereby ruling out long range and/or high frequency). The four problems selected were:

Test Case 1 - Range Dependent Surface Duct
Test Case 2 - Bilinear Profile
Test Case 3 - Range-Independent Shallow Water Environment
Test Case 4 - Basin/Slope/Shelf Configuration for Geoacoustical Bottom

Details of these test cases will follow in later sections.

Participants were encouraged to exercise their PE programs for as many test cases as possible even though the programs may not have been designed to treat all cases, e.g., applying a PE program to Test Case 3 that is not designed to treat attenuation, density, and sound speed discontinuities. The objective was not to encourage a poor showing but rather to determine the consequences of applying a PE to a test case it was not designed to handle and at the same time determine the consequences of applying some other PE that was designed to handle that same test case--thereby permitting an assessment of the value of such modifications or improvements. That objective was met with a fair degree of success.

Table 2 summarizes the characteristics of the PE programs that were exercised against the test cases. In this table, and in ones that will follow, we use the shorthand notation given in Table 3. Abstracts of these PE programs are given in Appendix B. Appendix B also contains abstracts for SNAP and FFP, the SACLANT ASW Research Centre programs that were used as "reference" calculations. The SNAP result is used as the reference calculation in the test case comparisons and is referred to in the figures as "MODE." Table 4 shows which test cases were attempted by each program. The X's that are underlined indicate that the test case was run but the results are not included in this report. The SAI-1 case 2A was not to the correct scale, there was a yet unidentified problem with the NOSC results for case 4, and the SAI-2 program contained a compiler error that affected all but cases 2B and 2C. The NUSC-2 program is not a typical PE (it uses a normal mode program to solve SPE), and the result for Case 2 is included primarily for comparison with the usual PE results.

B. COMMENTS ON WORKSHOP

In fairness to the workshop participants some general comments should be made. First, there were scaling problems at the workshop that precluded definitive comparison of results. This was due in part to requiring a less-than-ideal plot scale for viewgraph presentation, and in part by not recognizing the consequences of the distortion introduced by reproducing viewgraphs from originals on a variety of machines. Second, some participants had the advantage of resources (e.g., normal mode programs) with which they could "tune up" their PE results. Ideally two types of results from each participant would have been extremely useful: (1) a routine run; and (2) a thorough analysis of the test case with a "tuned up" run. Since resources varied, initial results spanned this range.

Because of the above considerations, it was decided at the workshop that everyone would be given the reference calculations (to be shown in later sections), and that participants could then submit new results, due a month after the workshop (May 1981), based on this information and knowledge gained at the workshop. Participants were also offered the opportunity to comment on their results, in writing, to aid in the analysis. However, the response from the authors of the various PE programs was minimal and the interpretation of the results is almost entirely due to the authors of this report. It was also decided to include the results of Gilbert (NORDA), although he had not presented them at the workshop because the program was described at the workshop, the results were delivered before May 1981, and the results provided additional evidence of the accuracy of the "high-angle" PE.

One additional comment is appropriate at this point. Most programs exercised at the workshop had been in existence for some time and were likely debugged. Other programs such as DREP (Thomson), NORDA (Gilbert), SAI-2 (Greene), and URI (Papadakis) were relatively new, and likely were not thoroughly debugged.

C. FORMAT OF TEST CASE RESULTS

Standardization and conventions are obviously necessary for comparison of test case results. To this end, a source is understood to be the fixed field point at zero range, and a receiver is the field point that varies with range. Unless otherwise noted, the sound speed is assumed to extend as constant beyond the deepest depth specified, i.e., an iso-velocity half space underlies each case and precludes the return of energy (a radiation boundary condition at $z \rightarrow \infty$). The sound speed is assumed to be a linear function of depth between given points. Transmission loss is in dB re 1 m and range is in km. Average TL results are intensity averaged over a

Table 2. Summary of PE program features

Program	Equation	Solution Technique	Initial Field	Phase Correction	Interface Conditions	Radiation Conditions	Computer
BTL	SPE	SS	G	CMOD	AB	FB	UNIVAC/AP 190L
DREP	HAC	FD	D	NONE	FULL	FB	XEROX SIGMA 7
NORDA	HAC	FE	NM	NONE	FULL	FB	CDC 6600
NOSC	SPE	SS	NM	NONE	AB	FB	UNIVAC 1110
NRL-1	SPE	SS	G,NM,U	CPA	AB	FB	TI ASC
NRL-2	SPE	SS	S	CMOD	AB	S	TI ASC
NRL-3	CIT	FD	G	NONE	FULL	FB	TI ASC
NUSC-1	SPE	FD	G	NONE	FULL	FB	VAX 11
NUSC-2	SPE	NM	-	-	-	-	VAX 11
SACLANT	SPE	SS	G,NM	CMOD	AB, smeared ρ	FB	UNIVAC 1106
SAI-1	SPE	SS	S	CMOD	AB	S	HP21 MX CDC 7600
SAI-2	HAG	CS	G	NONE	FULL	FB	TI ASC
URI	SPE	FD	G	NONE	IMP	IMP	VAX 11

Table 3. Notation used in test cases

SPE	Standard PE
CIT	Tappert's Co-independent PE
HAC	Claerbout's high-angle PE
HAG	Greene's high-angle PE
G	Gaussian source
S	SAI source
D	DREP source
NM(r)	Normal mode source at range r
U	User input
SS	Split-Step algorithm
FD	Finite difference
FE	Finite element
CS	Cubic splines
FULL	Full bottom treatment
IMP	Impedance boundary conditions
AB	Attenuating bottom, smeared sound speed
FB	False bottom with attenuating layer
Δ	Range increment
δ	Depth increment
-	Not relevant
?	Not known to authors

Table 4. Programs exercised against test cases

	TEST CASES											
	1			2			3		4			
	A	B	C	A	B	C	A	B	A	B	C	D
BTL	X	X	X	X	X	X	X	X		X		X
DREP	X	X	X	X	X	X	X	X	X	X	X	X
NORDA							X	X				
NOSC	X	X	X									X
NRL-1	X	X	X	X	X	X	X	X	X	X	X	X
NRL-2	X	X	X	X	X	X	X	X				
NRL-3							X	X	X	X	X	X
NUSC-1	X	X	X	X	X	X	X	X	X	X	X	X
NUSC-2				X	X	X	X	X				
SACLANT	X	X	X	X	X	X	X	X	X	X	X	X
SAI-1	X	X	X	X	X	X	X	X	X	X	X	X
SAI-2				X	X	X	X	X	X	X	X	X
URI	X	X	X	X	X	X	X	X	X	X	X	X
REF				X	X	X	X	X	X	X		X

specified interval. It is worth noting that participants used different averaging schemes and it should be recognized that this can contribute to differences between results.

D. INTERPRETATION OF RESULTS

In the following sections (V-VIII), for each test case: (1) the test problem is defined, (2) the PE program results are presented, and (3) the results are interpreted. The first two are straightforward. An explanation of why each PE performed as it did is not so straightforward, and is best left to the author of that PE since he alone knows how he parameterized the particular test case to fit within the limitations of his PE. It would be a monumental undertaking for the authors to "dissect" every PE for every test case, especially Case 4. The analysis for each test case is therefore superficial in the sense that we speculate on the origin of differences among various PE results based on treatments of: (1) initial field, (2) interfaces, (3) radiation conditions, and (4) type of PE equation. Our interpretive remarks tend to be general rather than specific, and are by no means conclusive. Finally, evaluation of how well a PE did is somewhat subjective and depends to a great extent on what features are the most important for the case in question. The results speak for themselves, and the reader can draw his own conclusions.

V. TEST CASE 1 (Range-Dependent Surface Duct)

A. DEFINITION OF PROBLEM

This test case has a range-dependent surface duct and consists of profile 1a from 0 to 20 km in the first region, a transition from 1a to 1b over the range interval 20 to 30 km in the second region, and profile 1b from 30 to 50 km in the third region. Pertinent parameters are shown in Table 5.

The profile in the transition interval is range dependent between depths of 0 and 300 m and is given by:

$$h(r) = 300 - 10(r-20),$$
$$C_s(r) = 1480 + 1.238(r-20),$$

and

$$C_d(r) = 1500 + 0.571(r-20),$$

where

$h(r)$ is the depth (m) of the duct,
$C_s(r)$ is the sound speed (m/s) at zero depth,
r is the horizontal range in km,

and

$C_d(r)$ is the sound speed (m/s) at the bottom of the duct.

There are three parts to this test case as defined by the receiver depths; (A) 25 m, (B) 250 m, and (C) 400 m.

The 25 m source is in the duct, as is the 25 m receiver. The 250 m receiver is initially in the duct in the first region, goes from in-duct to below-duct in the

Table 5. Parameters defining Test Case 1

TEST CASE 1

Frequency = 25 Hz

Source Depth = 25 m

Receiver Depths = 25, 250 and 400 m

Max Range = 50 km

Profile 1a:

Depth (m)	Sound Speed (m/s)	Density (g/cm3)	Attenuation (dB/km)
0	1480	1.	0.
300	1500	1.	0.
1000	1460	1.	0.

Profile 1b:

Depth (m)	Sound Speed (m/s)	Density (g/cm3)	Attenuation (dB/km)
0	1492.38	1.	0.
200	1505.71	1.	0.
300	1500.00	1.	0.
1000	1460	1.	0.

Plots--TL vertical scale 60-130 dB at 10dB/inch
Separate plots for each receiver depth
0 to 50 km at 5 km/in

transition region, and is below-duct in the last region. The 400 m receiver is always below the duct.

Modal analysis of this case shows only one trapped (but slightly leaky) mode in the first region, that transitions into an untrapped mode in the last region. This should be an easy test for any PE program since phase errors should not be a problem (there is only one mode and C_o can be selected with confidence), since the range dependence of the environment is weak, and since attenuation, sound speed and density discontinuities or rapid variations are not present. That is to say that all PE programs should agree and give the "correct" answer. See Table 6 for a summary of the PE program parameters used for Test Case 1.

B. RESULTS AND SUMMARY FOR TEST CASE 1

No reference calculation was available for this problem over the full range (0 to 50 km); however, the test results of NRL-1, NUSC-1, BTL, and SACLANT are virtually identical and agree with range-independent environment normal mode results up to 20 km. Figure 1 shows the NUSC-1 results for the three receiver depths and is typical of NRL-1, BTL, and SACLANT.

The results from other programs exhibited slightly different behaviors, and several types of problems were uncovered by this test case. These problems are examined using part C (400 m receiver) as the example. The first is the problem of "false" bottom returns and is shown in Figure 2 comparing NRL-2 with NUSC-1 for the 400 m receiver. The spurious oscillations in the NRL-2 result are due to medium- or high-angle energy returning into the problem from the bottom, i.e., caused by insufficient attenuation in the bottom or by transform artifacts (sidelobes or aliasing) which redistribute the energy into higher angles. This is also typical of the SAI-1 result (not shown). Both use the SAI filter (Hanna) to determine the initial field and eliminate higher angle energy as the solution progresses in range. The difficulty is caused by the algorithm that determines the mesh size (δ) and problem extent (z_{max}) from the requested beamwidth. The algorithm yields an effective beamwidth greater than or equal to that requested. For this particular problem the half-beamwidth is greater than 90° regardless of the beamwidth requested, and there is little or no attenuation of bottom returns. Brock was able to correct the NRL-2 result for this problem by using a new z_{max} inversely proportional to the beamwidth. The result (not shown) is virtually the same as NUSC-1.

False bottom returns would have also been present in the NUSC-1, NRL-1, BTL and SACLANT results had a $z_{max} = 4/3$ W been used, i.e., a false bottom layer of 333 m. The problem was avoided however by using a larger layer depth, as indicated in Table 6. The degree to which the false bottom duplicates the radiation condition is obviously dependent on the attenuation in the layer and the layer thickness.

Oscillations are also present in the DREP result compared in Figure 3 for the 400 m receiver depth. Their origin is not easy to determine, since the false bottom used in the DREP calculation extended to 6000 m. The spurious oscillations in the URI results, shown in Figure 4 for a receiver depth of 400 m, cannot be attributed to a false bottom since impedance conditions were employed. Papadakis attributes this to numerical noise that can occur when the signal gets low; however, in this case, we see the level is on the order of 90 dB in the 10 to 30 km interval.

Finally, the NOSC result is shown in Figure 5 for a receiver depth of 400 m. In this case a normal mode solution was used to generate the field to a range of

Table 6. PE program parameters for Test Case 1.

Program	C_o(m/s)	Source	Half Beam Width(°)	δ(m)	Δ(m)	Profile Samples (m)	Phase Correction	False Bottom Layer (m)
BTL	1500	G	30	5	25	100	NONE	1500
DREP	1500	D	20	15	100	2500	NONE	5000
NOSC	1500	NM(20)	-	5	10-100	10-100	NONE	280
NRL-1	1465	G	30	6	125	500	NONE	5400
NRL-2	1482	S	90+	21	171	1000	CMOD	330
NUSC-1	1483	G	30	1	10	10	NONE	2000
SACLANT	1460	G	37	4	100	1000	CMOD	3000
SAI-1	1460	S	90+	10	50-200	1000	CMOD	330
URI	1483	G	30	5	10	10	NONE	IMP

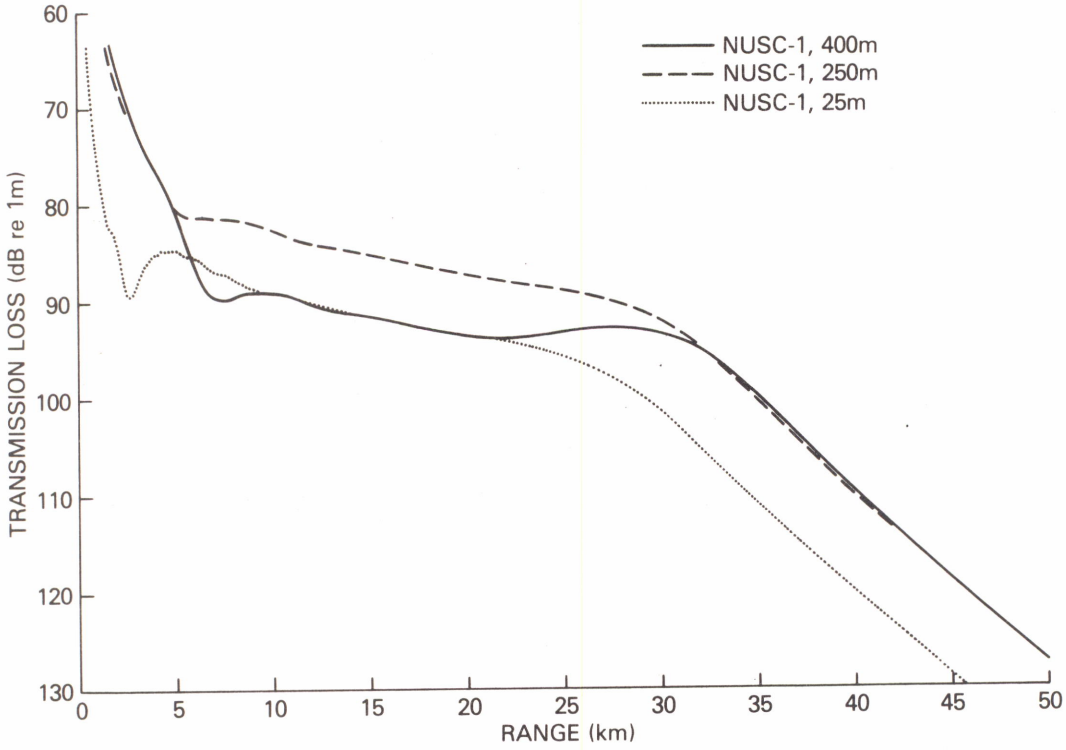

Figure 1. NUSC-1 PE results for Test Case 1

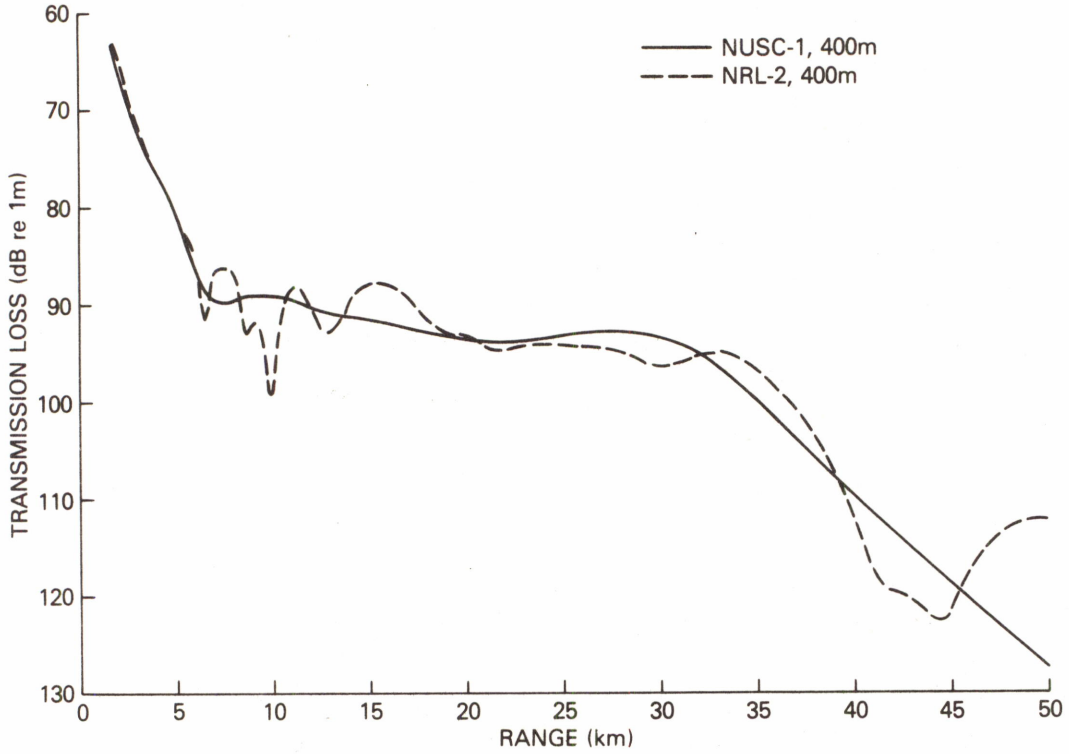

Figure 2. NRL-2 PE results for Test Case 1C compared with NUSC-1 PE

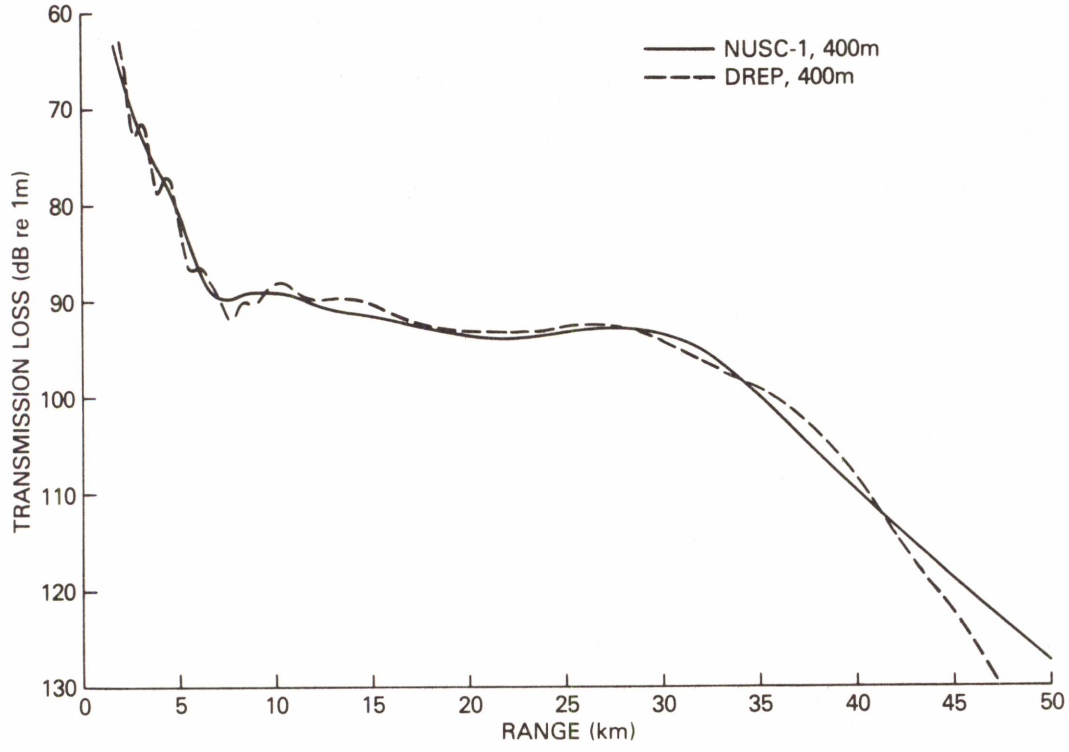

Figure 3. DREP PE result for Test Case 1C compared with NUSC-1 PE

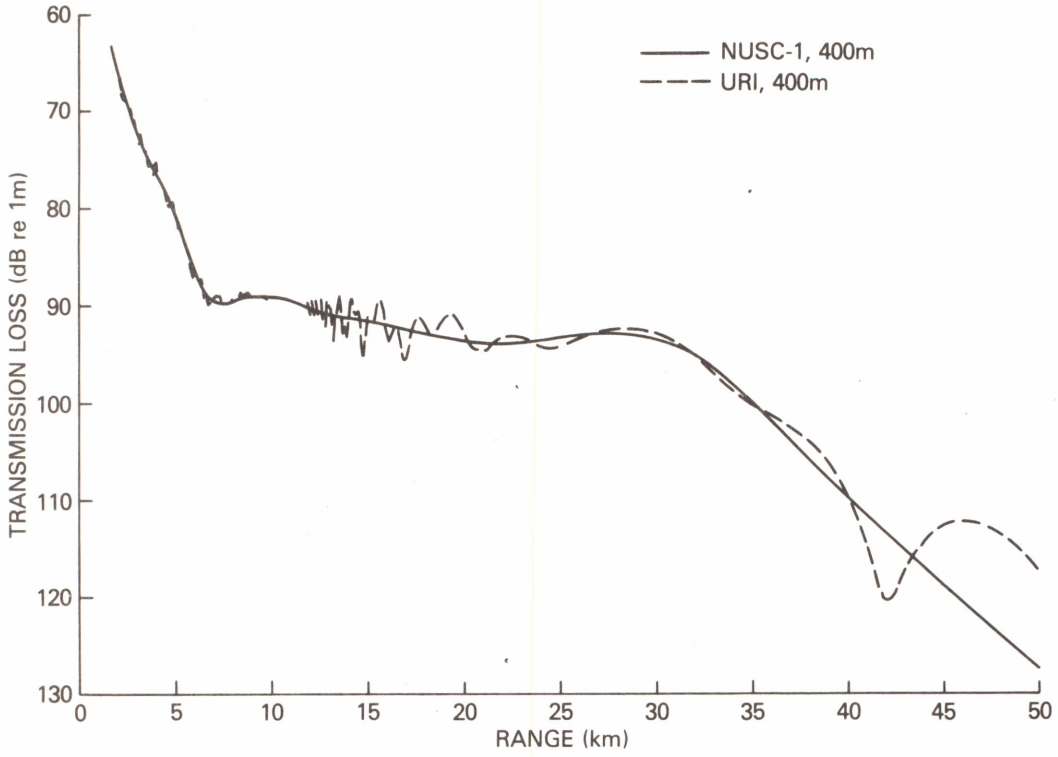

Figure 4. URI PE results for Test Case 1C compared with NUSC-1 PE

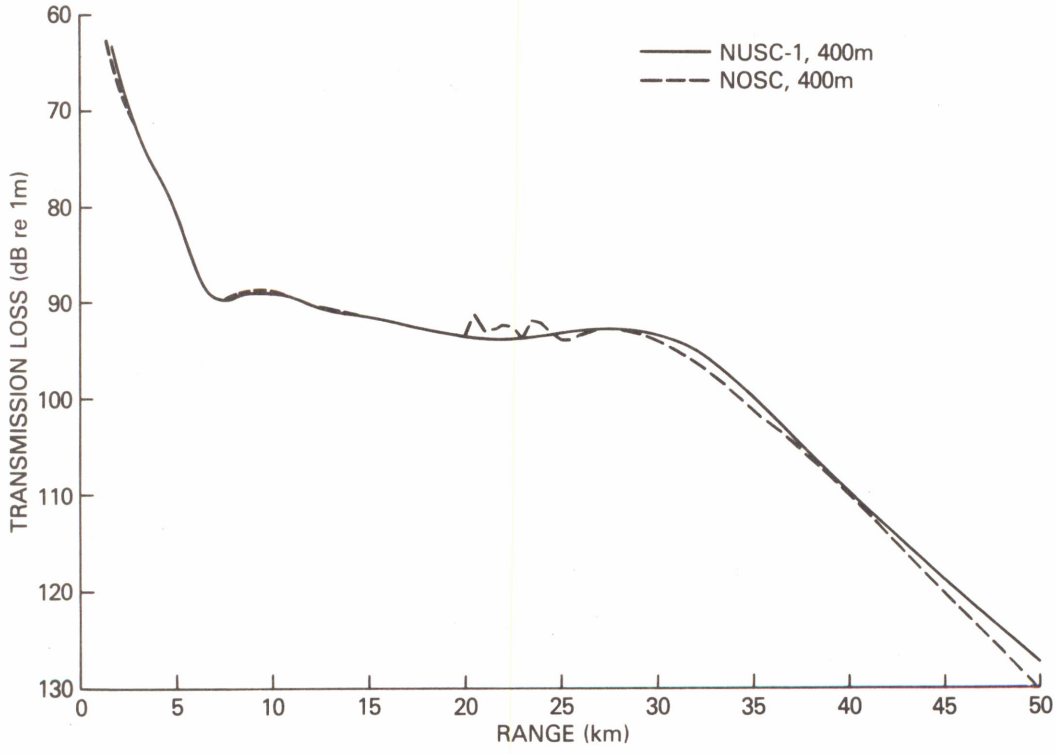

Figure 5. NOSC PE results for Test Case 1C compared with NUSC-1 PE

20 km where the PE calculation is initiated. We have no explanation of the oscillations between 20 and 25 km, but they are likely due to matching the PE calculation to the normal mode field.

This test case has demonstrated that PE results for a narrow beam problem with no drastic range dependence of the environment and no bottom complications (other than that the radiation condition be satisfied) are relatively insensitive to computer type, starter, z and r mesh, phase corrections, choice of C_o, and whether solved by SS or FD.

Questions raised by this test case, but not answered, are: (1) what is the most effective way of approximating the radiation condition, and (2) how often should a range dependent environment be sampled?

VI. TEST CASE 2 (Bilinear Profile)

A. DEFINITION OF PROBLEM

In this test case the environment is range-independent with a bilinear sound speed in the water column and a half-space bottom. It consists of three parts and the parameters are given in Table 7.

The rationale for this case is to test the beamwidth capabilities of a PE program without the complications of bottom interaction other than ensuring that no energy returns to the water column. Case 2A requires a 15° half-beamwidth capability, 2B a 30° half-beamwidth capability, and 2C a 40° half-beamwidth capability. There is a continuous spectrum in this problem because of the branch point at z=1500 m; however, this contribution is negligible beyond 10 km for all three cases, and SNAP (which does not treat the continuous spectrum) and FFP (which does treat the continuous spectrum) should agree, as they did. The reference calculation for this case is the SNAP result which we refer to as MODE.

We would anticipate that all PE programs should be able to do well on 2A and, without a high-angle capability, they should have some difficulty with 2B and have serious problems with 2C. Initial field conditions (amplitudes of corresponding PE modes) and phase errors will govern the accuracy of the results. See Table 8 for a summary of PE program parameters used for Test Case 2.

B. RESULTS FOR CASE 2A

For this test case, which required a 15° half-beamwidth capability, all PE's did well with little disagreement in detail. The most accurate result was NRL-1 with CPA. We do not show it because it is virtually the same as the MODE result. We show instead in Figure 6 the MODE reference calculation along with the envelope formed by the DREP, NRL-1 (no CPA), NUSC-1, NUSC-2, SACLANT, and URI results. This is an extremely tight envelope and there is little to choose between the various results.

Two model results are singled out, not because they are "bad", but because they are not quite as accurate as the other and are to some degree different. The first is shown in Figure 7 which compares NRL-2 with MODE. The "kinks" in the NRL-2 curve are due to straight-line connections between range point solutions. We believe the NRL-2 result is an example of the cumulative errors caused by a crude range step size. The BTL result, shown in Figure 8, is not so easily explained. The level is

Table 7. Parameters defining Test Case 2

TEST CASE 2

Frequency = 25 Hz

Source Depth = 500 m

Receiver Depth = 500 m

Density = 1 gm/cm^3

Attenuation = 0 dB/km

Depth (m)	Sound Speed (m/s)		
	Part A	Part B	Part C
0	1500	1500	1500
1000	1520	1520	1520
1500	1563	1744	1971

Plots--separate plots for each part from 10 to 20 km.

--TL vertical scale 60 to 130 dB at 10 dB/in.

Table 8. PE program parameters for Test Case 2

Program	C_o(m/s)	Source	Half Beam Width(°)	δ(m)	Δ(m)	Phase Correction	False Bottom Layer (m)
BTL	1500	G	30	4	25	CMOD	700
DREP	1510	D	(a) 20 (b) 30 (c) 40	10	25	NONE	2340
NRL-1	(a)1521 (b)1551 (c)1586	NM	-	2	(a)100 (b) 20 (c) 20	(a)CPA (b)NONE (c)NONE	500
NRL-2	1510	S	(a) 20 (b) 30 (c) 40	(a) 66 (b) 45 (b) 35	(a)590 (b)181 (c) 98	CMOD	(a)2738 (b)1399 (c) 753
NUSC-1	(a)1521 (b)1551 (c)1589	G	30	10	25	CMOD	500
SACLANT	1500	G	37	11	25	CMOD	1300
SAI-1	1500	S	90+	16	35	CMOD	500
SAI-2	-	G	30	5	4	NONE	500
URI	(a)1521 (b)1551 (c)1589	G	30	10	25	NONE	IMP

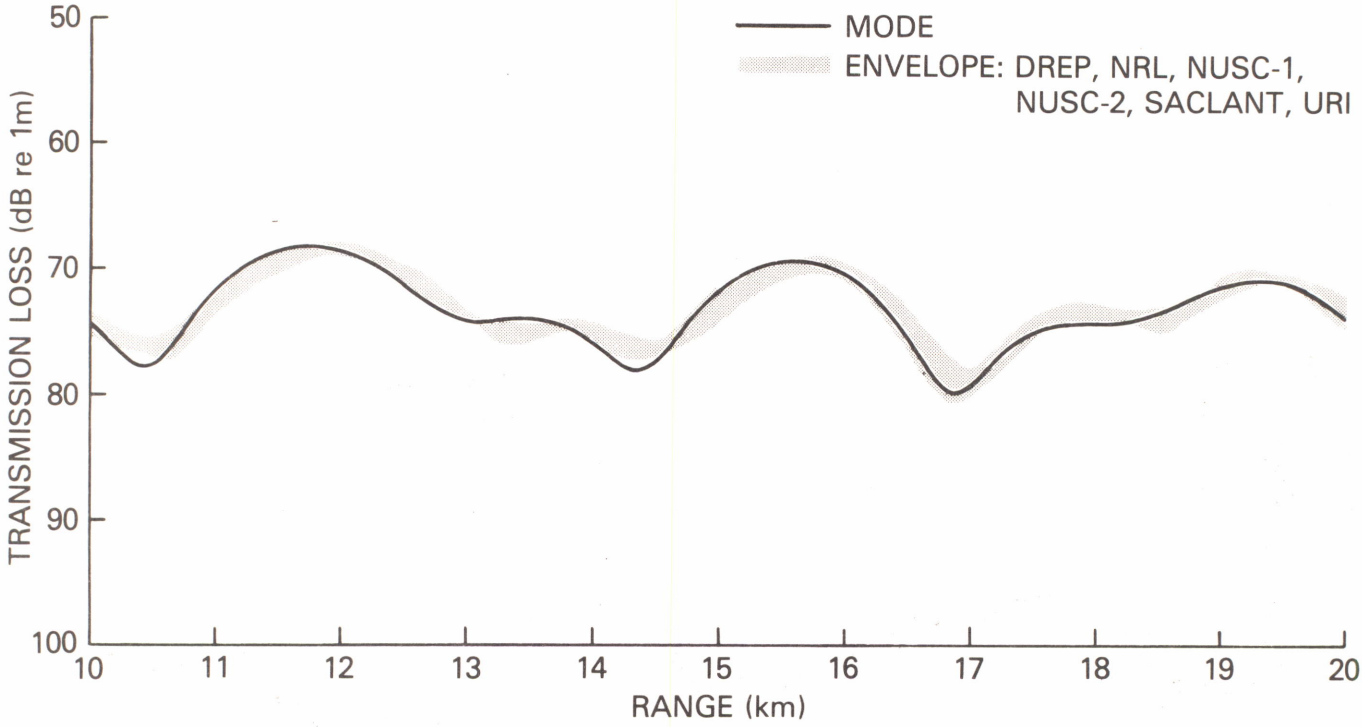

Figure 6. Envelope of various PE results compared with reference calcuation (MODE) for Test Case 2A

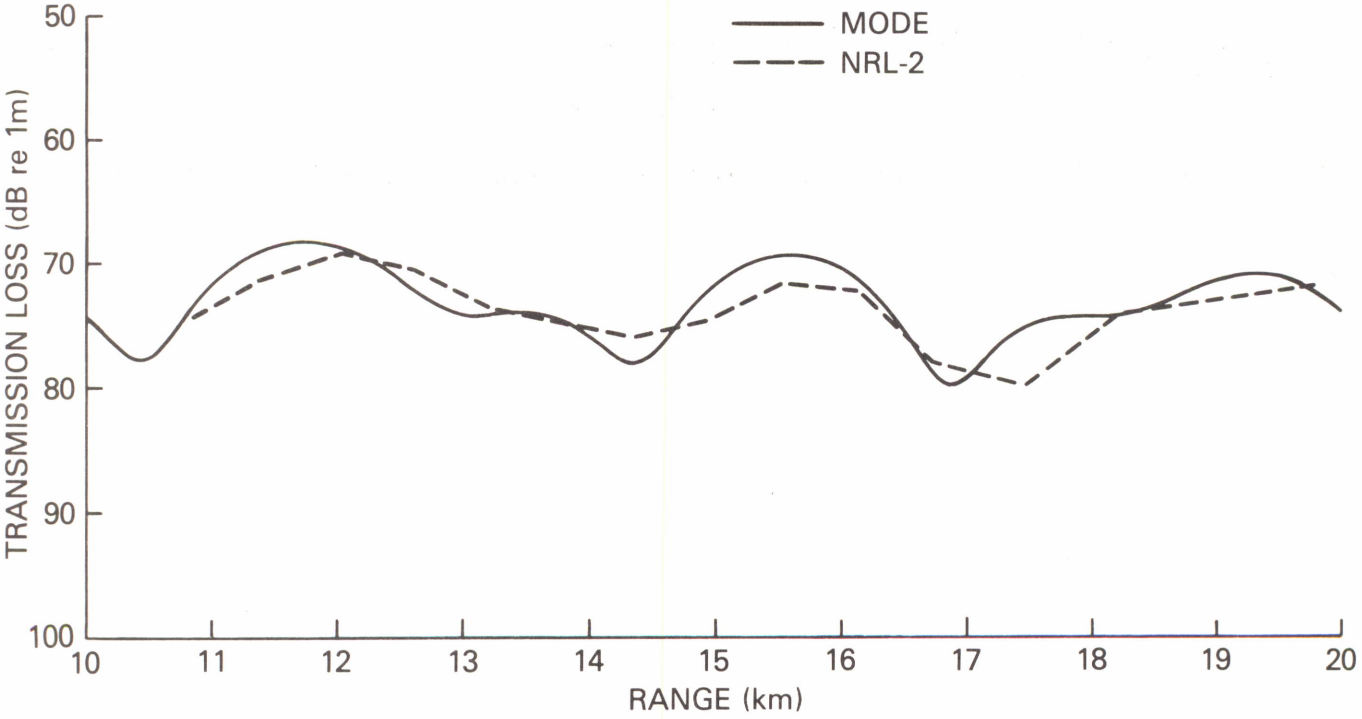

Figure 7. NRL-2 PE result compared with reference result (MODE) for Test Case 2A

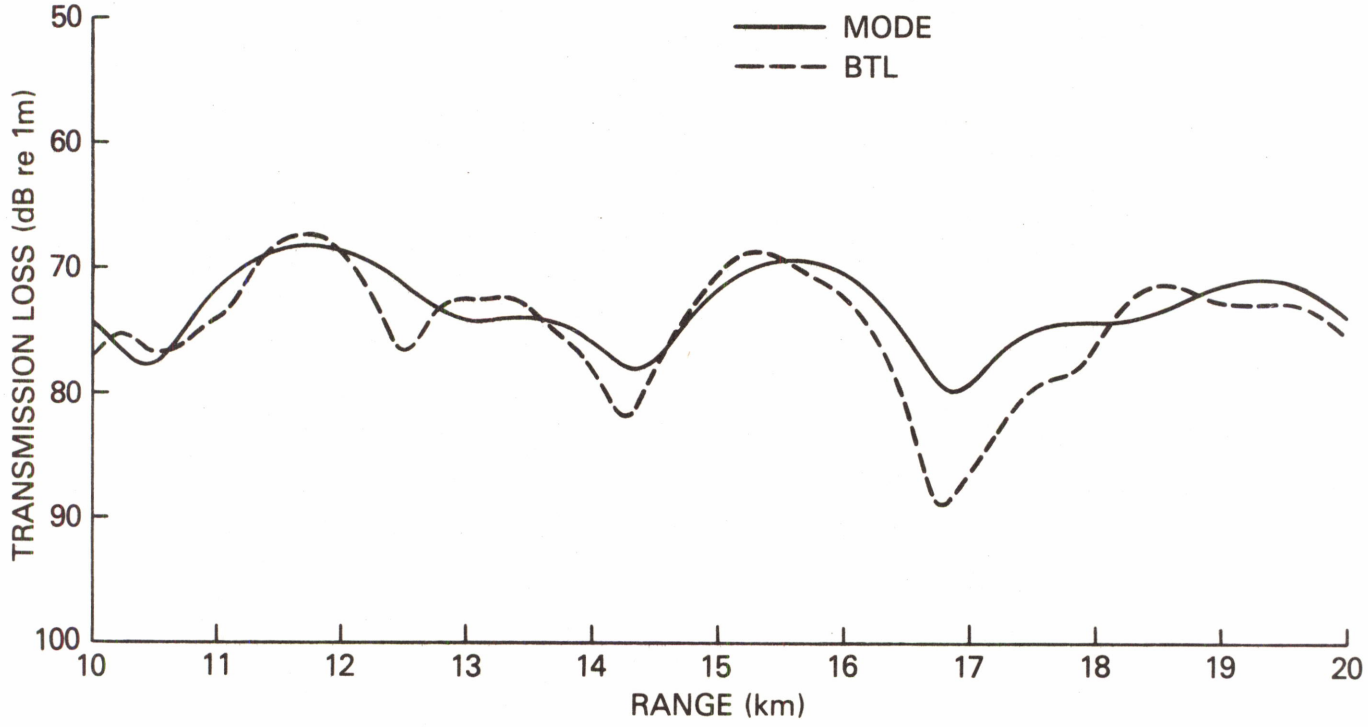

Figure 8. BTL PE result compared with reference result (MODE) for Test Case 2A

good but we are unable to account for the disagreement in detail. We would have expected this result to fall within the envelope shown in Figure 6.

One conclusion evident from this test case is that CPA is effective when the SPE phase error is small, seemingly more effective than CMOD (used in the SACLANT result in Fig. 6). However, SPE without corrections is very accurate, and any corrections should be small. Since this is the only case where CPA is used, we cannot evaluate its effectiveness in later cases where the SPE phase error is not small.

C. RESULTS FOR CASE 2B

All PE's did well on the average for this case but differed in detail. A half-beamwidth capability of 30° is required. We show first the SAI-2 result in Figure 9, compared with the MODE solution. This is the most accurate PE solution for this case and gives surprising agreement in detail (the pattern in Fig. 9 is caused by the interference of 22 modes). This is an excellent demonstration of the capability of the rational linear (high angle) approximation. We should note that there was a compiler error in Greene's program (discovered after the workshop) that produced spurious results for most of the test cases. While the consequences of that error are included in Figure 9 (as well as in Fig. 13 for Test Case 2C), we assume that elimination of the error can only improve the accuracy. This was demonstrated after the workshop by results Greene obtained using a some what different program, but still a rational linear approximation.

In this same connection Figure 10 compares the DREP result against the MODE result. Although the level is reasonable, the detailed agreement is poor. This is difficult to account for since the DREP program also solves PE in a rational linear approximation.

Results from the remaining programs are best sorted out in terms of whether or not the CMOD phase correction was applied. Figure 11 shows the envelope formed by the NRL-1, NUSC-1, NUSC-2, and URI results, none of which used the CMOD correction while Figure 12 shows the envelope formed by the BTL, NRL-2, SACLANT, and SAI-1 results, all of which used the CMOD correction. These figures show that the CMOD correction produces significant differences, greater than the differences within the two envelopes caused by beamwidth, mesh size, etc. It would appear that CMOD improves the results.

D. RESULTS FOR CASE 2C

Results for 2C, which required a 40° half-beamwidth capability, are similar to those for Test Case 2B. Transmission loss levels over the range interval are fair, but the details are not very good except for SAI-2 shown in Figure 13. This is strong evidence that a "high-angle" PE can give accurate results for problems having beamwidths up to 40°. The DREP result, Figure 14, has the correct level but again serious phase problems.

As in Test Case 2B, the remaining results are best presented in terms of whether or not a CMOD correction was applied. Figure 15 shows the envelope formed by the NRL-1, NUSC-1, NUSC-2, and URI results, none of which used the CMOD correction, while Figure 16 shows the envelope formed by the BTL, NRL-2, SACLANT and SAI-1 results, all of which used the CMOD correction. As for Test Case 2B, the differences between the envelopes are greater than the differences within the envelopes. It is not clear whether CMOD improves the overall results in this case.

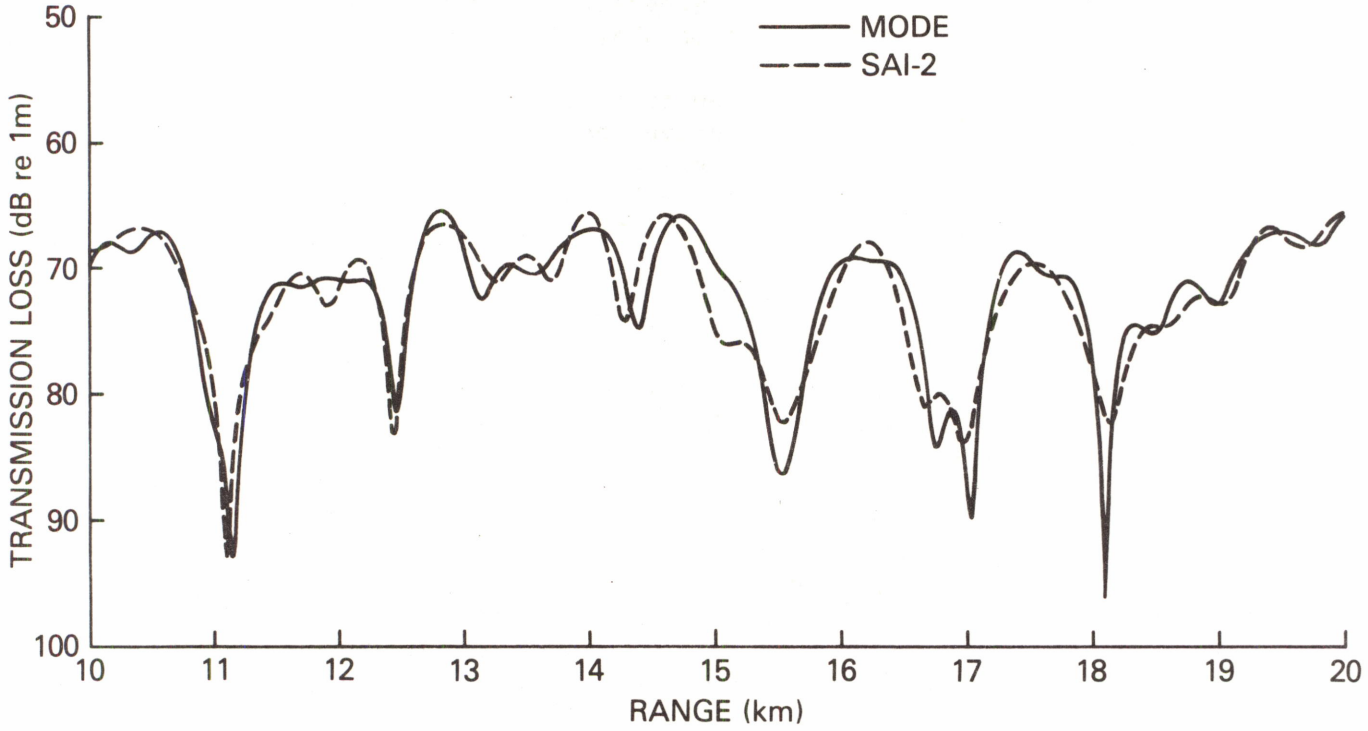

Figure 9. SAI-2 PE result compared with reference result (MODE) for Test Case 2B

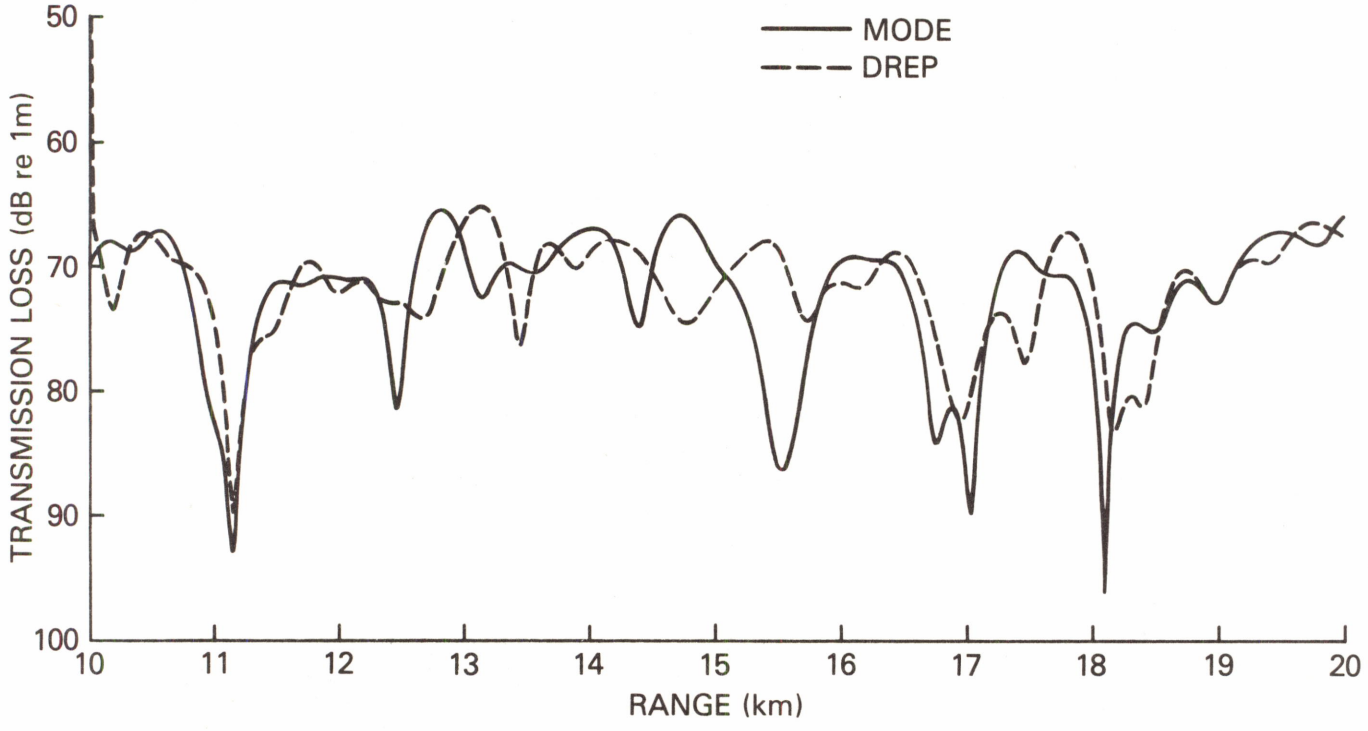

Figure 10. DREP PE result compared with reference result (MODE) for Test Case 2B

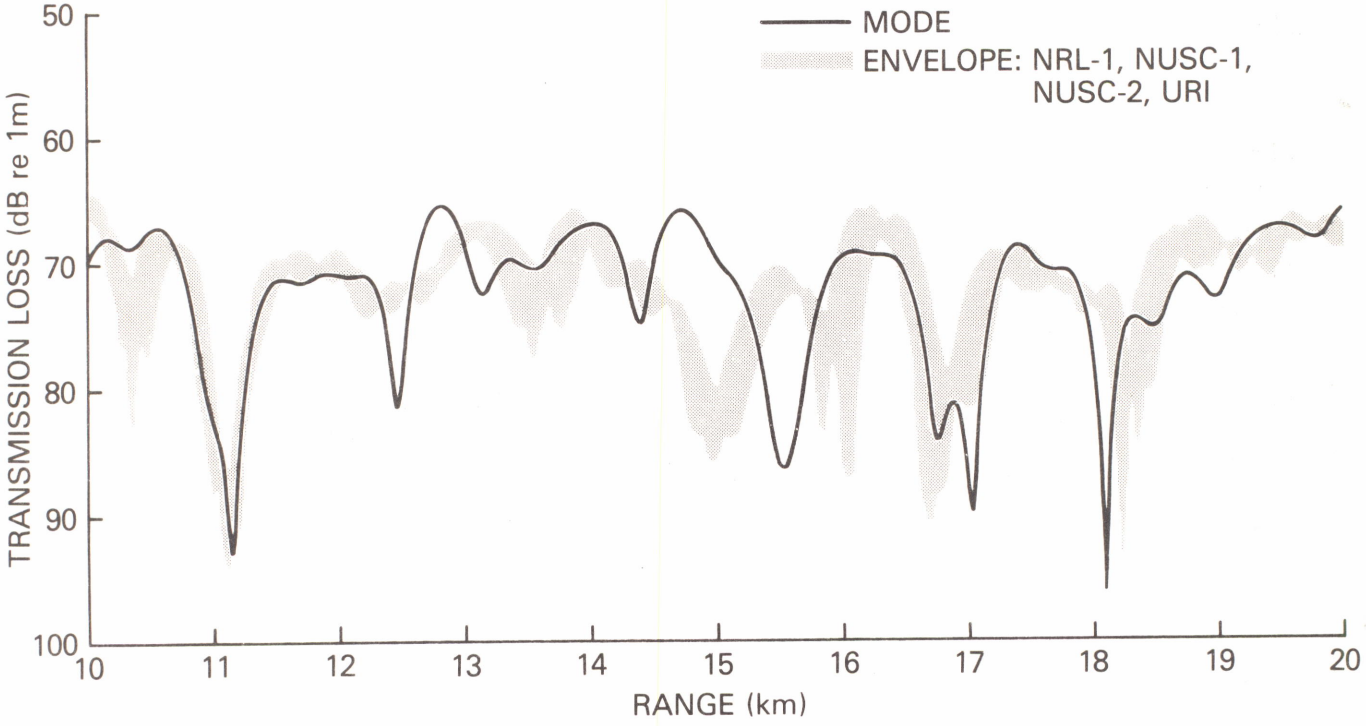

Figure 11. Envelope of results of PE programs that did not use CMOD compared with reference result (MODE) for Test Case 2B

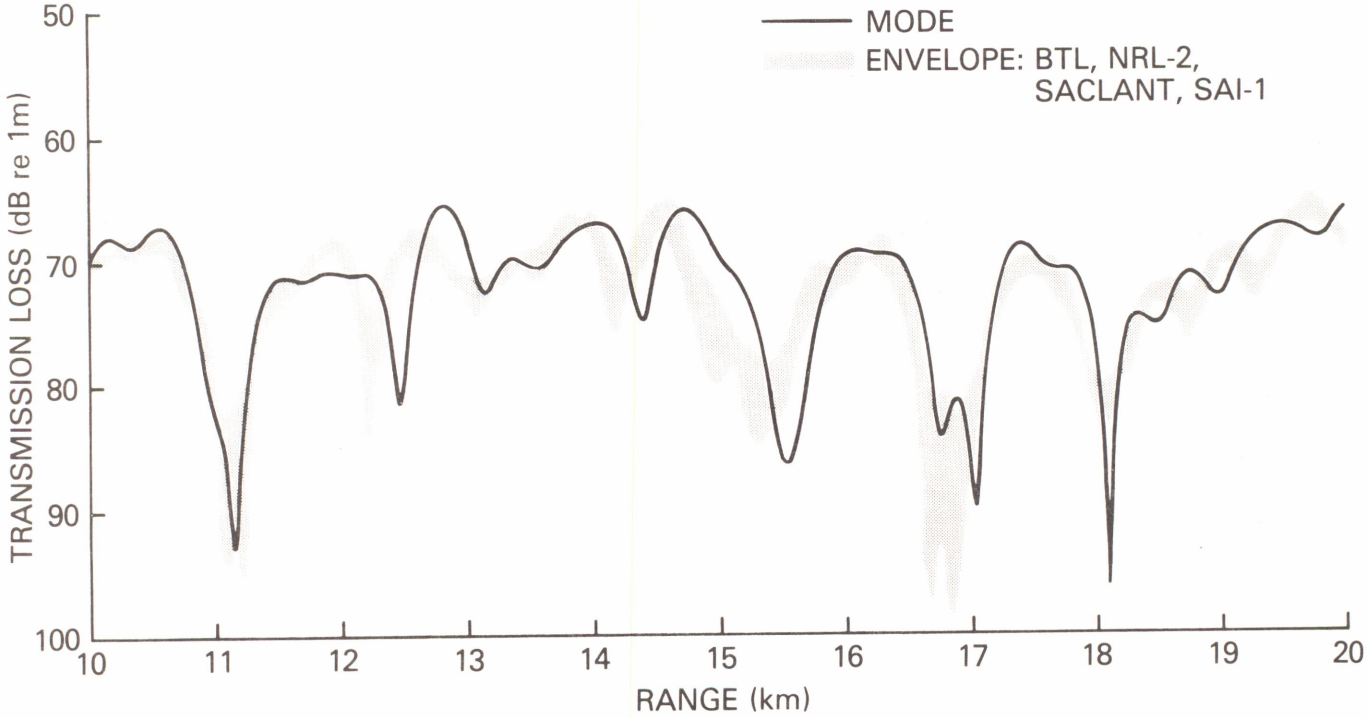

Figure 12. Envelope of results of PE programs that did use CMOD compared with reference result (MODE) for Test Case 2B

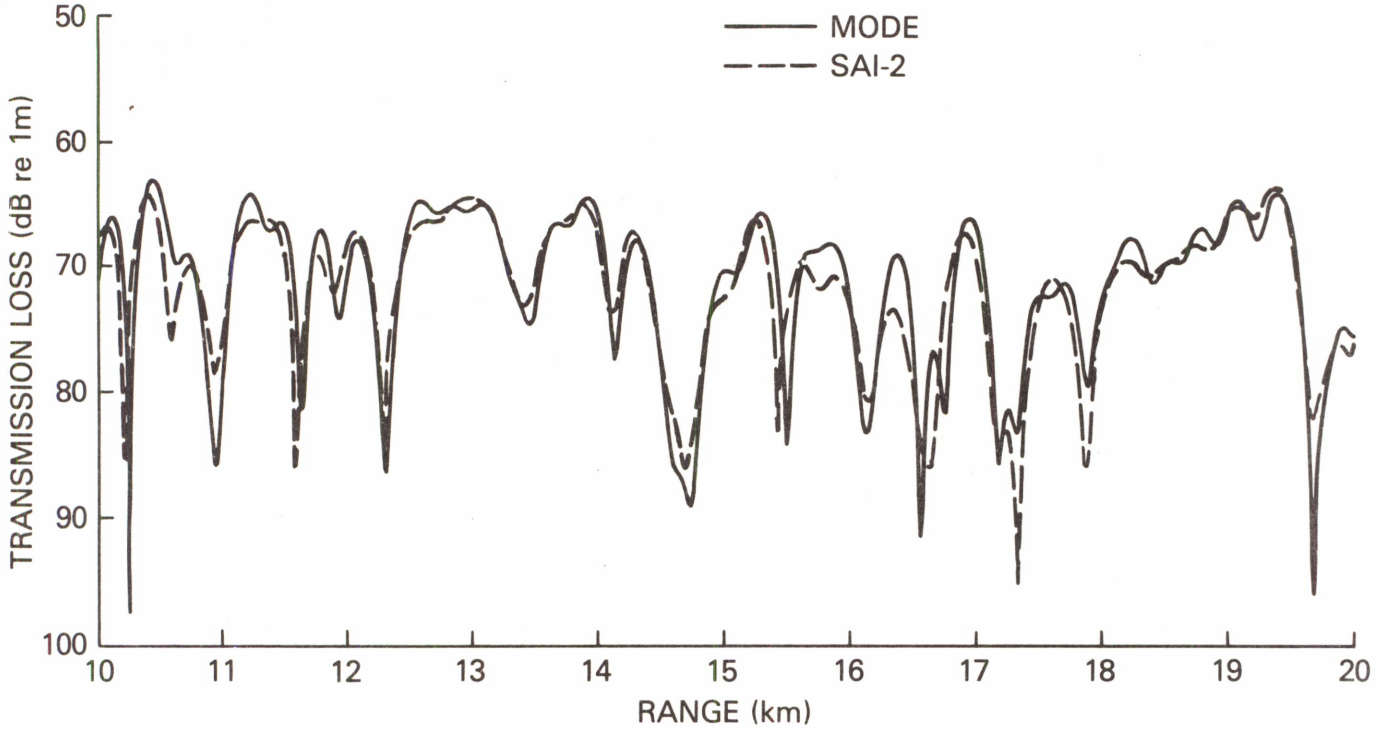

Figure 13. SAI-2 PE result compared with reference result (MODE) for Test Case 2C

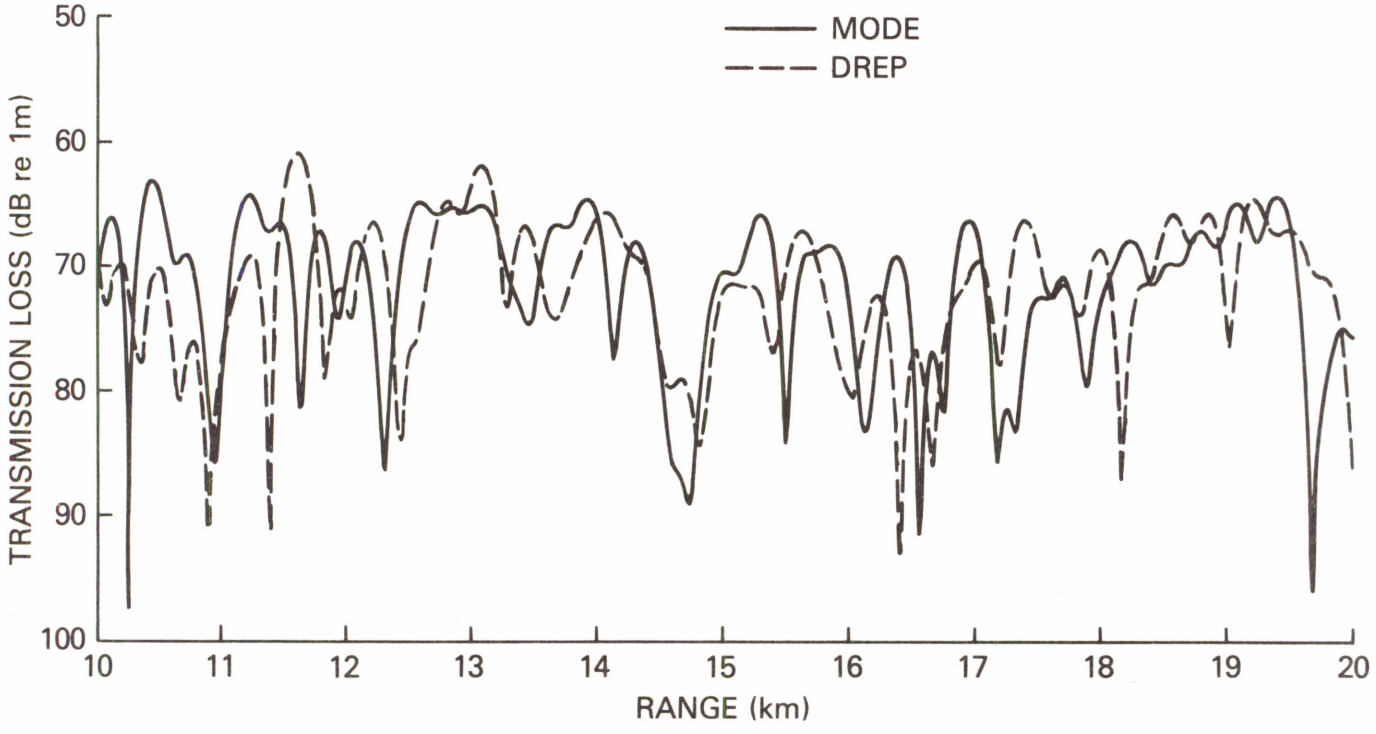

Figure 14. DREP PE result compared with reference result (MODE) for Test Case 2C

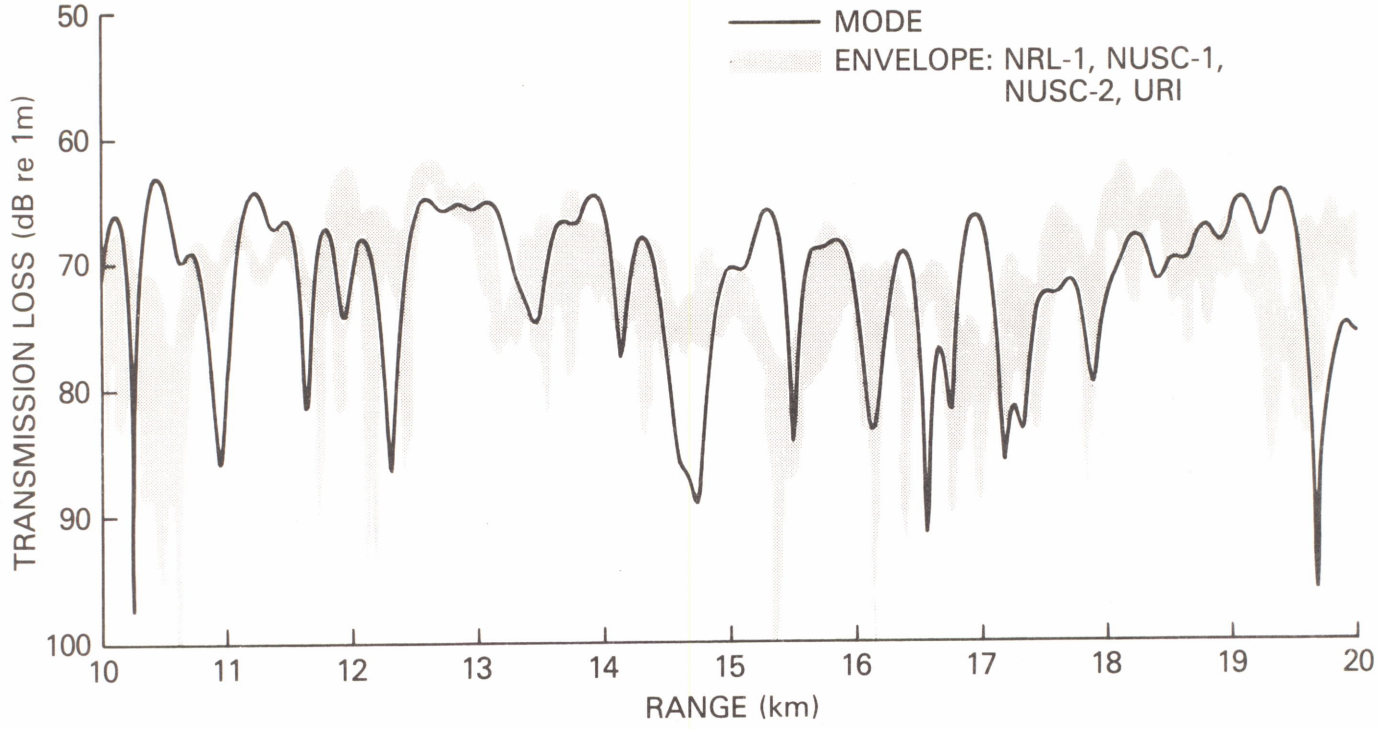

Figure 15. Envelope of results of PE programs that did not use CMOD compared with reference result (MODE) for Test Case 2C

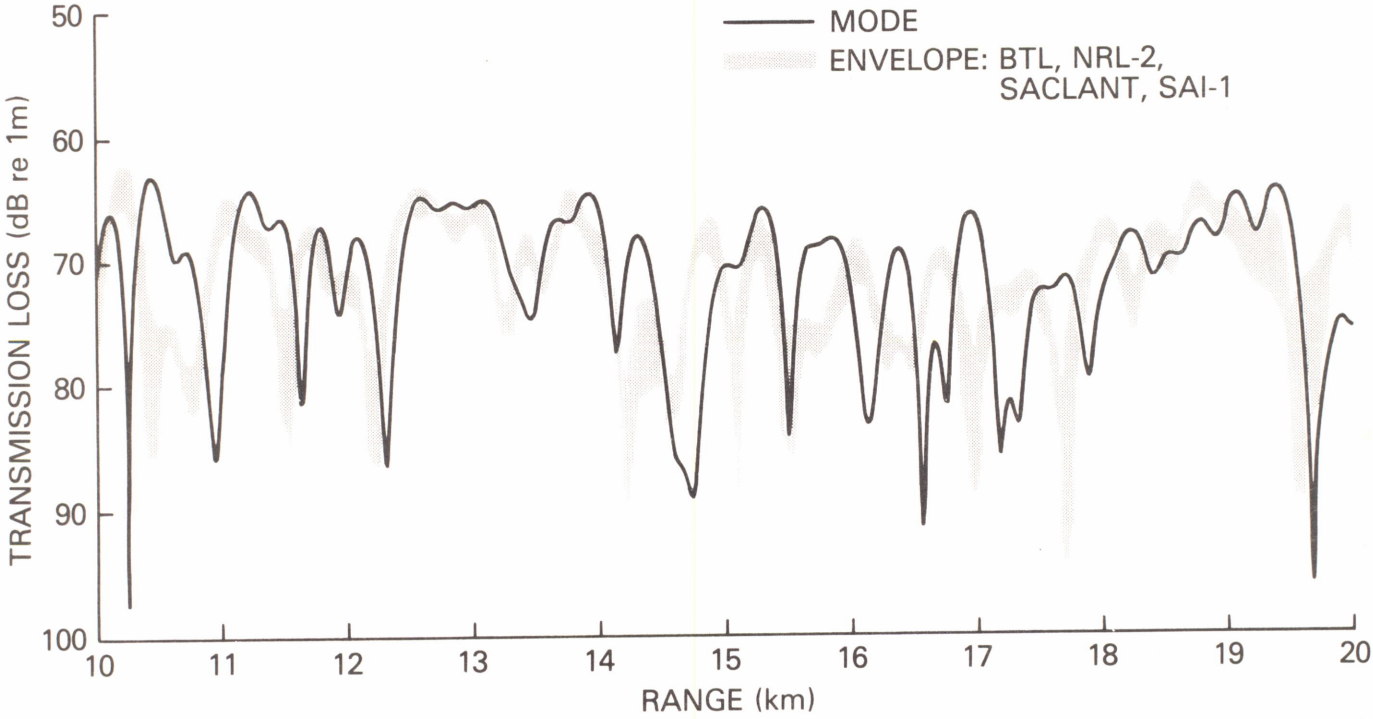

Figure 16. Envelope of results of PE programs that did use CMOD compared with reference result (MODE) for Test Case 2C

E. SUMMARY FOR CASE 2

Test Case 2 has demonstrated that SPE can give an accurate answer for a small beamwidth problem if there are no sound speed, density, or attenuation discontinuities, whereas for larger beamwidth problems average levels are predicted well but phase errors cause disagreement in detail. It has also demonstrated that a "high-angle" PE, in this case Greene's rational linear approximation, can provide a good approximation to the elliptic solution for a range-independent problem containing half beamwidths up to 40°. In addition this test case indicates that in a situation where the phase errors are small (i.e., SPE is very accurate), CPA provides a more accurate correction than CMOD. For larger beamwidth problems all SPE's give essentially the correct level but are unable to reproduce the details. CMOD appears to slightly improve this situation. It is not known whether CPA would provide an improvement in general. The PE results are relatively independent of r-z mesh, initial field, details of imposing the radiation condition, and method of solution, i.e., split-step or finite difference.

VII. TEST CASE 3 (Shallow Water)

A. DEFINITION OF PROBLEM

The environment for this case is range-independent and consists of an isovelocity water column over an isovelocity half-space bottom. Parameters for the two parts of the problem are given in Table 9. It represents an idealized shallow water environment and was designed to test whether PE can accurately handle sound speed, density, and attenuation discontinuities for a simple problem where the half-beamwidth requirements are less than 20°.

There is a continuous spectrum in this problem because of the branch point at 100 m. However, its contribution is negligible beyond 5 km, and thus the SNAP and FFP results should agree, as they do (comparison not shown). There are 11 propagating modes (corresponding to a half-beamwidth of 18.5°). However, with the source and receiver in the middle of the water column, a 7 mode solution (corresponding to a 12° half-beamwidth) is fairly accurate in the 5 to 10 km range and a 9 mode solution (corresponding to 15° half-beamwidth) is extremely accurate in the 5 to 10 km range. Thus a half-beamwidth capability between 12 and 15° should be adequate to accurately handle Case 3A. For Case 3B, with the source and receiver just off the bottom, the higher modes are more strongly excited, and all 11 modes are required for an accurate solution in the 5 to 10 km range interval. This in turn requires a half-beamwidth capability of 18.5°.

It should be noted that for Case 3B, where the source is within 0.08 wave lengths of the bottom interface, we also have a test of the initial field employed if it assumes that the source is a few wavelengths from any boundary. See Table 10 for a summary of PE program parameters used for Test Case 3.

As mentioned in Sec. III-F, the NORDA program employed as a starter a normal mode solution based on a simplified initial environment. This environment was isovelocity, constant density, with zero absorption and with pressure release boundary conditions at $z = 0$ and $z = 650$ m.

B. RESULTS FOR CASE 3A

Results for this case are mixed and for the first time some PE's have incorrect levels. It is worth noting that CMOD was not applied for this test case (both parts

Table 9. Parameters defining Test Case 3

TEST CASE 3

Frequency = 250 Hz

Water Depth = 100 m

Sound Speed in Water = 1500 m/s

Density in Water = 1.0 g/cm^3

Density in Bottom = 1.2 g/cm^3

Attenuation in Water = 0

Bottom Attenuation = .5 db/λ

Bottom Sound Speed = 1590 m/s

Max Range = 10 km

Part A:

Source Depth = 50 m

Receiver Depth = 50 m

Part B:

Source Depth = 99.5 m

Receiver Depth = 99.5 m

Plots--Separate plots for each part from
5 to 10 km at 0.5 km/in.

Table 10. PE program parameters for Test Case 3.

Program	C_o(m)	Source	Half Beam Width (°)	δ(m)	Δ(m)	False Bottom Layer (m)
BTL	1550	G	30	1	variable	450
DREP	(a)1500 (b)1550	D	40	1	5	100
NORDA	1506	NM	30	2	2.5	550
NRL-1	1500	NM	-	.1	5	33
NRL-2	(a)1525 (b)1500	S	90+	(a) .4 (a) .2	(a) 3 (b) 1.6	33
NRL-3	1500	G	30	variable	1.5	?
NUSC-1	1500	G	30	.25	1	150
SACLANT	1500	G/NM	37	.5	5	67
SAI-1	1500	S	?	?	5	?
URI	1500	G	30	.5	2	IMP

A & B) as it is not appropriate for isovelocity problems. The most accurate result was that of NORDA shown in Figure 17; it is essentially the same as the MODE result. This accuracy is the result of proper treatment of discontinuities and, as will shortly become evident, of the efficacy of the rational linear approximation. On the other hand the DREP result, shown in Figure 18, seems to be off by a constant range shift, for which we have no explanation. The compiler error encountered by Greene (SAI-2) seriously affected the results for this test case and plots are not shown. His corrected version and new program give results comparable to the NORDA results.

The next best results are shown in Figure 19, which displays the envelope of the NRL-1, NRL-3, NUSC-1, SACLANT and URI transmission losses. The level and detail are good, and the envelope is fairly tight despite the difference in equations being solved, treatment of the bottom, starter, and solution technique. Notice in particular that NRL-1 does very well, although it does not have a bottom treatment appropriate for this problem (see Table 2).

An extremely important observation can be made upon comparison of the NORDA prediction (Figure 17) and the envelope of Figure 19: the high angle PE is more accurate than SPE for a case requiring a half-beamwidth of less than 15°. The point made by this result is that high-angle PE is not only more accurate in phase than SPE for large angles, but is also more accurate in phase at small angles. The SPE phase errors in this test case are evidently just enough to prevent forming the precise mode interference pattern. Since phase errors are accumulative in range, this has important implications for relatively narrow beam, long range propagation problems.

The NRL-2 result is presented in Figure 20. This result is not bad, but is different from those in Figure 19. The difference, we believe, is primarily due to the range step size and to some degree the treatment of the bottom. The SAI-1 and BTL results are shown in Figure 21. Here the levels are considerably in error and the details are completely different.

C. RESULTS FOR CASE 3B

This was an extremely difficult case as illustrated by the comparison of MODE (SNAP) and FFP in Figure 22. Agreement is excellent except near the null in the vicinity of 7 km. There are obvious numerical problems that can arise when 11 modes must almost exactly cancel. Other normal mode results (not shown here) indicate that the FFP solution is correct; however, we will, as for the previous test cases, use the MODE (SNAP) results as reference. The null at 7 km is on the order of 1/2 km wide and is interesting in its own right. It is also predicted by a fully coherent ray theory calculation. Ray theory analysis indicates that there is a complicated interaction of well-known effects which, by happenstance, combine to produce a null. It is not appropriate to present that analysis here, nor to examine the circumstances under which it can occur. Of more present interest is that the analysis shows that its reproduction requires an accurate treatment of the phase and water/bottom interface.

This test case posed problems for PE both in level and in detail; however, the NORDA result shown in Figure 23 is very accurate (recall that the MODE result does not faithfully reproduce the null). This is further supporting evidence that a high-angle PE with proper bottom treatment is an extremely powerful approximation.

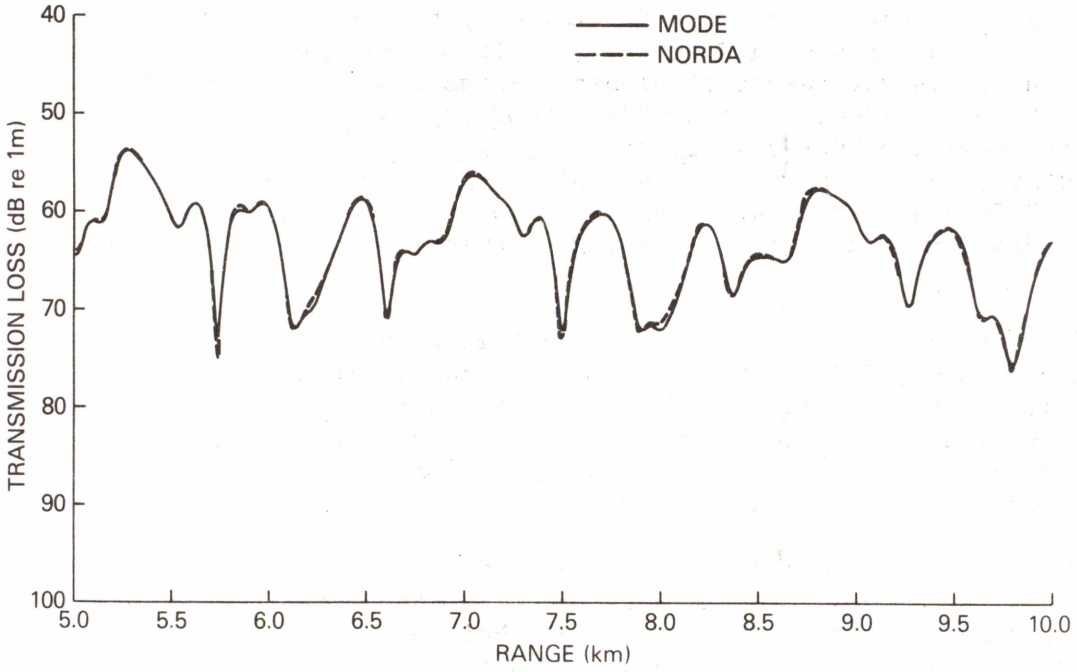

Figure 17. NORDA PE result compared with reference result (MODE) for Test Case 3A

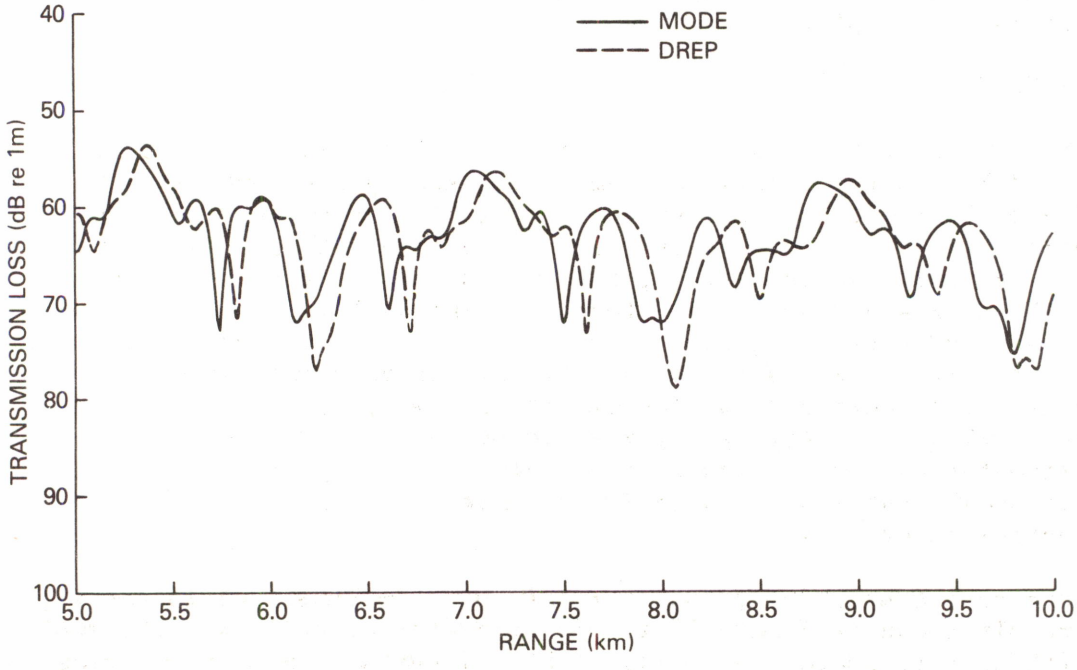

Figure 18. DREP PE result compared with reference result (MODE) for Test Case 3A

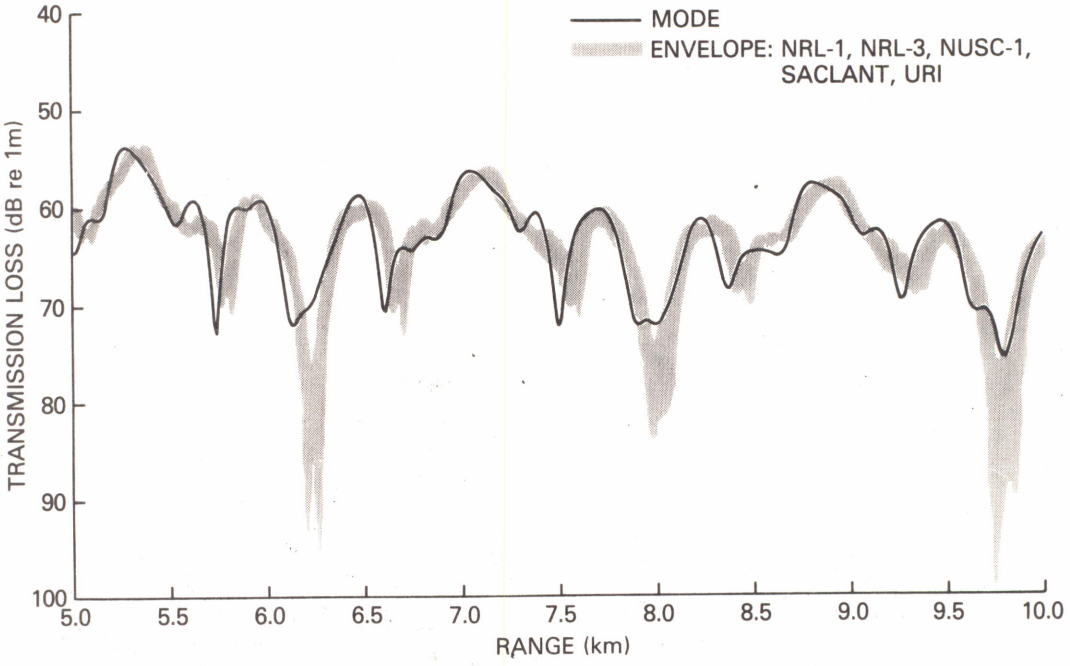

Figure 19. Envelope of the results of a group of PE programs compared with reference result (MODE) for Test Case 3A

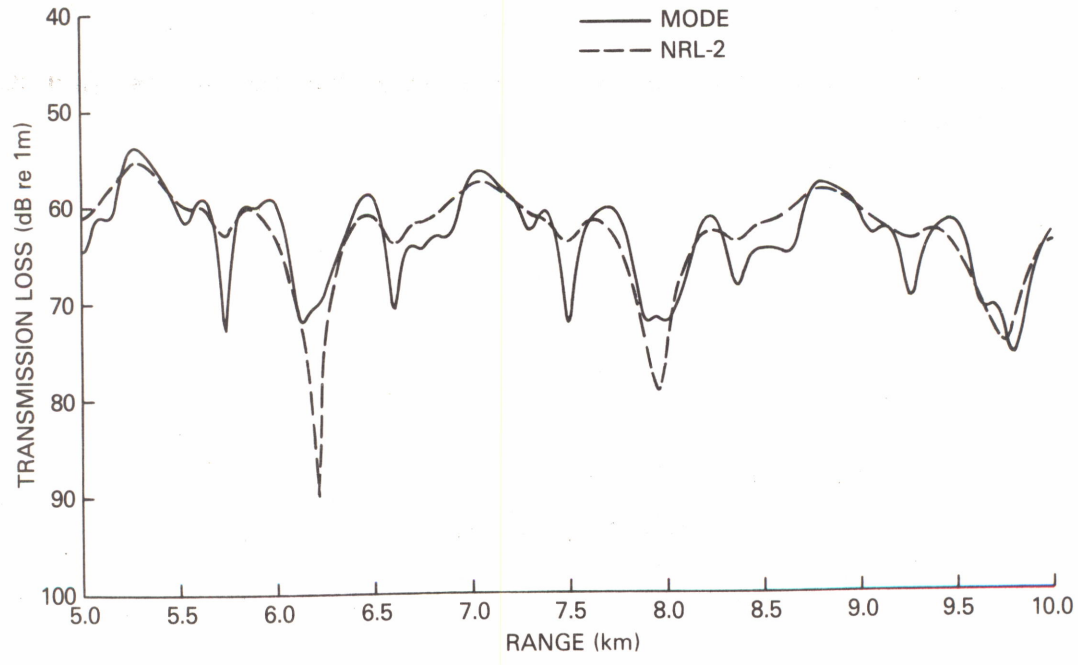

Figure 20. NRL-2 PE result compared with reference result (MODE) for Test Case 3A

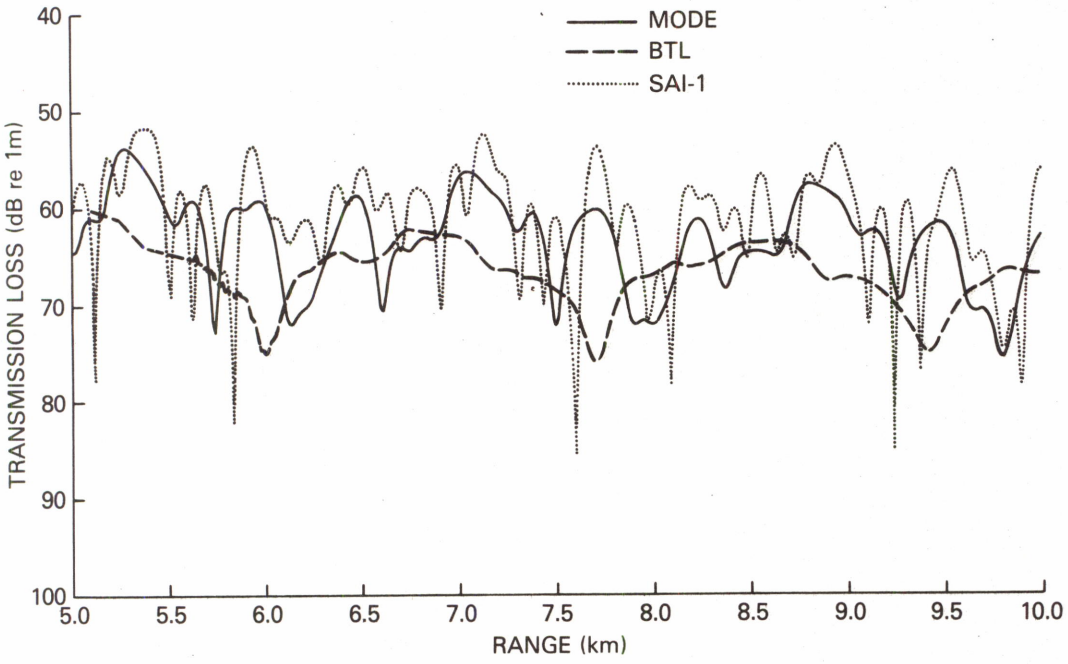

Figure 21. BTL and SAI-1 PE results compared with reference result (MODE) for Test Case 3A

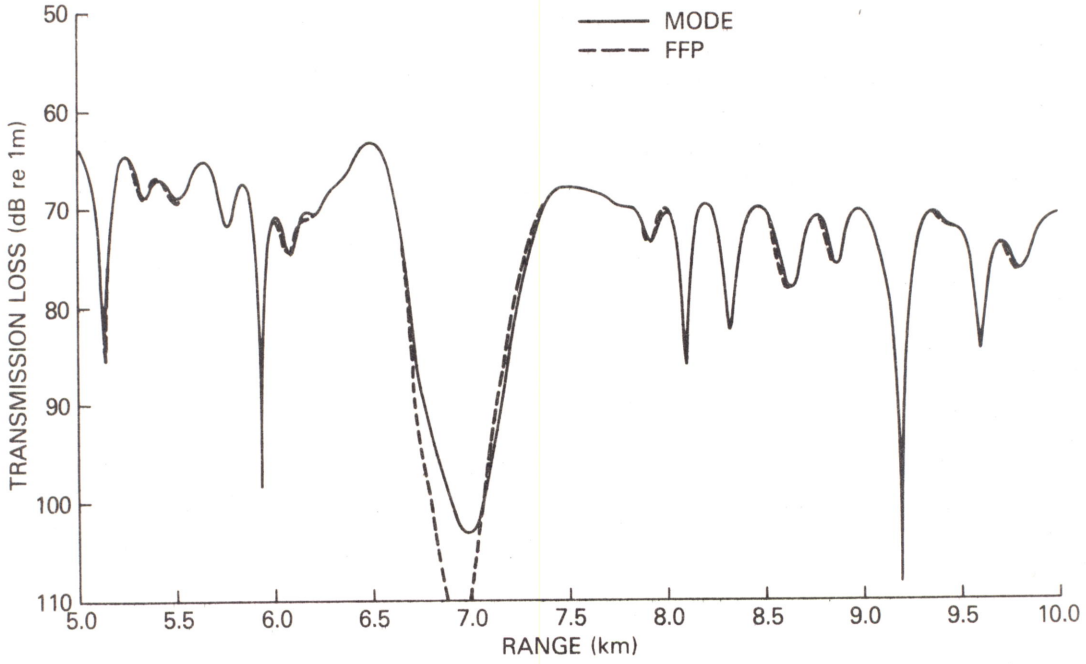

Figure 22. Comparison of MODE (SNAP) and FFP results for Test Case 3B

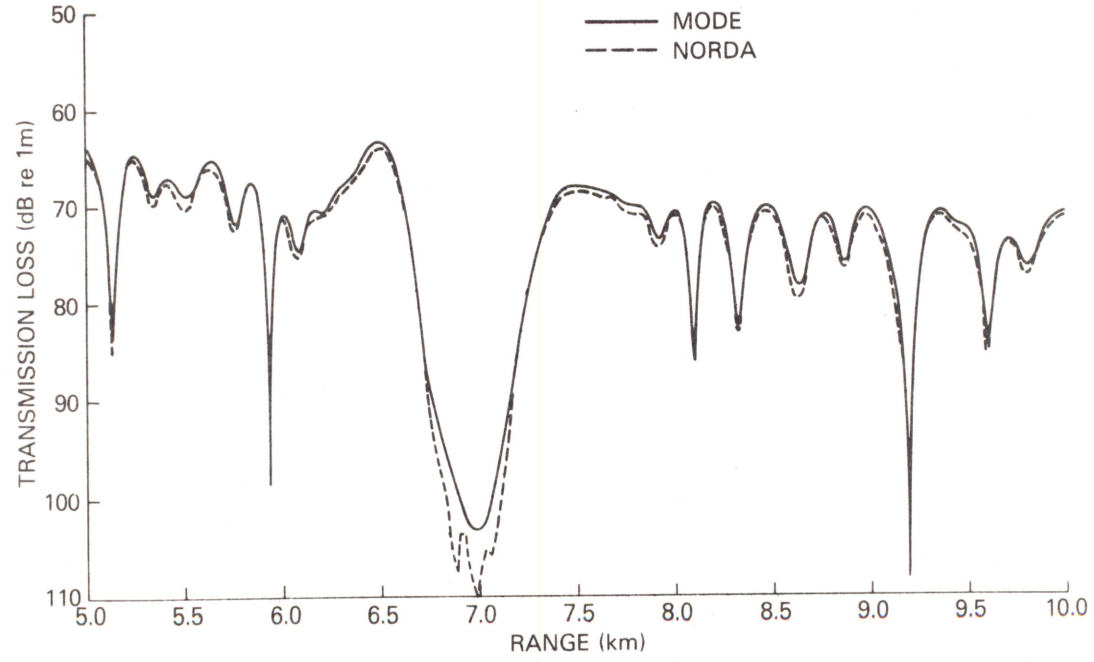

Figure 23. NORDA PE result compared with reference result (MODE) for Test Case 3B

Figure 24 shows the envelope of the NRL-1, NUSC-1, and URI results, all SPE's. Notice that the average level is good but the detailed pattern is not good. Figure 25 is the SACLANT result and is shown separately as an indication of how C_o can be selected to reproduce a particular feature. In this case the null at 7 km is reproduced, but the details at other ranges are no more accurate than the Figure 24 results. The NRL-2 transmission loss is shown in Figure 26; it is neither better nor worse than the SPE's in Figure 24, but is different. The DREP and NRL-3 results are shown in Figure 27. These again are no more or no less accurate than the results in Figures 24 and 26. The SAI-1 and BTL results are shown in Figure 28 and quantitatively the same as for Test Case 3A, i.e., the levels and details are off.

Finally, note that a display of the sensitivity of transmission loss to source treatment is obscured by the lack of agreement of any method, except NORDA's, with the reference. Even though the source is .08 wavelengths from the water/bottom interface, the fact that the NORDA normal mode starter is based on a homogeneous medium (no discontinuities) suggests that the form of the initial field is not very important for this case. Other results, such as the envelope of Figure 24, in which models utilizing a variety of source types yield similar predictions, support this conclusion.

D. SUMMARY FOR CASE 3

We repeat here several specific results of this test case which appear to be generalizable. First, PE can do well in predicting average transmission loss levels for bottom interaction problems only if some reasonable approach to handling the bottom is included in the PE algorithm. This approach may be crude in some specifics, such as in this case where several programs used constant density even though there was a density change. The conclusion holds whether SPE or other PE forms are used and whether the PE is implemented through split-step, finite difference, or finite element techniques. Second, correct detail in the range dependence of the transmission loss is lacking unless energy at even relatively low angles (10°) is treated accurately. Third, the high angle approximation can represent this energy much more accurately than SPE and, because of this, can track transmission loss through a larger range of levels. The last point, one which has long been accepted, is that the choice of C_o appears to have little effect on average level, but can have major effects on specific detail, and in fact can be chosen to produce "special effects" such as the proper location of the deep fade in part B.

VIII. TEST CASE 4 (Basin/Slope/Shelf with Geoacoustical Bottom)

A. DEFINITION OF PROBLEM

This test case has a range-independent sound speed in the water column, a range-dependent bottom depth consisting of a basin-slope-shelf configuration, and a simple geoacoustic bottom (a sediment layer overlying a basement) with sound speed proportional to that at the bottom of the water column. The parameters defining this case are given in Table 11. This is perhaps the most realistic of the test cases and is a modified version of a recent SEAS problem of interest. The 700 m receiver has a positive depth excess of 1346 m in the basin, becomes bottom limited on the slope at a range of 171 km, and strikes the bottom slope at a range of 192 km. The 150 m receiver is bottom limited throughout. Because of the test case parameter values, energy up to angles of 40° returns to the water column. This case is therefore a stringent test for any PE because it requires proper treatment of interface conditions (discontinuous sound speed and density at the water column-sediment and sediment-basement interfaces), a large half-beamwidth capability, and

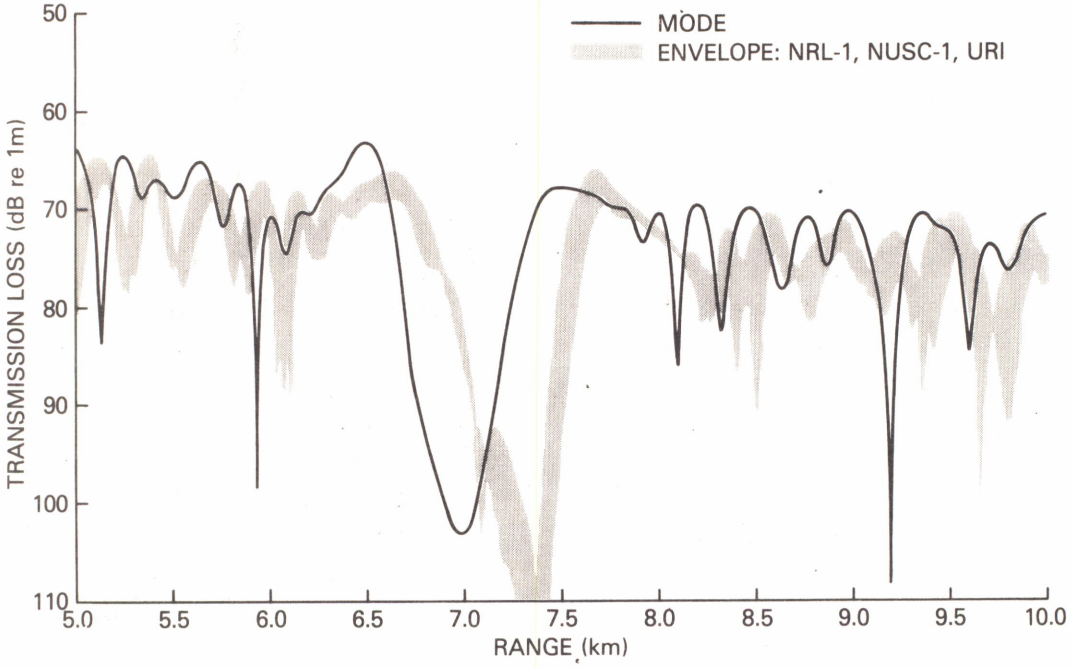

Figure 24. Envelope of NRL-1, NUSC-1, and URI PE results compared with reference result (MODE) for Test Case 3B

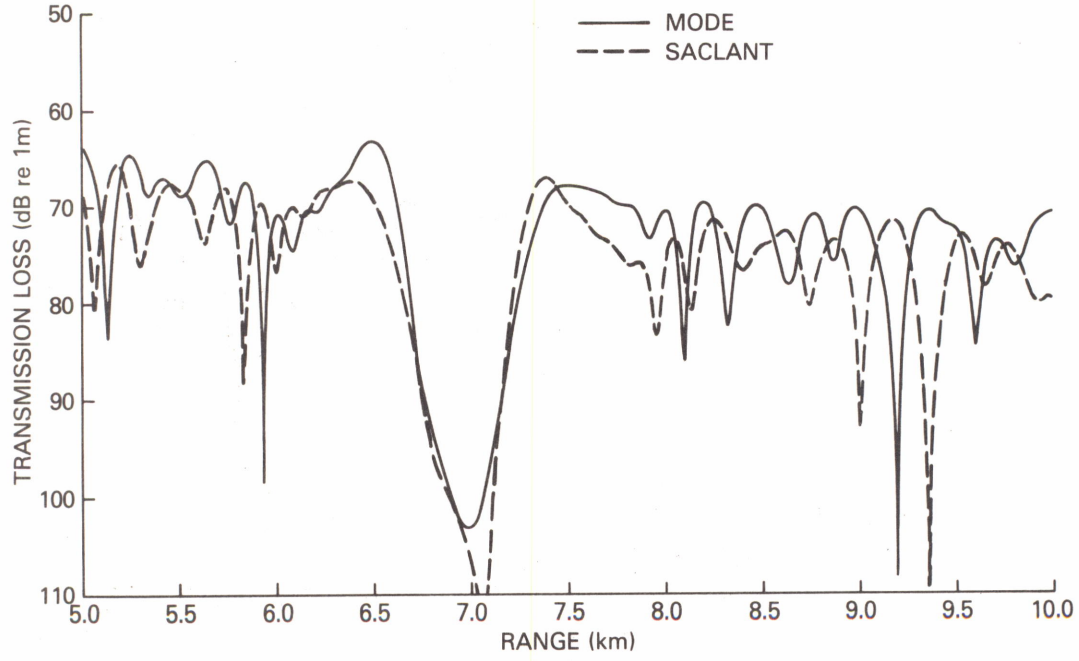

Figure 25. SACLANT PE result compared with reference result (MODE) for Test Case 3B

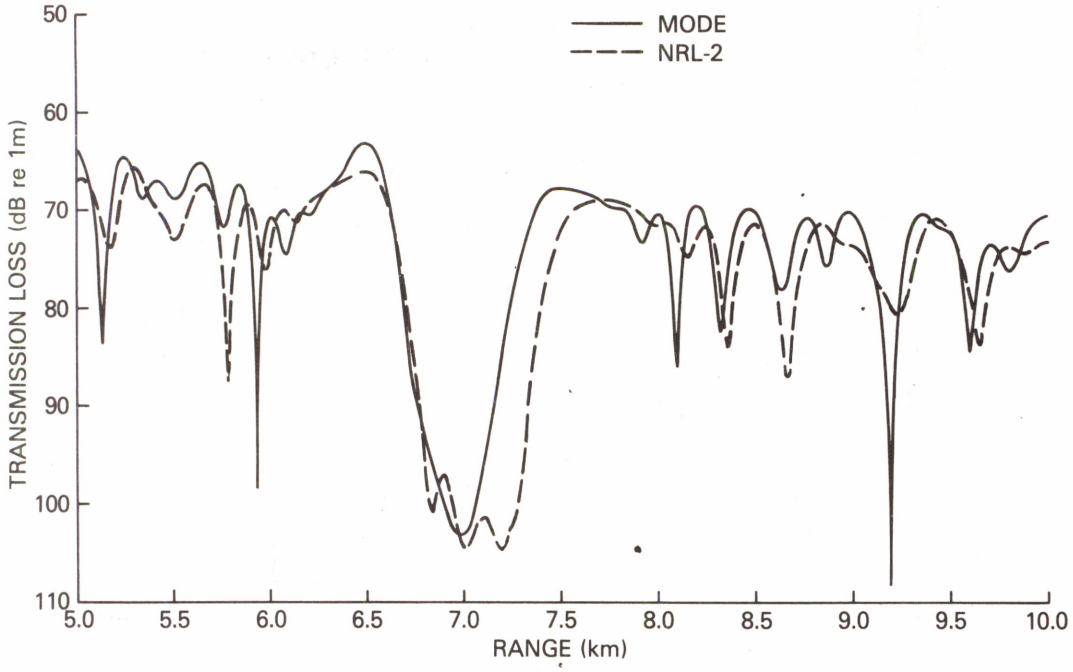

Figure 26. NRL-2 PE result compared with reference result (MODE) for Test Case 3B

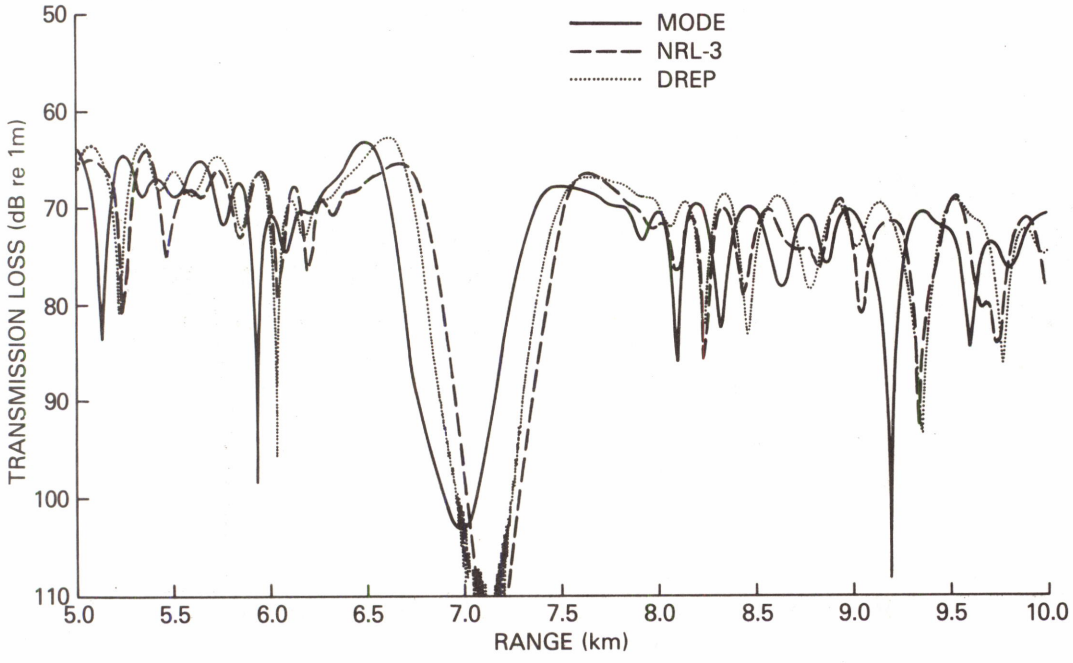

Figure 27. NRL-3 and DREP PE results compared with reference result (MODE) for Test Case 3B

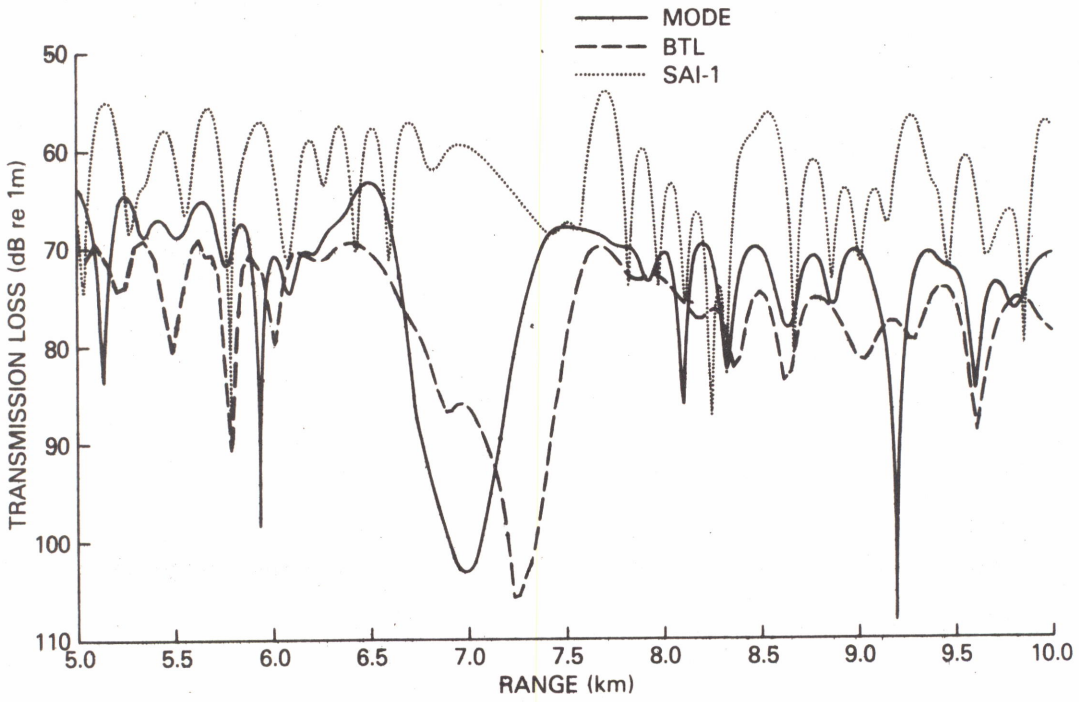

Figure 28. BTL and SAI-I PE results compared with reference result (MODE) for Test Case 3B

Table 11. Parameters defining Test Case 4

TEST CASE 4

Frequency = 25 Hz, Source Depth = 600 m, Maximum Range = 250 km

WATER COLUMN PARAMETERS

Depth(m)	C(m/s)	Density (g/cm^3)	Attenuation (dB/km)
0	1539.3	1.	0.
30	1539.8	1.	0.
200	1534.2	1.	0.
600	1502.4	1.	0.
700	1495.4	1.	0.
800	1491.8	1.	0.
1000	1488.0	1.	0.
1100	1487.5	1.	0.
1200	1487.9	1.	0.
3410	1525.0	1.	0.

BOTTOM DEPTH

Range	Bottom Depth
0-150 km	Constant 3410 m
150-200 km	Linearly decreasing with increasing range from 3410 m to 200 m
200-250 km	Constant 200 m

SEDIMENT

Sound speed at top of sediment is $CT_s(r) = .975 \times C_W(r)$ where $C_W(r)$ is the sound speed at the bottom of the water column. Sound speed at the bottom of sediment is $CB_s(r) = 1.305 \times CT_s(r)$

Sediment thickness = 454 m (constant in range)
Attenuation = 0.015 dB/km/Hz
Density = 1.5 gm/cm^3

PLOTS: 700 m RECEIVER DEPTH

4a - 1.0 km average from 10 to 50 km at 4 km/in
4b - 20 km average from 0 to 250 km at 25 km/in

150 m RECEIVER DEPTH

4c - 1.0 km average from 175 to 225 km at 5 km/in
4d - 20 km average from 0 to 250 km at 25 km/in

For additional clarification at a range of 200 km: Water depth = 200 m; C_W (200 km) = 1534.2 m/s; CB_s (200 km) = 1952.1, CT_s (200 km) = 1495.8; and Basement depth = 654 m.

a range sufficiently great (250 km) that cumulative phase errors can significantly distort the resultant PE field.

Details of normal mode predictions for the range-independent portion of this problem were found to be sensitive to particular mode program's treatment of sound speed interpolation in depth, density discontinuities, etc. It was therefore decided to avoid comparisons of the details of the field. It was decided instead to first compare intensity average results on a fine enough scale (1 km) in particular regions of interest to allow meaningful comparison of the relative behaviors, yet not so fine a scale as to make comparisons unduly difficult, if not meaningless. At the other extreme, a gross intensity average (20 km) provides an overall comparison of levels and trends. Since this 20 km average is roughly equivalent to an incoherent mode sum, the PE results should be relatively insensitive to phase errors.

Another and perhaps more important driving factor in the use of intensity averages versus detailed transmission loss is that the reference calculation (SNAP or FFP) can be used with confidence only in the basin area (0-150 km). The "correct" solution in the slope and shelf areas (150-250 km) is not known and comparison of results is somewhat of a "bootstrap" situation. Although an adiabatic SNAP solution is used as a reference result for the 150 m source (20 km intensity average case from 0 to 250 km), it should be recognized that it is an approximate solution and its accuracy relative to the "true solution" is not presently known. A coupled mode solution for Test Case 4 would have been desirable but was not available. Thus, we will be comparing PE results that contain full coupling but have beamwidth constraints with an adiabatic mode result which has no beamwidth constraints but ignores mode coupling. Consider an additional complication in comparing average results: for any detailed intensity-range function, the average result will be sensitive to the weighting of the values within the given interval (e.g., uniform or nonuniform) and to the range values for which the average is generated (e.g., a running range step average, or an average for every range value corresponding to the mid-point of the range interval).

The test rationale for each of the cases is as follows:

4A. Capability to treat, on a 1 km average level of detail, a case that has positive depth excess, but considerable bottom interaction.
4B. Capability to correctly partition water column and bottom interaction energy for a case that has positive depth excess but considerable bottom interaction.
4C. Capability to track on, a 1 km average level of detail, up a slope and onto a shelf under strong bottom limiting conditions.
4D. Capability to correctly partition energy across a basin up a slope and onto a shelf under strong bottom limiting conditions.

For Test Case 4 we found it difficult to identify patterns, similarities, etc., among the various PE results which would allow sensible groupings for graphical presentations. Rather than presenting the results individually (which makes intercomparison almost impossible), the results are all presented in one figure for each test case. Table 12 gives the PE program parameters for Test Case 4. For convenience, in Table 12 we use the following short-hand notation to describe the type of intensity averaging used:

Table 12. PE program parameters for Test Case 4.

Program	C_o(m)	Source	Half Beam Width (°)	δ(m)	Δ(m)	Phase Correction	Average
BTL	1488	G	30	2	variable	CMOD	EXP-R
DREP	1500	D	(a) 60 (b) 40 (c) 40 (d) 40	15	50	NONE	LIN-R
NRL-1	1531	NM	40?	5	158	NONE	LIN-R
NRL-3	-	G	30	variable	8	NONE	LIN-I
NUSC-1	1507	G	30	5	10	NONE	LIN-R
SACLANT	1500	G	37	5	25	NONE	LIN-R
SAI-1	1488	S	?	?	30-500	CMOD	LIN-R
URI	1507	G	30	10	20	NONE	LIN-R

LIN - equal weighting of points within the averaging interval
EXP - exponential weighting of points within the averaging interval
R - average over the interval for each range-step
I - average over the interval for each range corresponding to the mid-point of the interval.

B. RESULTS FOR CASE 4A

The PE results for the 700 m receiver case (1 km intensity average) are mixed and are shown in Figure 29 with the MODE result given by the black line and the various PE's color coded according to the legend. It is clear from Figure 29 that no one PE does well throughout the range from 10 to 50 km. As an aid in understanding these results see Figure 30 which shows the MODE result for modes 1 through 16 (corresponding to a 12.5° half-beamwidth), modes 1 through 56 (corresponding to a 30° half-beamwidth), and the full solution modes 1 through 77 (corresponding to a 40° half-beamwidth). The 16 mode solution contains only RR paths while the 56 and 77 MODE solutions include bottom-interacting paths. Notice the small spread of the various PE results and agreement with the MODE result in Figure 29 at ranges (34 to 40 km and near 46 km) where in Figure 30 the RR paths are important. In all other regions the RR paths are not important, and the spread in the various PE results is greater. The 56 mode solution and the 77 mode solution are nearly the same except in the range interval from 10 to approximately 14 km. Notice also in Figure 29 that all PE's over estimate the loss from 10 to 14 km because the higher angle paths are not present. Apart from the RR region, detailed agreement is poor and average agreement is fair. Although they are not really designed to handle this wide a beamwidth, the NRL-1 and SAI-1 results compare surprisingly well; this is probably due to the large half beamwidths (greater than 30°). The primary reason for lack of better agreement of PE in the 16 to 30 km region is the impact (on a 1 km intensity average level of detail) of the phase errors associated with SPE. An exception to this is the DREP result for which we have no explanation.

C. RESULTS FOR CASE 4B

A reference calculation for the 700 m receiver depth (20 km intensity average) case was available only in the basin region and is shown in Figure 31 as the black line along with the various PE program results (color-coded). The DREP result appears to be the most accurate. Apart from the NRL-1 result which underestimated the loss (and which employed a 40° half-beamwidth) the remaining PE's tend to overestimate the loss and form a relatively small envelope that decreases in width with increasing range to less than 2 dB at a range of 150 km. This envelope is even smaller if we do not include the NUSC-1 and URI results which consistently overestimate the loss on the order of a dB or so (probably due to the 30° half-beamwidth employed). In the plain region (0 to 150 km) the results are a measure of whether a PE can include all of the pertinent energy (up to 40°) and whether the interfaces are treated accurately enough to return energy from the bottom.

The results should not depend strongly on phase errors since the 20 km intensity average is roughly equivalent to an incoherent mode sum. Thus, for programs that attempt to take discontinuities into account, the transmission loss should be greater the smaller the beamwidth. This appears to be the case.

The results start to diverge on the slope (150 km) to the range where the receiver depth and bottom depth are the same (192 km). We cannot comment on the

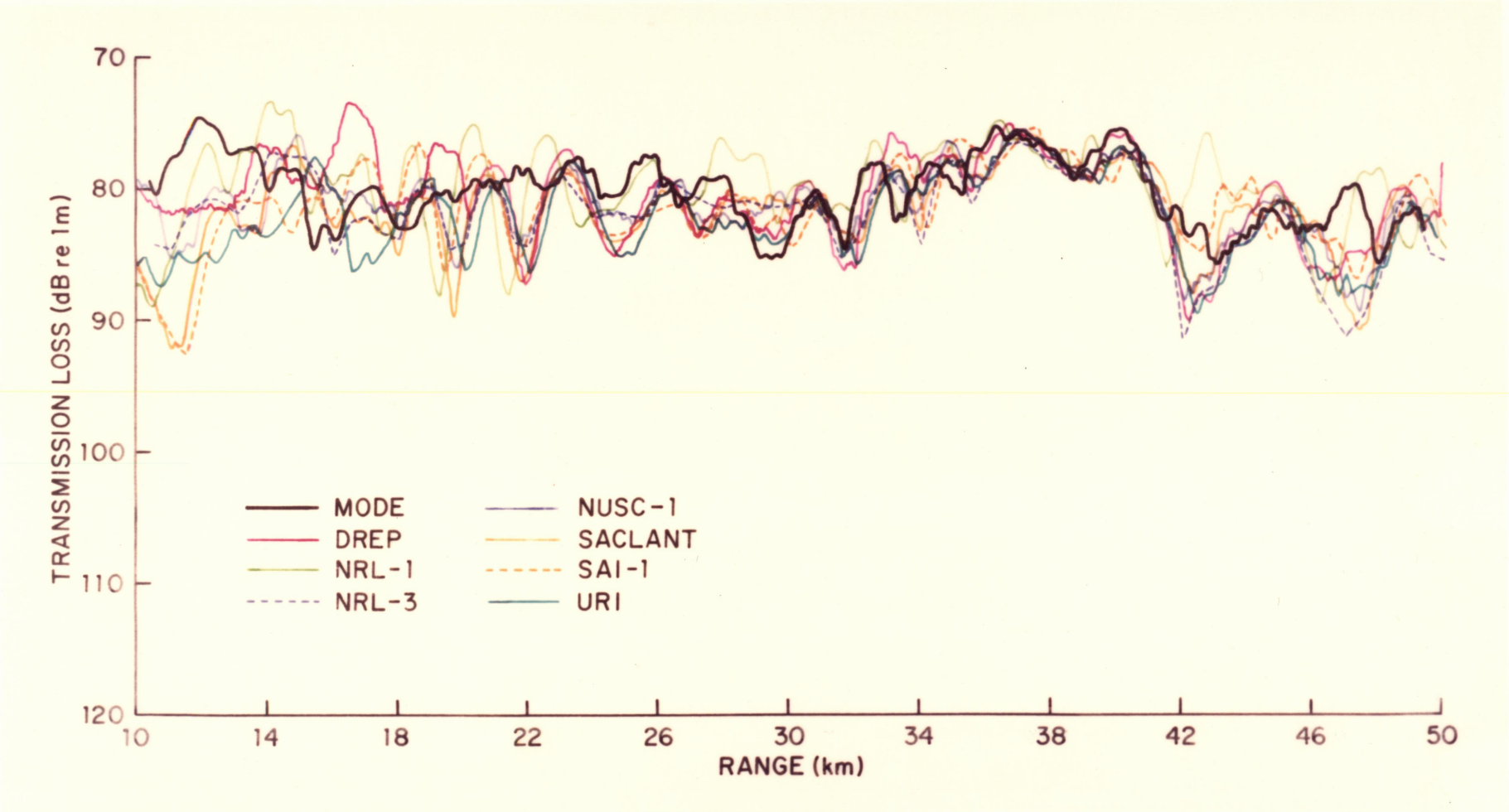

Figure 29. PE program results (1 km intensity average) compared with reference result (MODE) for basin of Test Case 4A

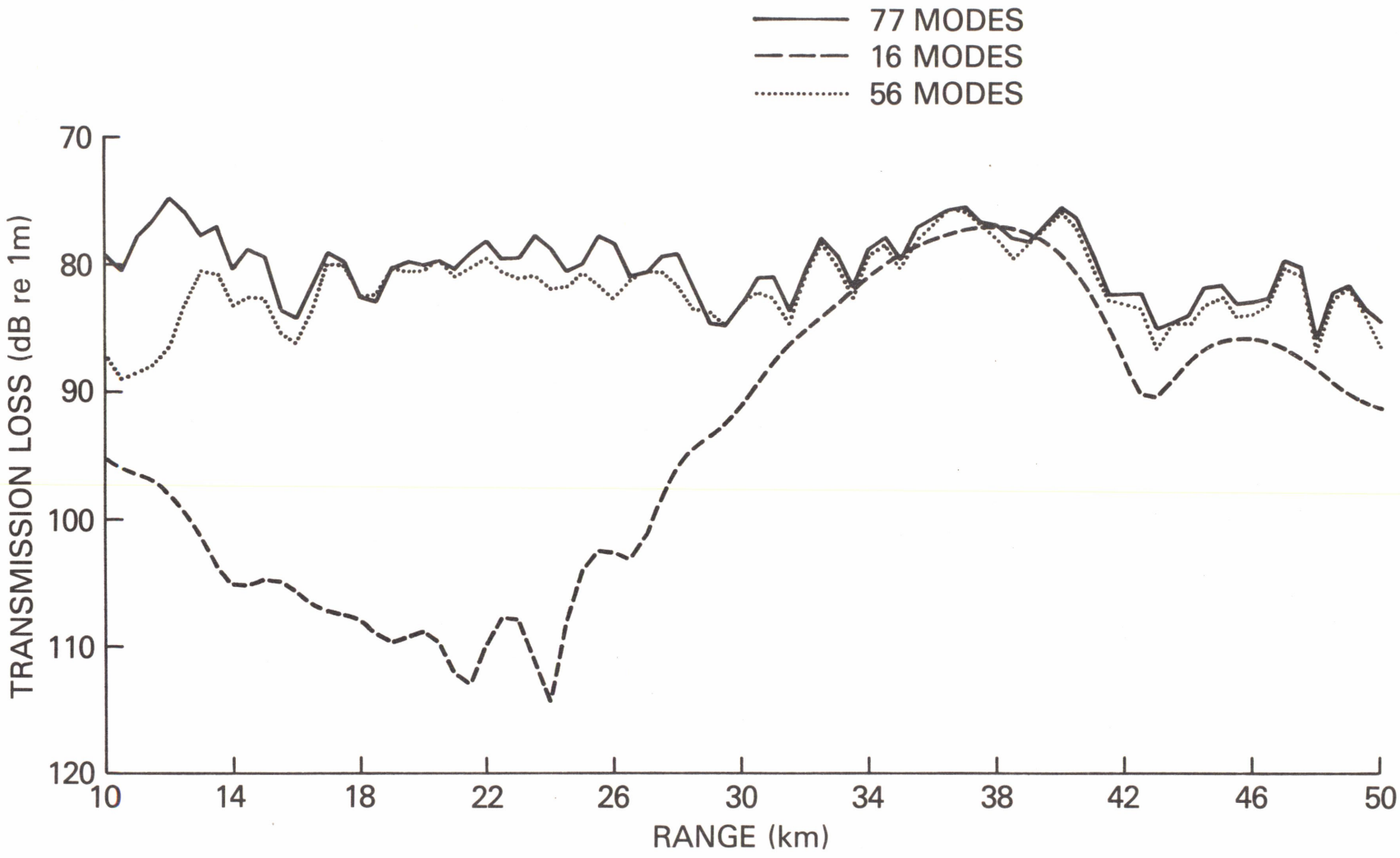

Figure 30. Effect of number of modes (beam width) on (1 km intensity average) transmission loss in Test Case 4A

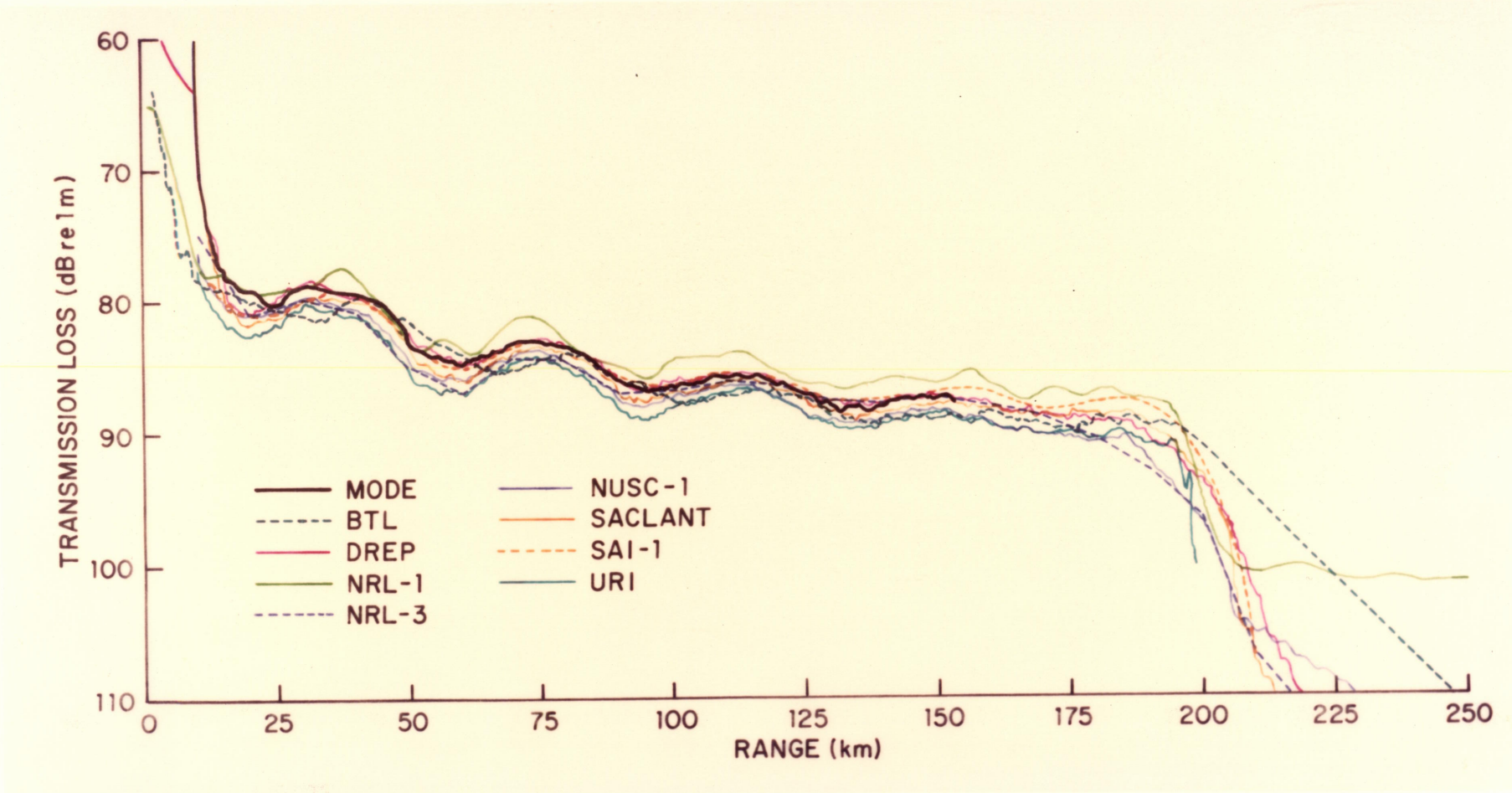

Figure 31. PE program results (20 km intensity average) compared to reference result (MODE) for Test Case 4B (basin/slope/shelf)

relative accuracies in this region as we have no reference calculation, but do note that the spread is on the order of 5 dB.

D. RESULTS FOR CASE 4C

PE results for Test Case 4C (150 m receiver depth) are shown in Figure 32, but no reference calculation is available. Information obtained after the workshop, but not included here, in the form of an adiabatic mode calculation (SNAP), indicates that the PAREQ result agrees with the SNAP result in general level but not in detail (i.e., interference pattern). To the extent of our confidence in SNAP, we can use PAREQ as a reference, but must keep in mind that SPE phase errors are large enough to preclude 1 km intensity average detail comparisons.

The agreement between the various PE's in Figure 32 is generally poor, as perhaps might be expected because of the different treatments of interfaces, method of solution, etc., but the large degree of disagreement is a little surprising. Notice, however, that there tends to be some agreement between PE's in the range interval 182.5 to 187.5 km (a spread of 2.5 dB at 185 km). This apparently is a "slope-conversion" effect, caused by conversion by the slope of small angle energy to high angle energy.* The agreement is not as good at shorter ranges (7 to 10 dB), and there is a large spread (as much as 15 dB) at greater ranges. Also, notice that there is a general decay in level beyond 200 km. Although the level is different for each PE, the decay rate appears to be the same. As will be seen in Section D, the PE's enter the slope region (150 km) with a spread in average level of 5 dB. This spread is primarily due, just as for the 600 m receiver case (4A, 4B), to initial beamwidth and treatment of interfaces and radiation boundary conditions.

Now the slope is approximately 3.7° and, therefore, from a ray perspective each encounter with the slope (water-column/sediment and/or sediment/basement interface) increases the angle by 7.4°. We speculate that the agreement at 185 km is due to (1) loss of higher angle energy that contributed to the disagreement in the plain region and (2) conversion by the slope of the RR energy (less than 15° in the plain) to higher angles. However, even though the conversion process persists at ranges from 190 to 200 km, the various PE's are now each converting differently and losing the higher angle energy at different rates. This conversion and loss process is sensitive to the treatment of the slope and the radiation boundary conditions, but the detailed investigation of this process for each PE is beyond the scope of this report.

E. RESULTS FOR CASE 4D

A reference calculation from the adiabatic mode program SNAP for the 150 m receiver depth (20 km intensity average) case was available throughout the range of the problem (0-250 km) and is shown in Figure 33 as the black line along with the various PE program results (color-coded). It is interesting to note that the SACLANT (PAREQ) result, which was accurate on a 1 km intensity average basis in the slope-shelf region in Case 4C (175-225 km), see Figure 32, displays the same accuracy in the slope-shelf region on a 20 km intensity average basis but overestimates the transmission loss in the basin region (0 to 150 km) by a few dB.

*The mechanics of this process are complicated, and include three competing effects on transmission loss: (1) increased bottom loss as paths become steeper, (2) decreased geometrical spreading loss as the waveguide constricts, and (3) reduced surface decoupling (surface image interference) loss at the receiver as steep paths become more important.

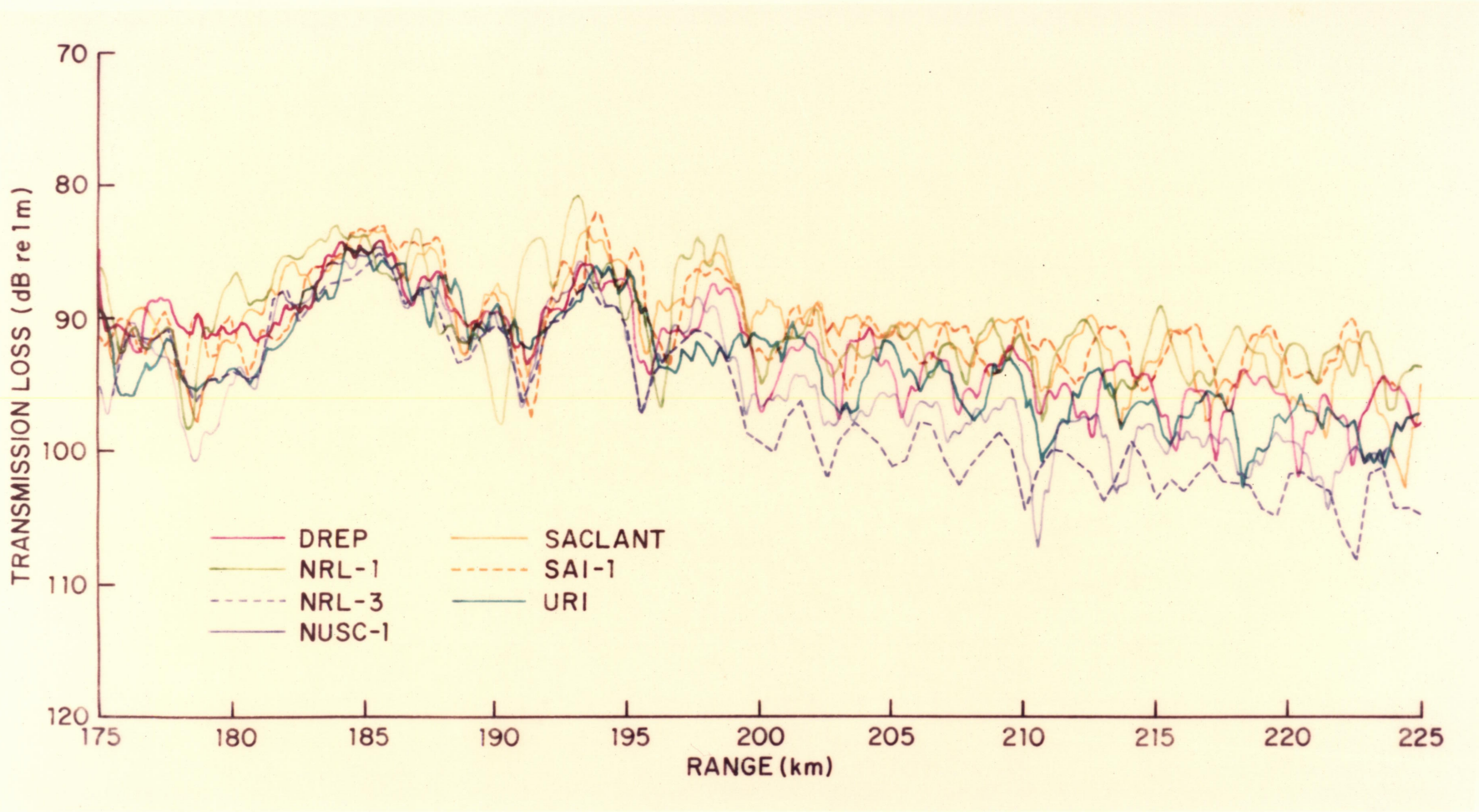

Figure 32. PE program results (1 km intensity average) for slope/shelf of Test Case 4C

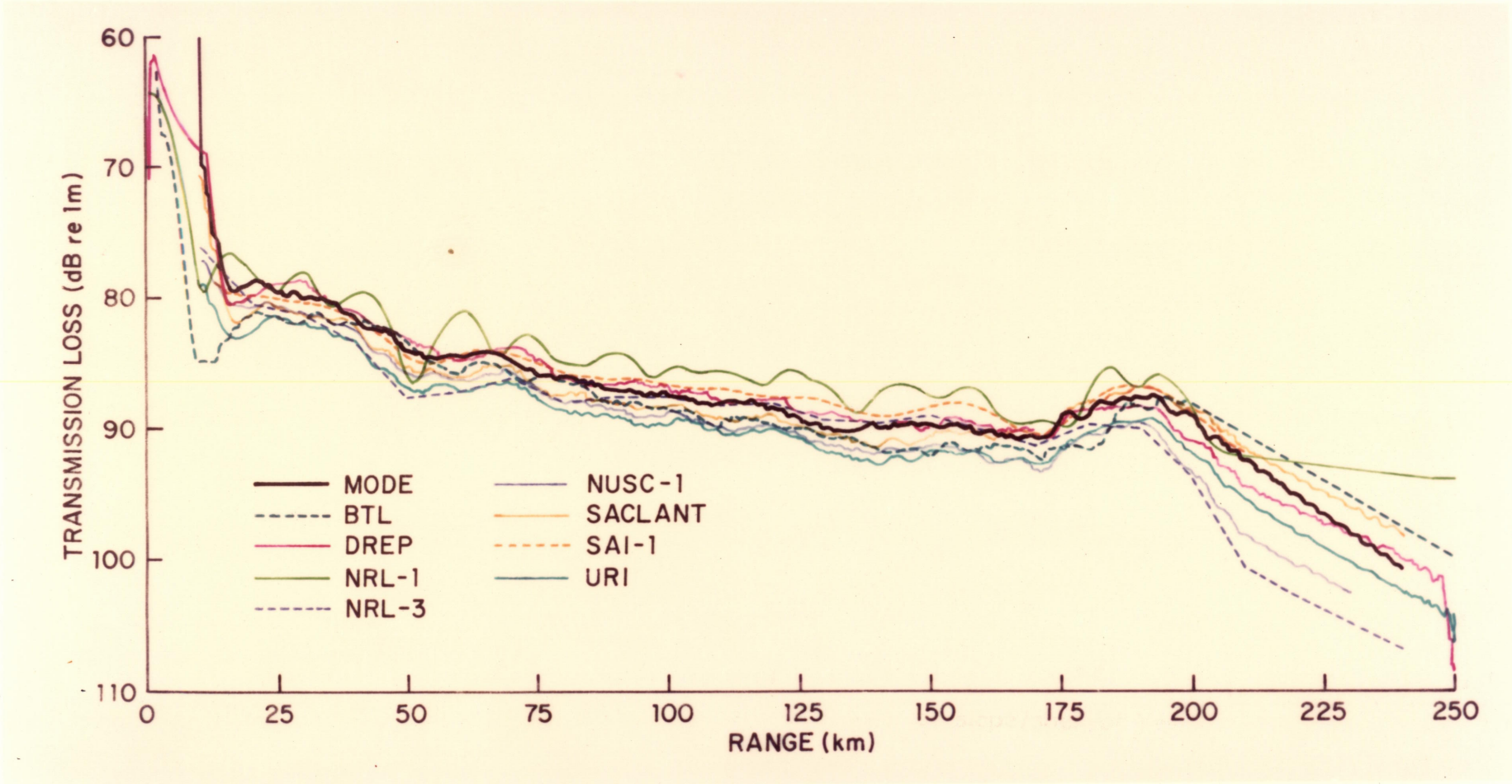

Figure 33. PE program results (20 km intensity average) compared to reference result (MODE) for Test Case 4D

Figure 33 is a dramatic example of the spread in average level (from 4 to 10 dB) of PE program results for a bottom limited wide beamwidth problem. The greatest spread is on the shelf, where we have the least confidence in the reference calculation. Notice that in the basin region (0-150 km) the URI, NUSC-1, and BTL results consistently overestimate the transmission loss (all use a half beamwidth of 30°), and both URI and NUSC-1 have a reasonable interface treatment, whereas the NRL-1 and SAI-1 results, which use constant density, underestimate the transmission loss (using a half beamwidth of 40° and 35°, respectively). The DREP result appears to be the most accurate in the basin and SACLANT on the slope and shelf. Again as mentioned in part C, the programs with smaller beanwidth (30°) appear to have removed too much energy in going up the slope. This speculation is reinforced if one notes that the decay rate is about the same for most of the PE's (and MODE) beyond about 205 km, but the spread in level is larger than in the basin.

F. SUMMARY FOR TEST CASE 4

This test case has provided some interesting, if somewhat disappointing, results. In general, the test shows the importance of careful treatment of interfaces in problems dominated by bottom-interaction effects. Also, it appears that a high angle PE (appropriately large beamwidth) is needed to adequately account for the bottom-interacting energy, especially for propagation up a slope and onto a shelf. The results in the basin region appear to be more dependent on beamwidth than on type of PE or depth-mesh, range-step or starter.

Specifically, these PE programs perform poorly at the 1 km level of detail in a case with considerable bottom interaction (Case 4A and 4C). In tracking up a slope and onto a shelf under bottom limiting conditions, they are not consistent (Case 4C), even at the incoherent (20 km average) level of detail (Case 4D). However, incoherent levels are predicted within a few dB in the range-independent (basin) environment (4B, 4D), and the PE's do very well even on the small scale when only RR (low angle) energy dominates (4A and 4C).

Test Case 4 has indicated a need for reference solutions to a set of range-dependent environment problems that could serve as benchmark test cases.

IX. SUMMARY AND CONCLUSIONS

This report has presented the results of the PE workshop held from 31 March to 3 April 1981. Two major objectives were met. The first objective was to provide a forum for exchange and stimulation of ideas for those presently active in theoretical and applied PE development, as related to underwater acoustic problems. This objective was accomplished partly in the new development section of the workshop and partly in the test problem section of the workshop. The appendix presents the abstracts for the new development portion of the workshop and also provides brief model descriptions for those programs exercised for the workshop. The second objective, a comparison of PE models and their predictions, was covered in the main text and is discussed below.

The first half of the main text reviewed model forms and solution techniques for PE as applied to underwater acoustic problems. First a general PE and then specific PE equations were discussed: from SPE (historically the first and the most common form in use) to C_0-independent PE and rational linear PE (the latest development in general use). The CMOD and CPA modifications, designed to correct SPE phase errors, were also outlined. Finally, several methods of solution were

discussed: split-step and finite difference for SPE, and schemes for the three high angle PE's presented at the workshop.

The second half of the main text presented and compared PE model results for a set of four ocean acoustic test cases. The test cases ranged from a simple problem, expected to be "easy" for any PE program, to a fairly realistic basin-slope-shelf configuration which had considerable bottom interaction and was expected to be a "difficult test" for all PE programs.

Detailed comparisons of test case results were not available at the time of the workshop, but were made by the authors afterward. Conclusions about the state of PE capability were then drawn, and are summarized as follows:

1. General

a. There are many PE models in operation today. They differ in form, in equation solved, in treatment of inputs, in boundary conditions and specifications, in numerical method, in computer implementation, and in display of the output. Each model has its regime of applicability, inherent assumptions, and idiosyncrasies. Not surprisingly, this diversity of models was, repeatedly, exemplified by a diversity of test case results. There is no "standard," all-purpose PE model.

b. Nonetheless, within its realm of applicability, a PE model can be a very powerful, efficient, and accurate predictor of sound transmission properties. This was borne out in those test cases for which there was an accurate reference solution. The lack of a reference solution for certain range-dependent environment problems serves as an illustration of the gap in technology which PE can fill.

2. SPE

a. The test problems reconfirmed that the accuracy of SPE is greatly dependent on the vertical-angle aperture (beamwidth) of dominant propagation paths. From a modal point of view, the smaller the extent of vertical wavenumbers or phase speeds for propagating modes, the smaller the SPE errors in phase. While a 20° half-beamwidth about the horizontal (or its equivalent "small angle" or vertical wavenumber limit about any depression angle) is a traditional rule of thumb for tolerable phase errors, in SPE, the detailed TL prediction suffers from the effect of cumulative phase errors as range increases, both for this and even for smaller apertures. This again was observed in the test problems.

b. For problems with a large beamwidth of propagating paths, SPE can predict range-averaged TL (because phase errors tend to average out), but not the details. For this case, and to a lesser extent the small beamwidth case, the detailed SPE predictions can be quite sensitive to choice of C_o.

c. The accuracy of SPE was also found to be very sensitive to the treatment of interface conditions, especially for larger beamwidth problems. Proper methods of dealing with abrupt changes of sound speed or density with depth are required.

d. In addition to the inherent limit of any PE to "slowly" range-varying environments, SPE was found to be sensitive to the treatment of range dependencies in sound speed and boundary conditions. This is as much an environmental as an acoustic problem.

e. Test case results tend to be insensitive to choice of z mesh, range step size, solution technique (split-step or finite difference), and starter, provided of course that all were within reason.

3. CMOD

The CMOD modification to SPE was found to reduce SPE phase errors and minimize sensitivity to choice of C_o, within the limits of the small beamwidth constraint.

4. CPA

The CPA modification to SPE was demonstrated in only one case, where SPE errors were small, and found to improve the results.

5. CIT

The C_o-independent version of PE showed no improvement over SPE in the test problems.

6. High Angle PE

Of the three models presented, one (NORDA) did only Test Case 3, another (SAI) had results only for Test Case 2, and the third (DREP) had inconsistent results (possibly caused by implementation problems in a new program). General conclusions cannot be drawn from this small sample, but individual cases suggest that a high angle PE can be quite accurate for beamwidths as large as $\pm 40°$. In addition, the finite difference and finite element approaches allow interface conditions to be accurately represented.

7. General Recommendations

a. There is a clear need for bench mark, reference solutions to a set of range-dependent environment problems.

b. PE development will continue. Persistent evaluation of new (and existing) models should be an integral part of that development.

ACKNOWLEDGMENTS

Special thanks are due to R. Evans of Ocean Data Systems, Incorporated, who provided support by aiding in the development of the test cases and in helping to unravel and interpret certain theoretical aspects of the PE programs. S. Chin-Bing and D. King of NORDA aided in the test case development and were largely responsible for ensuring that the mechanics of the workshop ran smoothly.

We also would like to thank F. Jensen and W. Kuperman of SACLANT ASW Research Centre for providing the reference calculations, SNAP and FPP, that proved invaluable in the evaluation of the test cases.

CDR K. E. Evans, modeling manager of the SEAS program, originated the idea for the workshop, and provided continual support and encouragement to bring the workshop to a successful conclusion, and CDR M. A. McCallister, the successor to CDR K. E. Evans as the SEAS modeling manager, continued to provide this support after the workshop.

Finally, we would like to thank the workshop participants, whose time, effort, and support ensured a successful workshop.

This work was performed under the Surveillance Environmental Acoustic Support Project program element 63785N.

APPENDIX A: ABSTRACTS OF FORMAL PRESENTATIONS

ALTERNATIVE DATA FOR PE MODELS

David H. Wood
Code 3342
Naval Underwater Systems Center
New London, CT 06320

The Parabolic equation is solved by numerical models that go forward in range one step at a time using previously computed values. The very first values, or initial data, must be provided to the model. By considering any initial data whatsoever after expansion as a weighted sum of normal modes, we can immediately see what the solution of the PE would be if the sound speed were not to depend on range. Matching this as well as we can* to the normal mode sum that satisfies the Helmholtz equation, and then extrapolating back to the initial range, we see that $\Sigma\emptyset_n(z_o)\emptyset_n(z)$ is the appropriate initial data. There are three deficiencies in the resulting approximation to the solution of the Helmholtz equation. The least important is an amplitude error for each mode that results from approximating the square root of the horizontal wave number for each mode by a single representative value*. More important is that each mode by is given a phase proportional to $k(1-1/2\sin^2\theta_n)$ instead of $k \cos \theta_n$ (the horizontal wave number of the n^{th} mode). This is the so-called phase error of the parabolic approximation and is small for small angles θ_n. Most important is a bizarre difficulty concerning the effervescent modes of the Helmholtz equation that decay rapidly with range because $\cos \theta_n$ is essentially pure imaginary. For these same modes, $1-1/2 \sin^2\theta_n$ is essentially pure real so that these modes <u>propagate</u> in the parabolic equation without the desired exponential decay.

*Prof. Tappert pointed out during the presentation that the initial data $\emptyset_n(z_o 0\emptyset_n(z) \cos^{-1/2}\theta_n$ would give an improved match by eliminating amplitude errors.

CONSTRUCTION OF A BANDLIMITED WAVENUMBER SOURCE FOR THE PARABOLIC EQUATION

John Hanna
Science Applications, Inc.
P. O. Box 1303
McLean, VA 22102

All solutions to the Parabolic Equation (PE) require specification of the initial pressure field as a function of depth (or wavenumber). It can be shown that an appropriate specification of the initial field in vertical wavenumber space for beamwidths of 30° or less is just

$$\emptyset(o,k) = \text{constant for } -k_b \leq k \leq k_b$$

$$= 0 \text{ otherwise,}$$

where

$$k_b = k_o \sin\theta_b,$$

$$k_o = w/c,$$

$$\theta_b = \text{desired source beamwidth.}$$

However, since most numerical solutions to the PE use FFT's, it is necessary to replace this rectangular function with one which has essentially the same shape, but also acceptable transform properties. For the SAI PE model, a low-pass finite-impulse digital filter was selected. At a given frequency this filter is implemented with the appropriate number of points to insure that a beamwidth of at least $k_o \sin\theta_b$ is achieved in wavenumber space. The principal advantage of this source function over the traditional Gaussian function is that it minimizes the transform size required for any desired beamwidth. (The difference in required transform size for the digital filter versus the Gaussian is typically a factor of four.)

If one constructs the ray theory equations for both the elliptic and parabolic equations and looks for the equivalent ray trajectory determined by each equation, the angle of a ray governed by the elliptic equation, θ_e, is related to the angle under the parabolic equation, θ_p, by

$$\sin\theta_e = \tan\theta_p.$$

So, for example, the 90° elliptic equation ray is equivalent to the 45° parabolic equation ray. If a pressure field from the elliptic equation has wavenumbers which correspond to $\sin\theta > 1$, (i.e., $k > k_o$) the energy corresponding to them is exponentially damped out as the field propagates. However, under the parabolic equation, energy at these wavenumbers is not damped out and the PE equivalent of elliptic rays for $\sin\theta > 1$ will

propagate. Such energy creates unphysical artifacts in the PE field. To insure against these artifacts, the digital filter wavenumber cutoff is constrained to the following interval

$$k_o \sin \theta_b \leq k < k_o$$

which achieves the desired beamwidth and prevents the artifacts.

As the field from a source propagates with range it becomes redistributed in depth and the influence of refraction and bathymetry is to redistribute the energy in vertical wavenumber space. Again, because most solutions to the PE are based on discrete Fourier transforms, the problem being solved is implicitly periodic in depth and wavenumber. To insure that aliasing does not occur in range as the energy redistributes in both depth and wavenumber, the low-pass filter is also used at each range step to suppress the energy at high wavenumbers and greatest depths. This is accomplished by simply multiplying the depth and wavenumber fields by the filter response which maintains suitably limited depth and wavenumber fields.

Early portions of this work are contained in a talk entitled "Construction of a New Source Function for the Parabolic Equation Algorithm" by H. M. Garon, J. S. Hanna and P. V. Rost (J. Acoust. Soc. Am. 61 (51), 512(A), 1977).

PULSE RESPONSE OF PROPAGATION CHANNELS NEAR CAUSTICS

Lan Nghiem-Phu
Daubin Systems Corporation
104 Crandon Boulevard #315
Key Biscayne, FL 33149

and

Frederick D. Tappert
University of Miami
RSMAS
4600 Rickenbacker (SWY)
Miami, FL 33149

A Pulsed Parabolic Equation (PPE) model has been developed for the purpose of analyzing the time-domain response of propagation channels for coherent broadband sources. The method is based on multi-frequency PE runs and Fourier transforms of the complex field amplitudes to yield the analytic signal in the time domain. The time domain signals are normalized such that transmission loss (re 1 yd) becomes a function of time and may be resolved into separate arrivals. The relative phase is also obtained as a function of time and is nearly stationary through the center of single arrival.

A careful study of the accuracy of the PPE model has been carried out in the time domain by comparison to ray trace calculation of arrival times and transmission losses of single arrivals. In the neighborhood of caustics for pairs of arrivals, we have obtained some new results on the pulse shapes.

A detailed study has been made for a range independent environment consisting of a bi-linear profile (iso-velocity ocean overlying a constant gradient loss-less bottom) and a directional source having 200 Hz bandwidth and 200 Hz carrier (100 Hz $\leq$ f $\leq$ 300 Hz). The pulse response was examined at several ranges as a function of depth. In particular, at 15 km range, a three-arrival region is obtained by ray theory with two bounding caustics, outside of which there are single-arrival regions.

Pulse response amplitudes were compared to known exact solutions (spherical spreading) for the direct arrivals in the iso-velocity region. After correcting for source beam pattern effects, the PPE transmission loss was found to be accurate to within 0.5 dB out to 15 km.

The accuracy of the PPE arrival times derived from phase information was found to depend somewhat on the choice of reference sound speed C_o and also on the equivalent ray angle with respect to the horizontal. For a poor choice of C_o and large angle (about 24°), the error in travel times to a range of 15 km could be as much as 10 msec. However, for an optimal choice of C_o and for angles less than 18°, we found that the error in travel times to the same range was reduced to less than 1 msec.

It was observed that the peak of the amplitude was not situated at the geometrical caustic location but was displaced towards the illuminated side. There was significant energy on the dark side which decreased exponentially away from the geometric caustic boundary, and resulted in pulse spreading due to the effective low-pass filter caused by diffraction in the shadow region. Complicated interference patterns developed as the caustic was approached from the illuminated side. Separated arrivals merged together when their relative phases differed by an integral multiple of a cycle of the carrier frequency. For arrivals that have interacted with the caustic, there was evidence of pulse deformation, resulting in a trailing tail.

Similar studies are in progress for a complex environment with range dependent profiles, complicated bathymetry, and range and depth dependent horizontal currents.

THREE-DIMENSIONAL ACOUSTIC PROPAGATION USING THE PARABOLIC-EQUATION METHOD

J. S. Perkins, R. N. Baer, E. B. Wright, and R. L. Dicus
Code 5160
Naval Research Laboratory
Washington, DC 20375

We have extended the parabolic-equation method for acoustic propagation to three-dimensions. A split-step technique results in an algorithm for marching the solution in range. We also present an approximation to this full three-dimensional (3D) algorithm which we call the Nx2D method. In this approach we solve N two-dimensional problems and combine the results to form an approximate three-dimensional solution. This technique allows wave-front bending, which is the dominant mechanism for water-borne propagation.

We show in several examples how horizontal variations in the ocean environment affect the spatial distribution of energy and the distribution of energy in azimuthal angle as seen by an array of hydrophones placed in the calculated complex-valued acoustic field. In the first example we consider a very strong linear cross-range gradient, designed to produce an obvious and predictable effect. Results from the Nx2D method are in excellent agreement with the results produced using the 3D algorithm. In another example, we investigate propagation through a strong (but realistic) ocean eddy. The presence of the eddy between source and receiver causes a change in the apparent source bearing of 0.5°. In this case the Nx2D method again proves to be an excellent approximation. In the final example, we use the full 3D algorithm to simulate the performance of a bottom-mounted array of hydrophones. The results suggest that reflection and diffraction from bathymetric features may have a significant effect on the performance of bottomed arrays.

NUMERICAL CALCULATIONS OF BOUNDS ON ARRAY PERFORMANCE USING THE PARABOLIC-EQUATION TECHNIQUE

David R. Palmer
National Oceanic and Atmospheric Administraton
Atlantic Oceanographic and Meteorological Labs
Ocean Acoustics Lab
4301 Rickenbacker Causeway
Miami, FL 33149

and

Marilyn L. Blodgett
Code 5120
Naval Research Laboratory
Washington, DC 20375

In order to evaluate the feasibility of proposed under-sea surveillance systems it is necessary to know the conditions under which the effects of ocean variability, i.e., internal waves, on system performance can be ignored. The standard approach to this question is to measure or calculate the mutual coherence function for the acoustic field since it enters directly into the calculation of measures of system performance such as array gain. Because of the great difficulties in determining, both experimentally and theoretically, the mutual coherence function, we have taken a different point of view. Rather than attempting to calculate, e.g., array gain, we seek only to bound it. Consequently, we calculate a limit on the degradation in system performance. The advantage of this approach is that the limit depends only on the mean pressure field, a quantity far easier to calculate than the mutual coherence function. The calculation of the mean field does require, however, the use of a generalization of the Markov approximation appropriate when diffracting and refracting effects are present. With this approximation the calculation of the mean field can be carried out with a slightly modified version of the parabolic equation technique of Tappert and Hardin. A case study is made for propagation in the Western North Atlantic with the following results: Independent of the length of a horizontal array, its gain will not be reduced by more than 3 dB for propagation to 1 convergence zone at 260 Hz, 4 convergence zones at 130 Hz, and at least 15 convergence zones at 50 Hz.

PRELIMINARY VERSION OF A FINITE-DIFFERENCE PE MODEL

Ding Lee and George Botseas
Code 3342
Naval Underwater Systems Center
New London, CT 06320

A general purpose computer model which calculates propagation loss, based on an implicit finite-difference solution to the parabolic wave equation, will soon be available. This model is designed to offer a number of useful features: modifications are easy to incorporate; it is easy to use; and reasonably accurate results can be obtained with reasonable computational speed. In shallow or deep water propagation, the present model is capable of handling multiple interfaces, irregular bottoms, arbitrary bottom boundary conditions, and artificial bottoms. All test results show excellent agreement with published results. This model was used to solve a set of NORDA workshop problems. These results will be discussed.

HIGH ANGLE PE

Robert R. Greene
Science Applications, Inc.
1710 Goodridge Dr.
P. O. Box 1303
McLean, VA 22102

High Angle PE is a full-wave range dependent propagation model similar in concept to PE. It is designed to handle the dual problem of bottom-interaction and high angles of propagation up to about 45 degrees. It is based upon an implicit tridiagonal range step and a cubic spline discretization in the vertical coordinate.

The most important observation about the method is that since it uses a finite difference approach to the problem rather than the split-step algorithm, a far better approximation to high angle propagation is used in the form of a "rational parabolic" as opposed to "parabolic" approximation.

The method also allows an accurate treatment of strong gradients in sound speed and discontinuities in sound speed and density. These are the main difficulties for PE in modeling bottom interaction. Strong gradients are not a limitation for a finite difference technique because the solution does not depend on splitting an operator into nearly commuting parts. Discontinuities in sound speed and density are treated accurately by matching cubic splines at the interfaces. The boundary conditions of the wave equation are the natural matching conditions for the splines.

The major application of the method will be over regions where bottom interaction and range dependent bathymetry are driving the problem. However, it can be used to model long-range propagation. It should be particularly appropriate for continental slope and shallow water applications.

The work is currently being funded by ONR Code 486.

A FINITE ELEMENT METHOD FOR THE PARABOLIC WAVE EQUATION

Kenneth E. Gilbert
Code 320
Naval Ocean Research and Development Activity
NSTL Station, MS 39529

A semi-discrete elliptic wave equation is derived and used to develop a parabolic equation which allows propagation angles of up to 40° with respect to the horizontal. The derivation is based on the minimization of a Lagrangian in which the vertical dependence of the acoustic field is written explicitly in terms of finite elements and the nodal values of the pressure and vertical particle velocity. Since the resulting wave equation is in terms of continuous field variables, discontinuities in sound speed and density are easily handled.

A FINITE-DIFFERENCE TREATMENT OF INTERFACE CONDITIONS

Ding Lee
Code 3342
Naval Underwater Systems Center
New London, CT 06320

and

Suzanne T. McDaniel
Applied Research Laboratory
The Pennsylvania State University
University Park, PA 16802

A finite-difference approach is introduced to handle both horizontal and irregular interface conditions. These interface conditions are developed to preserve continuity of pressure as well as continuity of vertical particle velocity. The formulation of interfaces is by means of a finite-difference scheme in conjunction with the Taylor series expansion, while the handling of the irregular interfaces is by line segmentation. The complete mathematical development will be outlined. The validity of this approach is clearly shown by the theory, however, test results will be discussed as supporting evidence.

A HYBRID PARABOLIC EQUATION CODE

H. Brock
Code 1721.2
Naval Research Laboratory
Washington, DC 20375

The Tappert-Hardin split-step Fourier algorithm is an accurate and efficient numerical technique for the solution of the parabolic wave equation, particularly on a vector computer. Difficulties arise, however, in simulating boundary conditions at interfaces. Discontinuities introduce complications, and the range step required is strongly dependent on the gradient of the index of refraction. Such boundary conditions can be handled by finite difference techniques, although, in general, for a given accuracy many more mesh points are required in both dimensions. In addition, on a vector computer the techniques available for the solution of the finite difference equations tend to be less efficient than the split-step algorithm. Since in many problems RSR propagation dominates over substantial ranges, on a vector supercomputer it is feasible to combine the split-step Fourier algorithm in RSR dominated regions with a finite difference algorithm in regions where bottom interactions are important. The resulting hybrid PE code changes both the parabolic approximation and the solution technique used dynamically with range during the execution of a given problem.

EQUIVALENT BOTTOM FOR USE WITH THE SPLIT-STEP PARABOLIC EQUATION ALGORITHM

Homer Bucker
Code 531
Naval Ocean Systems Center
San Diego, CA 92152

The split-step parabolic equation algorithms (SSPEA) have become the standard Navy model for acoustic calculations in range dependent ocean areas. This occurred because SSPEA is extremely simple, runs rather quickly on a computer, and does a good job of modeling the refraction of sound caused by changes of sound speed with depth and range. However, SSPEA has problems when used in areas of strong bottom interaction. These are due to density discontinuities at the ocean bottom, sediment rigidity which results in shear waves in bottom sediments, and sound scattering from ocean bottom irregularities.

The equivalent bottom is a set of absorbing liquid layers that have the same density as the bottom water and thickness equal to the vertical sampling interval used in the SSPEA. The sound speed and density of each layer is adjusted so that the equivalent bottom has the "correct" bottom reflection properties. That is, the equivalent bottom should have the same plane wave reflection coefficient as a function of grazing angle as the actual ocean bottom. In addition, restrictions on the maximum change in sound speed and attenuation between adjacent layers insures that range steps in the SSPEA can be kept as large as possible. Also, insofar as scattering effects can be incorporated into the reflection coefficient, they are automatically transferred to the sound level calculation.

A HIGH FREQUENCY RAY BASED PARABOLIC EQUATION

Frederick D. Tappert
University of Miami
RSMAS
4600 Rickenbacker (SNY)
Miami, FL 33149

No abstract was submitted for this presentation.

IMPEDANCE FORMULATION OF THE BOTTOM BOUNDARY CONDITION FOR THE PARABOLIC EQUATION MODEL IN UNDERWATER ACOUSTICS

John S. Papadakis
Department of Mathematics
University of Rhode Island
Kingston, RI 02881

In implementing impedance conditions along the bottom interface for the parabolic equation, it is assumed that the subbottom region is homogeneous, semi-infinite and the field satisfies a radiation condition at $z=\infty$.

The derived impedance is a condition on the total parabolic field $p(r,z_B)$, and in the form of an integral equation along the bottom interface $z=z_B$

$$p(r,z_B) = -\frac{i^{\frac{1}{2}}\rho_B}{(2k_o\pi\rho)^{\frac{1}{2}}} \cdot \int_o^r e^{i\frac{k_o}{2}(n_B^2 - 1)(r-s)} \cdot (r-s)^{\frac{1}{2}} p_z(s,z_B)ds \quad ,$$

where ρ_B/ρ are the densities in the bottom/water, $k_o=2\pi f/c_o$ and n_B is the index of refraction in the bottom.

The integral equation is approximated by a finite sum and is incorporated in an implicit finite difference algorithm for the parabolic equation. The resulting model advances the parabolic field only in the water column and does not require the introduction of an artificial subbottom layer.

Research is in progress on models with sloping bottom interfaces as well as elastic subbottom effects.

PERUSE: A PE CODE INCLUDING ROUGH SURFACE SCATTERING

Lewis B. Dozier
Science Applications, Inc.
1710 Goodridge Dr.
P. O. Box 1303
McLean, VA 22102

A new model has recently been developed which treats rough surface scattering in the context of PE. The surface is assumed to be piecewise linear and frozen in time. A sequence of conformal mappings locally flattens each linear surface segment, whereupon the split-step Fourier algorithm can advance the solution for one step in each transformed space.

Numerical PERUSE (PE Rough Surface) results for surface ducts are analyzed by resolving them in depth into Labianca's virtual modes ("mode-matching"). The resulting modal intensities are then plotted as a function of range, and decay rates are estimated for each mode. Comparison with simple Rayleigh theory shows no obvious correlation. A fullwave coupled mode model is currently being investigated to explain the PERUSE results.

PROPAGATION MODELING WITH THE PARABOLIC EQUATION

F. B. Jensen and W. A. Kuperman
SACLANT ASW Research Centre
La Spezia, Italy

A series of basic propagation problems are solved using the parabolic equation. First we show results of some mode coupling studies[1,2] comprising propagation in a wedge-shaped ocean (up-slope and down-slope) and propagation in a shallow-water channel with an abrupt profile change. Then we apply the PE model to study Lloyd-mirror patterns. These results are interesting since we here obtain field plots that explicitly show the effect of the small-angle approximation inherent in the PE technique. In this connection we also study the diffraction of Lloyd-mirror beams over the top of a wedge. Finally, we demonstrate the application of PE theory to modeling sound propagation over a seamount. Here, theory is compared with broadband experimental data.

1. F. B. Jensen and W. A. Kuperman, "Sound propagation in a wedge-shaped ocean with a penetrable bottom," J. Acoust. Soc. Am. 67, 1564-1566 (1980).

2. F. B. Jensen and W. A. Kuperman, "Range-dependent bottom-limited propagation modeling with the parabolic equation", in Bottom-Interacting Ocean Acoustics, edited by W. A. Kuperman and F. B. Jensen (Plenum Press, New York, 1980) pp. 451-466.

APPENDIX B. PE PROGRAM ABSTRACTS

BTL

ARRAY PROCESSOR PE

J. D. Seals
Bell Telephone Laboratory
Whippany Road
Whippany, NJ 07981

The BTL version of the parabolic code (APPE) was developed to provide production runs with turnaround times on the order of minutes rather than hours. This was achieved by careful implementation of the code on an AP-190L array processor interfaced to an UNIVAC 1108 host. The full potential of the array processor was realized only by wholly implementing the P.E. approximation and step size algorithm in the array processor. While the array processor propagates the code forward one or more steps, the host sets up physical input for the next step(s). When the array processor finishes the propagation, a minimal I/O exchange occurs and the process repeats until completion. A pre-cursor routine looks ahead to warn of major changes in physical properties so that step reduction occurs before rather than after the fact.

Additional features of the BTL code include both linear and triangular sectors interpolation of velocity profiles, range dependent Q^{-1} and bottom sound speed gradients, pseudo discontinuities at the water/sediment interface, mixed data units, full diagnostic capabilities, data checking, linear and exponential averaging of TL data, and extensive graphic capabilities.

Although the current version of the code was developed for production, its highly modular and structured format provides an excellent base for future program study and development.

DREP

A FINITE-DIFFERENCE PE MODEL

D. J. Thomson
Defence Research Establishment Pacific
FMO Victoria, B. C.
CANADA VOS 1BO

A finite-difference scheme (hastily invoked for the NORDA workshop) is described for the so-called heterogeneous formulation[1] of the parabolic equation, which allows for spatial variation in the material properties. The sound-speed, density and absorption may be specified at each grid point of a finite-difference mesh, and the (internal) boundary conditions are everywhere satisfied implicitely. Discontinuities in material properties can be accommodated. The Crank-Nicolson algorithm is used to march out the numerical solution to the parabolic equation. A source function, designed to be band-limited in vertical wavenumber, is used to begin the solution process. Promising features of this approach include the ability to treat parabolic equations with variable coefficients, the use of non-uniform step sizes in depth, and the possibility of adapting recently developed absorbing boundary conditions[2] to limit the vertical extent of the computational grid. While not thoroughly tested (or even possibly debugged), the new code was applied to each of the suggested test problems.

[1]K. R. Kelly, R. W. Ward, S. Treitel, and R. M. Alford. Geophysics, Vol. 41(1), pp. 2-27, (1976).

[2]R. W. Clayton and B. Engquist. Geophysics, Vol. 45(5), pp. 895-904, (1980).

NORDA

A FINITE ELEMENT HIGH ANGLE PE

K. E. Gilbert
Code 320
Naval Ocean Research and Development Activity
NSTL Station, MS 39529

The NORDA program solves the wave equation in Claerbout's rational linear approximation, i.e. a high-angle parabolic equation. The discrete representation is based on the minimization of a Lagrangian in which the vertical dependence of the acoustic field is written explicitly in terms of finite elements and the nodal values of the pressure and vertical particle velocity. Since the resulting wave equation is in terms of continuous field variables, discontinuities in sound speed, attenuation and density are easily handled. This program presently treats only range independent environments. A normal mode solution is used for the initial field, and the radiation condition at the bottom is approximated by a "false" bottom. The program is implemented on the NORDA Cyber 171 computer.

NOSC

PARABOLIC EQUATION COMPUTER PROGRAM

D. Gordon
Naval Ocean Systems Center
San Diego, CA 92152

This underwater acoustic propagation loss program is a split-step parabolic equation algorithm using an FFT with no corrections or extensions. It is designed to be started from a normal mode field input at any desired range. Sound speed profiles are normally entered as linear layers in $1/C^2$. A constant attenuation can be added to any layer. The attenuating layer has a large value of attenuation at the bottom of the attenuating layer, and decays exponentially in dB/Δr upwards so that attenuation is negligible at the top of the attenuating layer and above it. The operator specifies Δz, Δr, and C_o. Outputs are printouts, storage on cards or files, and plots.

NRL-1

THE NRL PARABOLIC EQUATION PROGRAM PACKAGE FOR ACOUSTIC PROPAGATION

John S. Perkins and Ralph N. Baer
Naval Research Laboratory
Washington, DC 20375

We solve the parabolic equation using the split-step technique. The program makes full use of the vectorizing and pipelining capabilities of the Texas Instruments Advanced Scientific Computer (ASC) at NRL. It is available to the Navy scientific community through the Navy Laboratory Computer Network (NALCON). In our implementation we have included the option to partially correct for the parabolic approximations [J. A. DeSanto, J. S. Perkins, and R. N. Baer, J. Acoust. Soc. Am. 64, 1664-1666 (1978)].

In order to begin the range-stepping algorithm, two preliminary programs are used to specify the environment and generate an initial pressure field. The first program reads environmental data, interpolates sound-speed profiles, writes the bathymetry and a list of profiles on a file, and draws a profile/bathymetry plot and a sound-speed contour. The second program writes a file containing the initial pressure field. The user can choose from three alternatives: (1) a normal mode calculation, (2) a functional form which is Gaussian in depth, or (3) supply a complex FORTRAN function which will override the Gaussian. A plot of the initial field is also generated.

In the main range-stepping program, the sound speed in the bottom is constant in depth, but can vary with range. An option allows the bottom sound speed to vary so that a constant critical angle is maintained. Below the water/bottom interface, the square of the index of refraction is given an exponentially increasing imaginary part which effectively produces an absorbing boundary at the bottom of the transform region.

The direct outputs of the main program are a listing and plot of transmission loss versus range for selected depths (the intensities can be smoothed with a Gaussian average prior to converting to transmission loss), and a solution file. Other plots are available through auxiliary plotting programs which read the solution file: (1) additional transmission loss versus range plots, (2) transmission loss versus depth plots, (3) histograms of transmission loss values in a specified range-depth region, and (4) gray-scale contour plots of intensity as a function of range and depth.

It is also possible to simulate the performance of a tilted array of hydrophones in the calculated pressure field. This is done in an auxiliary program which provides either gray-scale or isometric plots of intensity as a function of arrival angle and range from the source, and estimates of array signal gain and 3 dB width.

NRL-2 AND NRL-3

VECTORIZED PE PROGRAMS

H. Brock
Naval Research Laboratory
Washington, DC 20375

The current PE program implements the solution of two different parabolic approximations. The "standard" (Leontovich-Fock) parabolic approximation (NRL-2) is solved using the Tappert-Hardin split-step Fourier algorithm. The second approximation, Tappert's Co independent equation (NRL-3) is solved with a finite difference algorithm that attempts to match interface conditions at boundaries. The finite difference algorithm is currently under development, and a number of problems have not been solved. The code makes use of the TI ASC vector hardware with explicit in-line generation of vector instructions and, hence, is not readily transportable to other machines.

The split-step code is basically a vectorized version of the program described in NORDA Technical Note 12, The AESD Parabolic Equation Model, with the following modifications and additions:

1. Data structures have been modified for more efficient vectorization.

2. The sine transforms of the real and imaginary parts of the field are performed in parallel to reduce overhead and generate longer vectors. The fast Fourier transform algorithm is a vector version that eliminates the bit reversal permutation sequence that is necessary in most scalar implementations.

3. Two source functions are available--a Gaussian or the filter function developed by SAI (Garon, Hanna and Rost).

4. The pseudo radiation condition boundary is imposed by using a low pass digital filter to attenuate the last quarter of the transform grid.

5. Triangular sector sound speed interpolation is used.

6. Two range step size estimates are made each step. In physical space the range step size estimate is based on the absolute value of the leading error term (third order in range step) resulting from the assumption that the exponential operators commute. In Fourier space a range step estimate is derived from the range interference length corresponding to the highest vertical wavenumber component 50 dB below the spectral peak. (The Fourier space estimate was derived by H. Garon of SAI.) The code selects the minimum of the two step size estimates.

NUSC-1

NUSC IFD* PE MODEL

*Implicit Finite-Difference

D. Lee and G. Botseas
Naval Underwater Systems Center
New London, CT 06320

A PE propagation loss model

The parabolic wave equation is solved by an IFD scheme

The code treats the propagation problem as an IBVP (Initial Boundary Value Problem)

Sound speed profile can be supplied in user's format

Some bottom boundary conditions are built-in (sloping bottom case)

User's bottom boundary conditions are acceptable

Automatic handling of horizontal interfaces

FORTRAN (NUSC VAX11 computer)

The workshop test problems were solved by this model using a Gaussian starter and the artificial bottom technique.

NUSC-2

THE SNAPE NORMAL MODE MODEL FOR THE PARABOLIC EQUATION

David H. Wood
Naval Underwater Systems Center
New London, CT 06320

A normal mode computer model for predicting how sound travels in the ocean generates solutions of the Helmholtz equation. Such models can be easily modified to instead solve the Parabolic equation by changing a few lines of instructions. Such a modified normal mode model is useful for validation of other Parabolic equation models based on other, more generally applicable, numerical techniques. This eliminates two difficulties usually encountered in such validation: the Helmholtz equation has a different solution than the Parabolic equation, and the latter is sensitive to a parameter that does not even enter into normal mode computations. A normal mode model can be further modified to use any desired starting values, which eliminates another source of variation in the outputs of Parabolic equation models. Roughly speaking, one merely replaces the functions $H_o^{(1)}$ (k r cos θ_n) that express the range dependence of each term of the normal mode sum in terms of the horizontal wave number k cos θ_n. These functions are replaced by the functions exp $-i(1/2)$ $k_o r(1-\sin^2\theta_n)$. As an example the SNAP model (SACLANTCEN Normal-Mode Propagation model) of Finn B. Jensen and M. C. Ferla based on the work of A. V. Newman and F. Ingenito was modified by Susan M. Bates of Science Consultants Incorporated of Newport, R.I., and renamed SNAPE. Numerical results for some PE workshop problems have been generated for both Gaussian initial data and mode-sum initial data. These examples and further details are given in NUSC TM No. 811080.

SACLANT

PAREQ

F. B. Jensen and H. R. Krol
SACLANT ASW Research Centre
LaSpezia, Italy

PAREQ[1,2] is a parabolic equation model; the computer program used in this study is a modified version of the one developed by AESD[3]. This model not only handles a variable profile in depth and range but also allows the bottom depth and bottom structure to vary in range. The bottom is characterized by a compressional speed profile, density (the density discontinuity is smoothed using a hyperbolic tangent function as suggested in Ref. 1) and attenuation which is included by using a complex sound speed. The second layer of the bottom has constant acoustic properties. There are two options for the initial field: Gaussian source or normal modes. This model is not only resident on a UNIVAC 1106 but also runs on an HP 21MX computer.

1. Tappert, F. D. The parabolic approximation method. In: Keller, J. B. and Papadakis, J. S. eds Wave Propagation and Underwater Acoustics. Lecture Notes in Physics 70. New York, Springer-Verlag, 1977: 224-287.

2. Jensen, F. B. and Krol, H. R. The use of the parabolic equation method in sound propagation modeling, SACLANTCEN SM-72. La Spezia, Italy, SACLANT ASW Research Centre, 1975.

3. Brock, H. K. The AESD parabolic equation model, NORDA TN-12. NSTL Station, Miss., Naval Ocean Reserch and Development Activity, 1978.

SAI-1

SAI PE

C. Spofford, L. Dozier, H. Garon, and R. Stieglitz
Science Applications, Inc.
1710 Goodridge Dr.
P. O. Box 1303
McLean, VA 22102

SAI PE is based on the original AESD PE version written by Harvey Brock. Changes in the original version implemented in SAI's PE:

1) A new source function. The original Gaussian beam source function left too much energy traveling at steep angles and not enough energy traveling at lower angles at the source. The new PE source function is an impulse response in physical space (approximately a sinx/x) which transforms to a filter function in vertical wave number space. This filter function is very close to the wave number spectrum of a limited aperture point source with most of the energy evenly distributed over the low wave numbers and a roll-off in the higher wave numbers to prevent aliasing.

2) A new range step calculation. This feature of SAI's PE was installed to save computer time. Basically PE now calculates the maximum angle of energy propagation and then determines the interference length (horizontal) between energy traveling at this angle and energy traveling horizontally. This interference length is the new range step. This algorithm avoids the necessity of calculating the third order truncation error term (which is too time consuming on our non-vectorizing machine) and provides the same results.

3) CMOD. CMOD is a transform of the environment, both the sound speed profiles and the input and output depths, in order to reduce the parabolic phase velocity error.

4) Bottom options. SAI PE regular allows the user to specify either a sound speed profile and attenuation function in a sediment layer or a transmission loss versus grazing angle curve.

SAI-2

HIGH ANGLE PE

Robert R. Greene
Science Applications, Inc.
1710 Goodridge Dr.
P. O. Box 1303
McLean, VA 22102

High Angle PE is a full-wave range dependent propagation model similar in concept to PE. It is designed to handle the dual problem of bottom-interaction and high angles of propagation up to about 45 degrees. It is based upon an implicit tridiagonal range step and a cubic spline discretization in the vertical coordinate.

The most important observation about the method is that since it uses a finite difference approach to the problem rather than the split-step algorithm, a far better approximation to high angle propagation is used in the form of a "rational parabolic" as opposed to "parabolic" approximation.

The method also allows an accurate treatment of strong gradients in sound speed and discontinuities in sound speed and density. These are the main difficulties for PE in modeling bottom interaction. Strong gradients are not a limitation for a finite difference technique because the solution does not depend on splitting an operator into nearly commuting parts. Discontinuities in sound speed and density are treated accurately by matching cubic splines at the interfaces. The boundary conditions of the wave equation are the natural matching conditions for the splines.

The major application of the method will be over regions where bottom interaction and range dependent bathymetry are driving the problem. However, it can be used to model long-range propagation. It should be particularly appropriate for continental slope and shallow water applications.

The work is currently being funded by ONR Code 486.

URI

IMPEDANCE + IFD COMPUTER MODEL

John S. Papadakis
Dept. Math. University of Rhode Island
Kingston, RI 02881

Test problems 1-4 were run using an experimental computer model, consisting of the implicit finite-difference model presently under development by D. Lee and G. Botseas NUSC, New London Lab. into which an "impedance" subroutine has been incorporated. It should be pointed out that the above IMPEDANCE+IFD computer model is in the experimental stage and under continuous evolution.

The impedance subroutine calculates the field at the advanced range along the bottom interface via a weighted sum of its normal derivative along the interface from range zero to the present range. This eliminates the need of introducing an artificial bottom in the IFD model, and the field is advanced only in the water column. The impedance subroutine can trace the field along horizontal bottom boundaries as well as sloping bottoms.

ADVANTAGES of the impedance approach versus introduction of an absorbing layer and a false bottom: (1) Problems because of jump discontinuities along the bottom interface of density and sound speed are eliminated since the domain of interest terminates at the real bottom. (2) The question of how deep the false bottom should be placed is also eliminated. (3) The number of mesh points in the z-direction is much smaller (in many cases half, since often, in the false bottom approach the water depth is doubled). (4) The computer time is substantially improved since, by (a) above a larger range step-size can be used, and by (b) the number of z-mesh points is smaller.

DISADVANTAGES: (1) If the whole weighted sum is used then a larger storage space is needed. However, in most applications because of the size of the weights, the sum is truncated and a constant number of terms is used throughout the computation. (2) Because of the use of a sum, when the intensity is very small along the bottom boundary, numerical noise is introduced. This can be seen in Test-Problem 1. Actually, the same disadvantage exists in the split-step, namely; since every point in the advanced range is calculated via a weighted sum of the field at the present range, if the intensity is down to a few significant figures numerical noise will be introduced. This problem does not appear in finite difference approach since a point at the advanced range is given in terms of not all the points in the present range as in the split-step but in terms of only three points. In other words the impedance as well as the split-step being approximations of integral operators are global operators with the above disadvantage where the finite difference being an approximation of a differential operator is a local operator.

SNAP

SACLANTCEN NORMAL-MODE ACOUSTIC PROPAGATION MODEL

F. B. Jensen and M. C. Ferla
SACLANT ASW Research Centre
La Spezia, Italy

SNAP (1) is a normal-mode model based on a program originally developed at the U.S. Naval Research Laboratory (2, 3); this program solves the eigenvalue problem by direct numerical integration of the depth dependent equation. Computation time for some of the key subroutines has been reduced and the program has been restructured to run interactively on a UNIVAC EXEC 8 system. The model allows for slight range dependence by employing the adiabatic approximation. SNAP was originally designed for a shallow water environment but a version now exists which handles high-frequency deep-water situations. Environmental inputs are: arbitrary velocity profile as function of depth (multiple profiles for range-dependent adiabatic computations) in the water column, density, attenuation and compressional velocity profile of sediment layer and density, shear and compressional velocity and shear and compressional attenuation of the basement. At present, the existing output options are: loss vs. range, loss vs. depth, depth-averaged loss vs. range, depth-averaged loss vs. frequency, contoured loss vs. depth and range, contoured loss vs. frequency and range, contoured depth-averaged loss vs. frequency and range, modal group velocity vs. frequency, modal phase velocity vs. frequency, mode function vs. depth, phase of field vs. depth, intensity of field vs. arrival angle, and sound speed vs. depth. The model has been compared with other models (4) and has been tested against various data sets (5).

1. Jensen, F. B. and Ferla, M. C. SNAP: the SACLANTCEN normal-mode acoustic propagation model, SACLANTCEN SM-121. La Spezia, Italy, SACLANT ASW Research Centre, 1979 (AD A 067256).

2. Miller, J. F. and Ingenito, F. Normal mode FORTRAN programs for calculating sound propagation in the ocean, NRL Memorandum Rpt 3071, Washington, D.C., U.S. Naval Research Laboratory, 1975.

3. Ingenito, F., Ferris, R., Kuperman, W. A. and Wolf, S.N. Shallow water acoustics, summary report (first phase), NRL Rpt 8179, Washington D.C., U.S. Naval Research Laboratory, 1978.

4. Jensen, F. B. and Kuperman, W. A. Environmental acoustical modeling at SACLANTCEN, SACLANTCEN SR-34, La Spezia, Italy, SACLANT ASW Research Centre, 1979 (AD A 081 853).

5. Ferla, M. C., Dreini, G., Jensen, F. B. and Kuperman, W. A. Broadband model/data comparisons for acoustic propagation in coastal waters. In: Kuperman, W. A. and Jensen, F. B. eds. Bottom-Interacting Ocean Acoustics. New York, Plenum Press, 1980.

FFP

FAST FIELD PROGRAM

H. W. Kutschale
Columbia University
Palisades, NY

FFP (1, 2) is a complete numerical solution of the range independent wave equation and hence includes the continuous part of the spectrum and the near field (distances greater than a wavelength). The model used in this study was developed at Columbia University (2). The model includes propagation of both compressional and shear waves and is therefore also suitable for seismic studies. In the original version, the depth dependent part of the wave equation was solved using the Thompson-Haskell matrix method where the water column is divided into isovelocity layers. An updated version (3) allows constant gradient in k^2 (equivalent to $1/c^2$ constant gradient) and therefore employs Airy functions in the Thompson-Haskell matrices instead of trigonometric functions. The inputs are the same as that of the normal-mode model (SNAP). There are two possible outputs: there is the "integrand" plot, which is essentially a plot of energy vs. wavenumber and it therefore has maxima corresponding to the normal-mode eigenvalues in the discrete part of the spectrum. The maxima in the continuous portion of the spectrum correspond to the so-called "virtual modes." The second output is loss vs. range; it should be noted that the present program requires a complete new run for a change of source or receiver depth. Hence, loss contours over range and depth are not practical as compared to normal mode or PE methods.

1. DiNapoli, F. R. Fast field program for multilayered media, NUSC Rept. 4103. New London, Conn., Naval Underwater Systems Center, 1971.

2. Kutschale, H. W. Rapid computation by wave theory of propagation loss in the Arctic Ocean, Rept. CU-8-73. Palisades, N.Y., Columbia University, 1973.

3. Kutschale, H. W. Unpublished communication.

UNCLASSIFIED

SECURITY CLASSIFICATION OF THIS PAGE *(When Data Entered)*

REPORT DOCUMENTATION PAGE		READ INSTRUCTIONS BEFORE COMPLETING FORM
1. REPORT NUMBER NORDA Technical Note 143	2. GOVT ACCESSION NO.	3. RECIPIENT'S CATALOG NUMBER
4. TITLE *(and Subtitle)* NORDA Parabolic Equation Workshop		5. TYPE OF REPORT & PERIOD COVERED Final 6. PERFORMING ORG. REPORT NUMBER
7. AUTHOR(s) J. A. Davis D. W. White R. Cavanagh		8. CONTRACT OR GRANT NUMBER(s)
9. PERFORMING ORGANIZATION NAME AND ADDRESS Naval Ocean Research & Development Activity Numerical Modeling Division, OSTL NSTL Station, Mississippi 39529		10. PROGRAM ELEMENT, PROJECT, TASK AREA & WORK UNIT NUMBERS 63785N
11. CONTROLLING OFFICE NAME AND ADDRESS Same		12. REPORT DATE September 1982 13. NUMBER OF PAGES 102
14. MONITORING AGENCY NAME & ADDRESS*(if different from Controlling Office)*		15. SECURITY CLASS. *(of this report)* UNCLASSIFIED 15a. DECLASSIFICATION/DOWNGRADING SCHEDULE

16. DISTRIBUTION STATEMENT *(of this Report)*

Unlimited

17. DISTRIBUTION STATEMENT *(of the abstract entered in Block 20, if different from Report)*

18. SUPPLEMENTARY NOTES

19. KEY WORDS *(Continue on reverse side if necessary and identify by block number)*

Parabolic approximation
Workshop
Ocean acoustics

20. ABSTRACT *(Continue on reverse side if necessary and identify by block number)*

A Parabolic Equation (PE) workshop, sponsored by the Surveillance Environmental Acoustic Support (SEAS) Project and hosted by NORDA's Numerical Modeling Division, was held at NSTL from 31 March to 3 April 1981. The purpose of the workshop was to provide a forum for those active in theoretical and applied PE development and to compare computer results for a set of ocean acoustic problems. Fifteen formal presentations were given, and thirteen different PE models were exercised against four test cases. The test cases ranged from one that any

DD FORM 1 JAN 73 1473 EDITION OF 1 NOV 65 IS OBSOLETE
S/N 0102-LF-014-6601

UNCLASSIFIED

SECURITY CLASSIFICATION OF THIS PAGE *(When Data Entered)*

PE should be able to handle to one that is a challenge for every PE. This report describes the results of that workshop and includes the theoretical bases for the models, the model descriptions, results of the test cases, and abstracts of the formal presentations.